Interactions between a Bacterial Tyrosine Kinase and its Cognate Phosphatase-

A Solution NMR Study

by

Deniz B. Temel

A dissertation submitted to the Graduate Faculty in Physics in partial fulfillment of the requirements for the degree of Doctor of Philosophy, The City University of New York

2012

This manuscript has been read and accepted for the
Graduate Faculty in Physics in satisfaction of the
dissertation requirement for the degree of Doctor of Philosophy.

Ranajeet Ghose, PhD

Date — Chair of Examining Committee

Igor Kuskovsky, PhD

Date — Executive Officer

Ranajeet Ghose, PhD

Ruth Stark, PhD

Zimei Bu, PhD

David Cowburn, PhD

Kaushik Dutta, PhD

Supervisory Committee

THE CITY UNIVERSITY OF NEW YORK

Abstract

Interactions between a Bacterial Tyrosine Kinase and its Cognate Phosphatase-
A Solution NMR Study

by

Deniz B. Temel

Advisor: Professor Ranajeet Ghose

Bacterial tyrosine kinases (BY-kinases) play a central role in a variety of physiological processes in bacterial cells. Most notable among these processes is the formation of antiphagocytic capsule and biofilm for survival under environmental stress conditions. BY-kinases constitute a unique class of prokaryotic enzymes sharing no sequence or structural homology with their eukaryal counterparts. BY-kinases are regulated by eukaryotic-like protein tyrosine phosphatases and several tyrosine kinase/phosphatase pairs, which have been identified in both gram-positive and gram-negative bacterial species.

The *Escherichia coli* (K12) BY-kinase Wzc is regulated by a cytosolic Low Molecular Weight Protein Tyrosine Phosphatase (LMW-PTP) Wzb through the autophosphorylation/dephosphorylation of five phosphorylatable tyrosine residues (termed the tyrosine cluster, YC) located in the C-terminal tail of the cytosolic catalytic domain of Wzc. The cycling between autophosphorylated form of Wzc and the Wzb-catalyzed dephosphorylated state, rather than the quantitative phosphorylation state of the YC, appears to play a central role in the synthesis and export of the exopolysaccharide, colanic acid. Despite biochemical evidence that Wzb dephosphorylates YC-phosphorylated Wzc, the

nature of the interactions between these two enzymes and the detailed regulatory mechanism has not been elucidated. The aim of this research was to identify the structural, dynamic and mechanistic aspects of the regulation of Wzc by Wzb.

We used state-of-the-art solution-state Nuclear Magnetic Resonance (NMR) techniques in order to illuminate the interaction between Wzc and Wzb. We have obtained near-complete resonance assignments of the catalytic domain of Wzc, the first for a BY-kinase. Utilizing these assignments and chemical shift titrations, we demonstrate that Wzb prevents oligomerization of Wzc by occluding its intramolecular interaction surface, that lies on the opposite face to that housing the Wzc catalytic site, thus facilitating the dephosphorylation of the exposed YC. The YC would be buried, and shielded from Wzb, in oligomeric Wzc. Similar chemical shift titrations on Wzb reveals that Wzc docks onto Wzb using a site proximal to the catalytic site of the latter. NMR spin-relaxation measurements confirm this hypothesis in addition to revealing interesting dynamics in the key regulatory elements in Wzc and Wzb.

Acknowledgements

I thank to my husband, Dr. Ertan Eryilmaz for his endless love, support and patience. He is the only one who has understood me the most since we have met…

I thank to my parents for their unconditional love. They taught me that nothing is more important than loving, respecting and caring for each other.

I thank to my brother Kerim Temel. I am so lucky to have his love and support next to me at all times.

I thank to Dr. Aswin Natarajan. He is one of the best things happened to me since I came to the USA.

I thank to Prof. Ranajeet Ghose. He is a great scientist, human being and mentor. I will never forget that he accepted me to his laboratory without any hesitation.

I want to thank my committee members for their support and advice during my research.

Especially, I thank to Dr. Kaushik Dutta who gave priority to my experiments. Subsequently my PhD work gained momentum and my research became more interesting.

I want to thank all the members of Ghose's laboratory for their patience with me especially during the last phase of my PhD work. This work could not be done without their support, advice and help.

I want to thank all my friends. They always think of me and care about me.

This thesis is dedicated to a great biologist and a teacher Aylin Ozturk who passed away at a very young age. After her leaving, once again I understand there is nothing more important than health and each other's love in this world.

Table of Contents

List of Tables

List of Figures

1. Introduction

The process of phosphorylation and subsequent dephosphorylation of proteins is a central process in intracellular signal transduction (Johnson, 2009; Tarrant and Cole, 2009). Phosphorylation, a post-translational modification catalyzed by enzymes called protein kinases, involves the transfer and covalent attachment of the γ-phosphate of ATP, to the sidechains of specific amino-acid residues on target proteins. The phosphate moiety is subsequently removed by the action of enzymes called phosphatases. The opposing actions of kinases and their cognate phosphatases occurs in all domains of life, and this tightly controlled level of protein phosphorylation plays a central role in a multitude of essential cellular processes such as gene expression, cell growth, differentiation, proliferation, regulation of metabolic pathways, transport across membranes, and apoptosis. Residues that are covalent modified by kinases include serine/threonine (by serine/threonine kinases), aspartate (by aspartyl kinases), histidine (by histidine kinases), and tyrosine (by tyrosine kinases).

While protein serine/threonine (PSTK) (Bakal and Davies, 2000) and tyrosine kinases PTKs) were recognized to be key components of intracellular signal transduction in higher eukaryotes (Hunter, 1995) and aspartyl/histidine kinases were considered to be the only phosphorylation-based signaling pathway in prokaryotes, the discovery of prokaryal PTSKs (Pereira et al., 2011) and PTKs (Bechet et al., 2009) have blurred this simplified picture. As described below, in this thesis we have chosen to focus on the regulation of the *E. coli* PTK, Wzc, as a representative prokaryotic PTK by its cognate phosphatase pair Wzb. The Wzc/Wzb system serves as a tractable model binary kinase-phosphatase system wherein to define the regulatory mechanism of similar systems in both gram-positive and gram-negative bacteria. While the biological and physiological outcome (Bechet et al., 2009; Cozzone et al.,

2004; Grangeasse et al., 2007) of the phosphorylation/dephosphorylation event in *E. coli* has been extensively studied, the structural and mechanistic aspects of the interactions between Wzc and Wzb remains poorly defined. We have attempted to rectify this situation using a variety of solution NMR techniques. We expect that our present findings will shed light on the process of tyrosine phosphorylation and dephosphorylation in prokaryotes and enhance our understanding of the intricacies of this important binary event.

2. Background

2.1. Protein Phosphorylation in Bacteria

Protein phosphorylation is a post-translational modification where a phosphate group is covalently attached to serine, histidine, threonine or tyrosine residue(s) of a protein. Phosphorylation (by kinases) and dephosphorylation (by phosphatases) constitute a central mechanism of intercellular signal transduction in prokaryotic and eukaryotic cells, controlling a wide variety of molecular processes in the cellular life cycle including gene expression, regulation of metabolic pathways, growth, differentiation, membrane trafficking, proliferation and apoptosis. Protein phosphorylation is carried out by kinases, which catalyze the transfer of the γ-phosphate group of ATP to specific residues on their target proteins. Phosphatases remove the phosphate group from their substrates by acting in opposition to the corresponding kinases (Cohen, 2002).

Since its discovery over 50 years ago (Burnett and Kennedy, 1954; Krebs and Fischer, 1956), the phosphorylation of proteins has been established as a key component of intracellular signaling in higher eukaryotes. In bacteria phosphorylated serines in *Escherichia coli* (*E. coli*) was detected by radioactive assays in 1964 (Kennelly and Potts, 1996; Rafter, 1964). Since then, many proteins have been discovered that are involved in several

phosphorylation pathways in bacteria. Up to now, there have been 86180 proteins are reported as a kinase in bacteria of which 3926 being in *E. coli*.

2.1.1. Classification of Bacterial Kinases

Bacterial kinases can be divided into three distinct groups according to the amino acids they phosphorylate: 1) Histidine and aspartate kinases which are part of the two-component regulatory systems (TCS) 2) serine and threonine kinases and 3) tyrosine kinases (Kobir et al., 2011).

(1) *Histidine and aspartate kinases*: These enzymes are part of the so-called two component regulatory systems which are regulated by a stimulus-response mechanisms (Kennelly and Potts, 1996). In a two-component system, the membrane bound sensor histidine kinase autophosphorylates its histidine residue in response to an external stimulus and subsequently transfers the high-energy phosphoryl group to an aspartate residue of a second protein called, the response regulator (Bechet et al., 2009; Gao and Stock, 2009). This two-step signaling pathway plays a central role in metabolism, development and virulence (West and Stock, 2001).

(2) *Serine and threonine kinases*: The first serine/threonine kinase, Pkn1 from *Myxococcus xanthus*, revealed the importance of this kinase in the normal development of bacterium (Munoz-Dorado et al., 1991). These enzymes are also called "eukaryotic type kinases" in the literature since they harbor so-called Hanks motifs ($HRDLX_3N$, where X_3 is usually KPE in serine/threonine kinases in which lysine residue being invariant) similar to their eukaryotic counterparts (Hanks et al., 1988; Kobir et al., 2011; Zhang et al., 1992). Serine/threonine kinases in bacteria play critical role in differentiation, spore formation, cell division and regulation of protein secretion (Kobir et al., 2011).

(3) *Tyrosine kinases*: Bacteria were thought to be devoid of tyrosine kinase even though first protein tyrosine phosphorylation activity was pointed out in *Escherichia coli* in 1982 (Manai and Cozzone, 1982). Ultimately, genetic and biochemical properties of the first tyrosine kinase, Ptk (Protein Tyrosine Kinase) from *Acinetobacter johnsonii* was indicated to undergo autophosphorylation at specific tyrosine residues (Duclos et al., 1996). Sequence analysis of Ptk indicated a possible involvement of this kinase in signal transduction, cell recognition and pathogenicity of bacteria (Grangeasse et al., 1997). Bacterial tyrosines kinases (now referred to as BY-kinases) will be discussed in greater detail in following section.

2.2. Bacterial Tyrosine Kinases (BY-kinases)

Autophosphorylation of the BY-kinases and phosphorylation of its substrate have been shown to be essential for survival in Gram-negative and Gram-positive bacteria. For example, in the DivL protein kinase autophosphorylation of Tyr550 is essential for cell viability and signal transduction control in cell division and DNA replication from *Caulobacter crescentus* (Wu et al., 1999). In *Salmonella tpyhimurium*, not only tyrosine but also serine and threonine autophosphorylation in kinase the PutA were found to suppress the proline-utilization operon (which allows proline to be used as a carbon, nitrogen and an energy source) and involved in the conversion of proline to glutamate (Ostrovsky and Maloy, 1995). In addition, still unidentified proteins have been observed to be phosphorylated which play an important role in aggregation and sporulation of *Myxococcus xanthus*. In *Pseudomonas syringae*, phosphorylation of a 66 kDa protein was found to be essential for bacterial adaptation to cold (Cozzone et al., 2004). Similarly, light-dependent tyrosine phosphorylation of an unidentified protein was detected in *Prochlorothrix hollandica* wherein under intense light exposure conditions the phosphorylation of the protein is triggered whereas low light conditions cause its dephosphorylation (Cozzone et al., 2004).

Even though, BY-kinases are found to be mostly involved in polysaccharide production through the autophosphorylation/dephosphorylation process, there have been several lines of evidence that BY-kinases take part in the regulation of several other functions in bacterial cells by phosphorylating endogenous substrates (Bechet et al., 2009). However, since the focus on the structure/function/regulation of BY-kinases is very recent, not many protein substrates have been identified till date. Several studies have shown that BY-kinases phosphorylate other protein substrates in order to regulate their functions. For example, the BY-kinase Etk from *E. coli* can phosphorylate the RNA polymerase sigma factor RpoH and anti-sigma factor RseA at a tyrosine residue on each protein (Tyr260 and Tyr38 respectively) to regulate the heat shock response (Klein et al., 2003). In addition, Ugd, UDP-glucose (Uridine diphosphate-glucose) dehydrogenase protein has been shown to be phosphorylated by BY-kinases in *Bacillus subtilis*, *Staphylococcus aureus* and *E. coli* to regulate the production of capsular polysaccharides, exopolysaccharides and antibiotic resistant sugar derivative UDP-4-amino-4deoxy-L-arabinose (L-Ara4N) (Lacour et al., 2008). It should also be noted that the integrase protein Int-HK022 that is responsible for regulation of the site-specific integration and lysogenization in bacteriophage is phosphorylated/dephosphorylated at its catalytic tyrosine (Tyr342) by the BY-kinase Wzc and its cognate phosphatase Wzb (Kolot et al., 2008).

In Gram-negative and Gram-positive bacteria the cyclic process of phosphorylation/dephosphorylation plays an important role the in synthesis and/or transport of polysaccharides that form capsule or bio-film. This capsule or bio-film becomes a critical virulence factor that causes bacteria to be pathogenic to its host (Cozzone, 2005).

2.2.1. Structural Features of BY-kinases

BY-kinases consist of two distinct domains namely: a trans-membrane activator domain (TAD) and a catalytic domain (CD) (Figure 1) (Jadeau et al., 2008). Catalytic domain and TAD domains are expressed in single polypeptide chains in proteobacteria and actinobacteria. Whereas, in firmicutes (phylum of bacteria mostly showing Gram-positive property) these two domains are expressed as two separate proteins wherein helix-helix interactions between CD and TAD triggers the kinase activity. The trans-membrane activator domain contains a two-pass trans-membrane helix with a large periplasmic loop (Grangeasse et al., 2007). Even though it has been suspected that the long extracellular loop could be connected to sensory mechanism, there is no concrete evidence for this (Kobir et al., 2011). However, a proline rich motif in the external loop seems to play a crucial role in extending the chain during polysaccharide synthesis in bacteria (Obadia et al., 2007). The catalytic domain lies in the cytoplasm and consists of α-β units where parallel β strands form the central part of the CD domain that is surrounded by α helices. The CD contains a tyrosine rich C-terminal cluster (YC-cluster) (Leipe et al., 2002). In addition, the CD encompasses nucleotide and ion binding motifs of $[G/A]X_4GK[S/T]$ (Walker A), $[ILVFM]_3DX_2P$ (Walker B) and an additional $[ILVFM]_3DXDXR$ (Walker A') that is sandwiched between the Walker A and B motifs. These motifs are involved in ATP binding and hydrolysis (Bechet et al., 2010). The YC-cluster contains four to seven tyrosine residues, which can undergo autophosphorylation (Figure 1). Further, the sequence alignment of BY-kinases revealed a conserved EX_2RX_2R motif that seemingly plays a central role in oligomerization (Bechet et al., 2010). Also found is an arginine-lysine-rich cluster (RK-cluster) that appears to be essential for nucleotide binding and/or hydrolysis (Bechet et al., 2010).

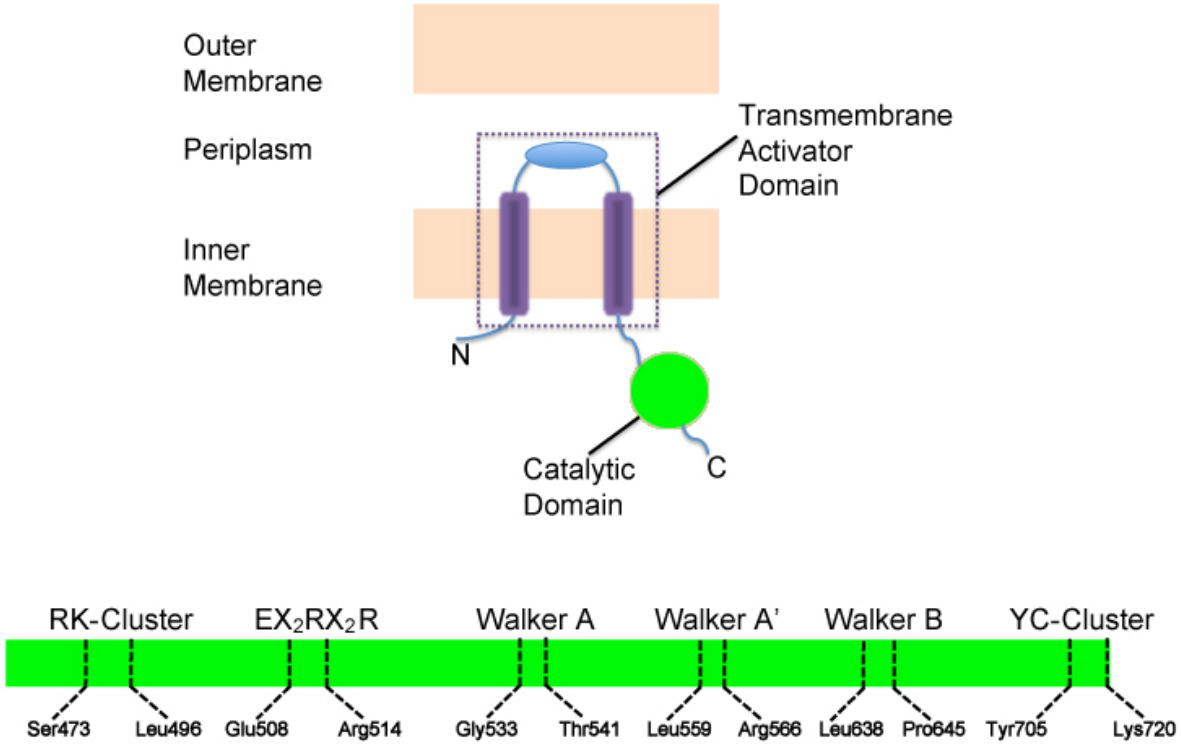

Figure 1: Schematic representation of the structural organization of the BY-kinase in proteobacteria. BY-kinase in proteobacteria contains a two-pass trans-membrane segment, a cytosolic kinase domain containing the Walker A, Walker A' and Walker B motifs and a C-terminal tyrosine cluster that is auto-phosphorylated.

Recent high-resolution crystal structures of the catalytic domain constructs of inactive Cap_{AB} from *S. aureus*, active Etk from *E. coli* K12 and inactive Wzc from *E. coli* K12 revealed the lack of structural similarity with eukaryotic protein tyrosine kinases (Figure 2 and Figure 3). However, BY-kinases' overall fold is strikingly similar with Mrp/MinD super family of P-loop GTPases (RMSD and Z-score between Wzc_{CD} and MinD are 2.7 and 16.4, respectively (Holm and Rosenstrom, 2010)) in spite of very low sequence identity (7.78% sequence identity with Wzc_{CD} *E. coli* K12).

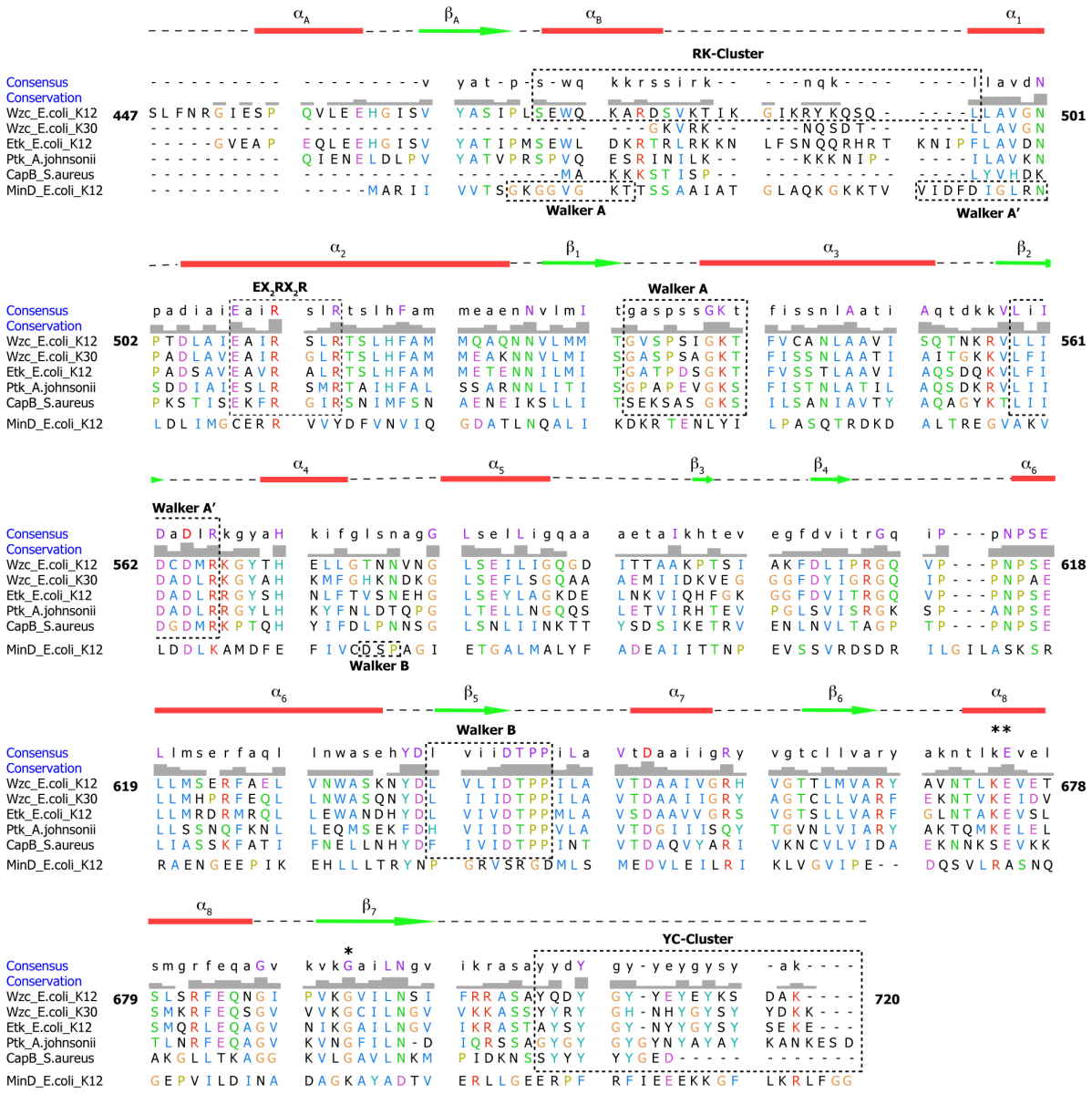

Figure 2: Sequence alignment of bacterial tyrosine kinases. The catalytic domains of Wzc from *E. coli* K12, Wzc from *E. coli* K30, Etk from *E. coli* K12, Ptk from *A. johnsonii*, CapB from *S. aureus* and MinD from *E. coli* were aligned by ClustalW2 (Goujon et al., 2010; Larkin et al., 2007). Dashed boxes indicate the key sequence motifs implicated in oligomerization, substrate binding and kinase activity. Secondary structure elements are indicated as: α helix - red rectangle , β strand - green arrow. The sequence identities of the catalytic domain of Wzc *E. coli* K12 with Wzc *E. coli* K30 is 58%, with Etk is 52%, with Ptk is 43%, with CapB is 29% and with MinD is 8%. Percent sequence identities were calculated using UCSF CHIMERA (Pettersen et al., 2004).

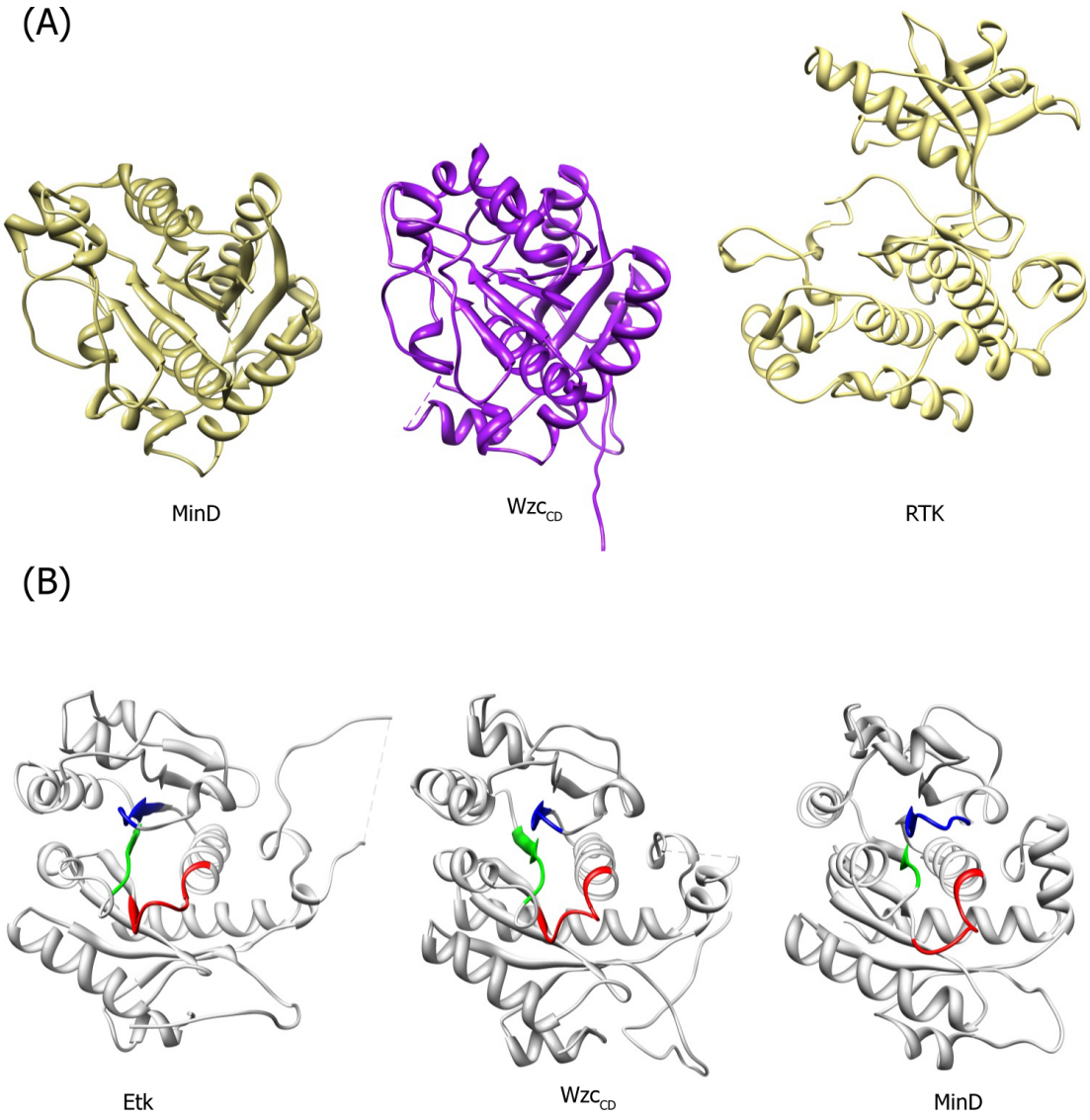

Figure 3: Structures of BY-kinases (A) MinD ATPase (dark khaki; PDB ID: 1G3R), BY-kinase Wzc_{CD} (purple, PDB ID: 3LA6) and human insulin receptor tyrosine kinase (RTK) (in khaki, PDB ID: 1IRK) are shown. The RMSD between Wzc_{CD} and MinD for 107 atom pairs is found to be 0.99 Å. (B) BY-kinases Etk (left; PDB ID: 3CIO) and MinD (right, PDB ID: 1G3R) and Wzc_{CD} (center, PDB ID: 3LA6) show high structural similarity. The Walker A (in red), Walker B (in green) and Walker A' (in blue) motifs are highlighted.

The phosphorylation state of the YC appears to play a major role in determining the oligomerization state of the kinase. Mutation of the Walker A Lys to Met inactivates Cap_{AB}(K55M) and Wzc_{CD}(K540M) resulting in unphosphorylated ring shape oligomers (Bechet et al., 2010; Olivares-Illana et al., 2008). This is in contrast to the monomeric structure of Etk for a fully-phosphorylated YC (Lee et al., 2008). Yet, the oligomeric state of BY-kinases is still controversial. A 3D-EM structure of Wzc_{CD} from *E. coli* K30 seems to show a tetramer (Collins et al., 2007) and the monomeric Etk crystal structure was successfully fitted into the tetrameric form (Lee et al., 2008). Whereas, crystal structures of dephosphorylated CapB from *S. aureus* and Wzc_{CD} from *E. coli* K12 form a ring-shaped octameric structure that dissociates to monomers upon phosphorylation (Doublet et al., 2002; Olivares-Illana et al., 2008). It was proposed that intermolecular autophosphorylation of the YC-cluster by adjacent kinase induces the dissociation of oligomer (Bechet et al., 2010). The oligomeric form is stabilized by the conserved EX_2RX_2R motif (Bechet et al., 2010; Olivares-Illana et al., 2008). The oligomerization of Wzc is described at length below (in Section 4.6.3).

Among the key regulatory elements in BY-kinases, the RK-cluster is important in nucleotide binding in proteobacteria, and its mutation in *E. coli* K12 Wzc diminishes autokinase activity and capsular polysaccharide synthesis (Bechet et al., 2010). Firmicutes do not contain an analogous RK-cluster. An internal tyrosine residue Tyr574 in Etk and Tyr569 in Wzc_{CD} is essential for nucleotide binding. This internal tyrosine was suggested to be phosphorylated in an intramolecular fashion, in a first of a two-stage YC-phosphorylation process, prior to facilitating the intermolecular autophosphorylation of the YC. The recent crystal structure of Wzc_{CD} seems to suggest that this scenario is highly unlikely since the presence of a phosphorylated Tyr569 would lead to drastic changes in the orientation of the loop housing the catalytic Asp564 leading to a conformation that would not be suitable for

catalysis. Therefore it appears that this residue plays a secondary yet crucial role in catalysis through its stabilizing hydrogen bonding interactions with the α-phosphate of the ADP (Bechet et al., 2010).

2.3. Protein Tyrosine Phosphatases (PTPs)

Protein tyrosine phosphatases (PTP) play an important role in signal transduction and cell cycle control by dephosphorylating their corresponding protein tyrosine kinases (Alonso et al., 2004). The first discovered PTP from human placenta, PTP1B (Tonks et al., 1988), with its characteristic CX_5RT/S motif (also called P-loop) opened a new avenue in research on protein phosphatases (Wang et al., 2003). Even though PTPs have very low sequence homology within themselves, these enzymes share the same conserved CX_5RT/S motif and perform almost identical hydrolysis of the phosphate group from their substrate (Wang et al., 2003).

The catalytic mechanism of dephosphorylation by PTP starts with the conserved cysteine residue in the P-loop, which serves as a catalytic nucleophile while the arginine in the same loop binds to the substrate (phosphotyrosine) moiety thus stabilizing the complex. The conserved serine/threonine residue in the P-loop stabilizes the transition state during the breakdown of the cysteine-phosphate intermediate of the substrate. Catalysis continues by closure of the WPD loop over the active site in PTPs. The aspartate residue in this loop acts as a general acid by donating a proton to the oxygen group of leaving substrate and as a general base, accepting a proton from the active site water (Figure 4) (Tabernero et al., 2008).

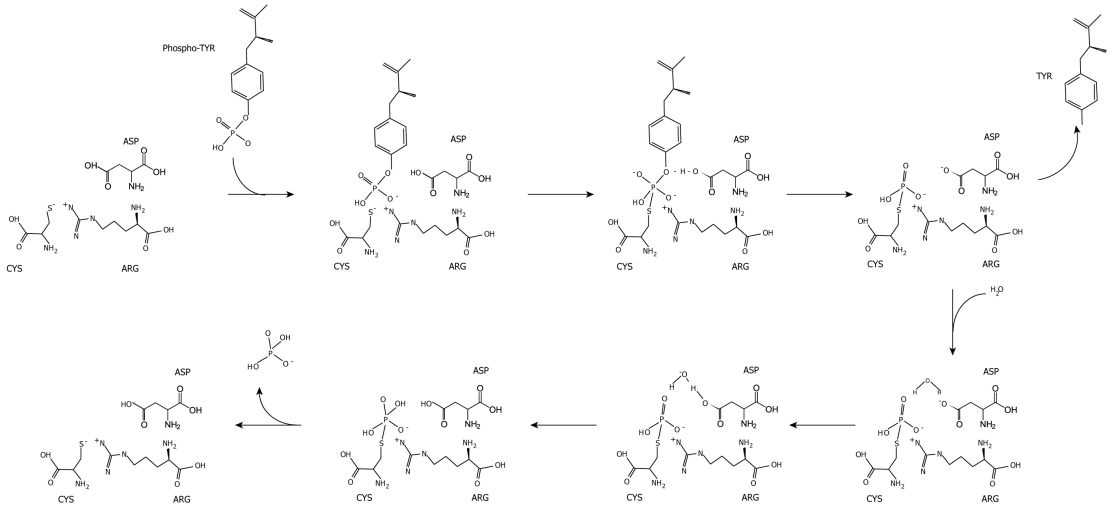

Figure 4: Catalytic mechanism of Cys based dephosphorylation in PTPs. The conserved CX_5RT/S motif plays a central in the dephosphorylation process where the Cys (nucleophile that forms a phospho intermediate). The conserved Asp residue in the WDP loop acts as a general acid and a general base.

2.3.1. Classification of Protein Tyrosine Phosphatases

So far 107 genes encoding protein tyrosine phosphatases have been found in the human genome (Alonso et al., 2004). They are divided into four categories according to their amino acid sequence of the catalytic domain:

(1) *The class I cysteine-based PTPs*: Based on their localization in the cell and their domain organization, class I Cys-based PTPs can be divided into two subfamilies, classical PTPs and dual-specificity phosphatases (Alonso et al., 2004). Classical PTPs are either non-receptor tyrosine phosphatases (NRTPs) that are present in the cytoplasm harboring only one catalytic PTPase domain or transmembrane receptor tyrosine phosphatases (RTPs) with putative extracellular ligand binding domain (Wang et al., 2003) containing one or two tandem catalytic domains (Schaapveld et al., 1997). Classical PTPs are specific to phosphotyrosines. Whereas, dual specificity phosphatases are more diverse structurally and functionally with their ability to target phosphoserine, phosphothreonine as well as

phosphotyrosine (Wang et al., 2003).

(2) *The class II cysteine-based PTPs*: They are smaller ~18 kDa cytoplasmic enzymes that are ubiquitous in eukaryotes and prokaryotes (Tabernero et al., 2008). They were previously identified as low molecular weight acid phosphatases because of their preference for acidic pH (Zhang and Van Etten, 1990). They were re-named as low molecular weight protein tyrosine phosphatases (LMW-PTPs) rather than non-specific acid phosphatase (Wang et al., 2003) since it was found that these enzymes are able to specifically dephosphorylate phosphotyrosines (Bottini et al., 2002). Except for the catalytic P-loop site which is present in the N-terminal region (in contrast to other PTPs sub-families where its located in the C-terminal region) and the DPYY-loop (similar to the WPD-loop) they do not have any sequence homology with class I PTPs (Wang et al., 2003). In prokaryotic cells, LMW-PTPs participate in extracellular polysaccharide synthesis and assembly on the cell surface in bacteria along with their cognate BY-kinases constituting the virulence factor in pathogenicity of the bacteria. This is discussed in greater detail in the following section.

It was shown that dephosphorylation mechanism by these ubiquitous enzymes is critical for cell signaling, differentiation and growth (Fiaschi et al., 2001; Hunter, 1995). Abnormal expression levels and functional aberration in LMW-PTPs may result in diverse diseases such as diabetes, obesity, allergy, asthma, rheumatoid arthritis, cardiomyopathy and Alzheimer's disease (Bottini et al., 2002). Hence, these LMW-PTPs have been considered as essential drug targets (Tabernero et al., 2008).

(3) *The class III cysteine-based PTPs*: These class of enzymes carry HCX_5R catalytic motif and they are known as Cdc25 phosphatases (Rudolph, 2007). Cdc25 phosphatases activate cyclin dependent kinases (Cdks) by dephosphorylating specific phosphotyrosine or phosphothreonine residues in their target proteins (Alonso et al., 2004). The activation of Cdks plays a crucial role in stages of cell division in eukaryotic cell cycle (Rudolph, 2007).

(4) *Aspartate based PTPs*: This class of phosphatases contains a DXDXT/V motif in the active site (Collet et al., 1998) and are able to dephosphorylate both phosphotyrosine and phosphoserine residues of their substrate kinases. Their dephosphorylation activity has been implicated in various developmental processes in Drosophila (Rayapureddi et al., 2003; Tootle et al., 2003) and in the salt stress response in yeast (Siniossoglou et al., 2000).

2.4. Prokaryotic Low Molecular Weight Protein-Tyrosine Phosphatases

Genes encoding the kinases and phosphatases pair in prokaryotes belong to the larger gene cluster related to synthesis and export of the exopolysaccharide or colanic acid in bacteria (Vincent et al., 2000). In Gram-negative bacteria, genes encoding the BY-kinases are located downstream of the gene encoding their corresponding protein tyrosine phosphatases. This positioning of the genes indicates the coordinative expression and production of these enzymes. In Gram-positive bacteria, BY-kinase expression depends on the successful production of two genes, which are next to each other. Their corresponding protein tyrosine phosphates genes are located either downstream or upstream of the set of BY-kinase genes depending upon the strain of the bacteria (Cozzone et al., 2004).

2.4.1. Structural Features of Low Molecular Weight Protein Tyrosine Phosphatases

In Gram-negative bacteria, most of the PTPs share majority of the conserved catalytic residues and are structurally homologous to with their eukaryotic Class II LMW-PTPs (Figure 5). Prokaryotic LMW-PTPs, like other protein tyrosine phosphatase superfamily members, contain the conserved CX_5RT/S P-loop active site (Ramponi and Stefani, 1997).

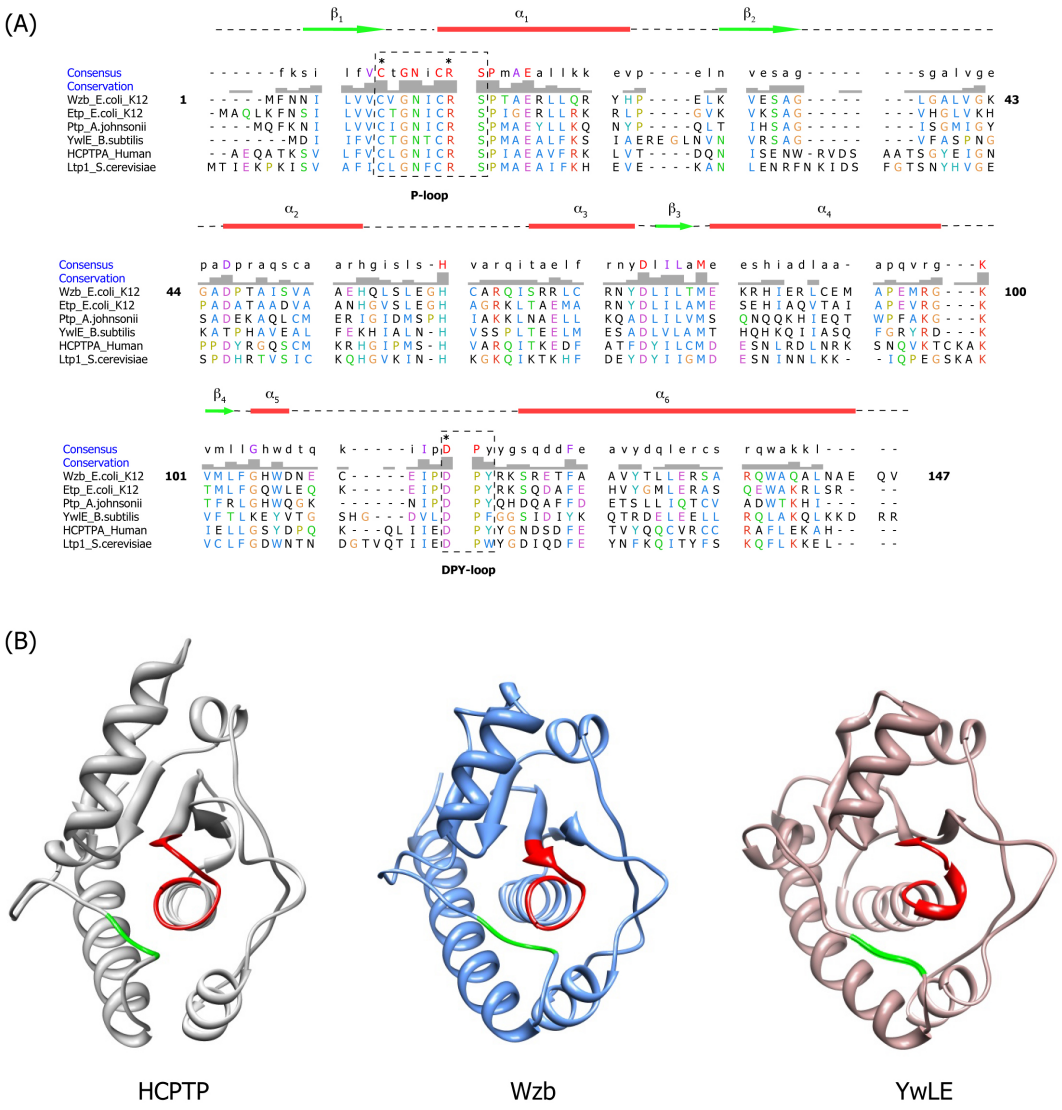

Figure 5: Sequence alignments and overall structural folds of LMW-PTPs. LMW-PTPs sequences: Wzb from *E. coli* K12, Etp from *E. coli* K12, Ptp from *A. johnsonii*, YwlE from *B. subtilis*, human HCPTPA and Ltp1 from *S. cerevisiae* are aligned by using ClustalW2. Secondary structure elements and catalytic motifs are indicated. Key catalytic residues are indicated by stars. Sequence identity between Wzb and other depicted LMW-PTPs calculated using UCSF CHIMERA are Etp 55%, Ptp 35%, YwlE 28%, HCPTPA 27%, and Ltp1 (BPTP) 25%. (B) The structures of human HCPTP (gray, PDB ID: 5PNT), *E. coli* K12 Wzb (blue, PDB ID: 2FEK) and YwlE from *B. subtilis* (brown, PDB ID: 1ZGG) are shown with the catalytic P-loop and DPY-loop highlighted in red and green respectively. These structures were aligned using UCSF CHIMERA. The RMSD between Wzb and HCPTPA and YwlE are 1.0 Å and 1.2 Å, respectively, over 107 atoms.

As shown in Figure 5 above, the overall structures of the LMW-PTPs in bacteria are highly similar to their eukaryotic counterparts (Lescop et al., 2006). However, there are significant differences seen around their catalytic side P-loop (Hagelueken et al., 2009; Lescop et al., 2006; Xu et al., 2006), which is explained in detail below.

The active site of all phosphatases in bacteria is fairly conserved with catalytic P-loop residues and the Asp residue in the WDP/DPYY-loop. The P-loop residues are responsible for binding the phosphate group of the phosphotyrosine substrate whereas the Asp in the WDP/DPYY-loop (Asp118 in LMW-PTP YwlE from *B. subtilis*, Asp115 in LMW-PTP Wzb from *E. coli* K12 strain and Asp129 in Human Cellular Protein Tyrosine Phosphatase A) is responsible for protonating the tyrosyl leaving group and acting as a nucleophile in the phosphorylated intermediate (Ramponi and Stefani, 1997; Xu et al., 2006). The conserved Arg residue in the P-loop along with the Asp residue in WDP/DPY-loop is essential for enzymatic activity in regards to recognition and positioning of the substrate in both prokaryotic and eukaryotic phosphatases (Lescop et al., 2006; Ramponi and Stefani, 1997). Substrate specific recognition in LMW-PTPs happens through stacking interactions between the phenyl ring of the phosphotyrosine substrate and the two other aromatic residues (e.g. the Trp49/Tyr131 pair in BPTP and HCPTPA; the Trp44/Tyr122 in *S. aureus* PtpA) (Ramponi and Stefani, 1997; Vega et al., 2011; Zhang et al., 1998). However, a recent NMR structure of *E. coli* K12 revealed that instead of these stacking interactions it is a hydrophobic residue (Leu40) that makes contact with the phenyl ring of the phosphotyrosine substrate. Absence of this stacking interaction appears to decrease substrate affinity (Lescop et al., 2006). However, the LMW-PTP YwlE from *B. subtilis* contains a Phe40/Phe120 pair located around the active site as seen in their eukaryotic counterparts, though Phe40 and Phe120 are not close enough to participate in stacking interactions with the aromatic ring of phosphotyrosine (Xu et al., 2006).

The cavity for the phosphotyrosine substrate is reasonably deep in all tyrosine specific PTPs, this likely explains the failure of these enzymes to hydrolyze the relatively shorter side chain phosphorylated serine and phosphorylated threonine (Lescop et al., 2006; Ramponi and Stefani, 1997). The edges of the active site cavity are surrounded by hydrophobic residues that likely interact with the aromatic ring of phosphotyrosine (Ramponi and Stefani, 1997; Zhang et al., 1998). A lack of conserved charged residues around the catalytic crevice suggests that prokaryotic LMW-PTPs do not require an electrostatic interaction between phosphotyrosine as in eukaryotic LMW-PTPs (Lescop et al., 2006).

Another type of PTP similar to the phosphoesterase domain of DNA polymerase and histindinol phosphatase (PHP) (Kim et al., 2011) was identified in Gram-positive bacteria. LMW-PTP and PHP-like PTPs show distinct differences in their sequences, structures and dephosphorylation mechanisms. PHP-like PTPs (e.g. CpsB from *Streptococcus pneumoniae*, YwqE from *Bacillus subtilis*), share neither sequence nor structural homology with LMW-PTPs (Hagelueken et al., 2009; Kim et al., 2011). Unlike LMW-PTP family, they do not require a catalytic Cys residue and/or P-loop. Their phosphatase activity is regulated by metal ions, specially manganese and this activity is highly dependent on pH (Mijakovic et al., 2005). High-resolution crystal structures of CpsB from *Stretococus pneumoniae*, YwqE from *Bacillus subtilis* indicate that the dephosphorylation of the phosphotyrosine takes place through two active site loops (loops I and II) where conserved phenylalanine and tyrosine residues as gatekeepers and switch the conformation of the enzyme between open and closed states (Kim et al., 2011).

2.5. Capsular Polysaccharides and Exopolysaccharides in *E. coli*

The serotypic categorization of *E. coli* depends on cell surface H, O and K antigens. H antigens are derived from flagellar proteins (Orskov, Orskov et al. 1977). O antigens are surface exposed bacterial lipopolysaccharides (LPS) (Guo et al., 2008) and participate in

outer membrane formation (Guo et al., 2008; Stevenson et al., 1996). They are seen in majority of serotypes of the bacteria (~170 different O-antigens) (Whitfield, 2006). LPS is not found to be absolutely necessary during the growth of the bacteria albeit important for its virulence (Guo et al., 2008).

K antigens are capsular polysaccharides, which are covalently attached to the cell surface (Guo et al., 2008). Capsular polysaccharides are classified into four different groups based on their biosynthesis and assembly system. Group 1 and 4 capsules are related to the LPS O-antigens. Group 1 capsules contain uranic acid repeat units whereas group 4 capsules contain different and more diverse sugar repeat-units (acetimido sugars). Group 1 and group 4 capsules are found in enteropathogenic, enterotoxigenic and enterohemorrahagic *E. coli* isolates, which cause intestinal infections (Whitfield, 2006). Group 2 and 3 capsules also contain more diverse sugar repeat units. This type of capsule formation causes extraintestinal infection (Whitfield, 2006). The non-serotype specific mucoid antigen (M antigen) production is also seen in enterobacteria. M antigen, the exopolysaccharide colanic acid, is capsular wall antigen and released onto the cell surface under specific growth conditions (Orskov et al., 1977).

Gram-negative bacteria synthesize two different polysaccharides, capsular polysaccharides (CPS) and exopolysaccharides (EPS). These polysaccharides are either attached to or released onto the cell surface (CPS and EPS, respectively) or participate in outer membrane formation (LPS).

CPS and EPS are essential for bacterial virulence and survival under environmental stress since they participate in capsule formation (Stevenson et al., 1996), a process regulated by the autophosphorylation of BY-kinases and their subsequent dephosphorylation by LMW-PTPs (Grangeasse et al., 2007; Vincent et al., 2000). For example, in *E. coli* two specific BY-

kinase/LMWPTP pairs exist and participate in physiologically distinct processes. The Wzc/Wzb pair the Etk/Etp pair is central to the synthesis of Group 4 CPS.

Colanic acid, an exopolysaccharide, is released onto the bacterial cell surface and makes a layer of mucous that envelopes the bacterial cell surface (Cozzone, 2005). This layer protects the bacterial cell from desiccation and environmental stress, facilitates adhesion for colonization and biofilm formation. Formation of capsules, on the other hand is often central to the virulence of pathogenic species. A poor antibody response to the capsule, ensures prevention of phagocytosis and macrophagy (Collins et al., 2006; Cozzone, 2005; Reid and Whitfield, 2005; Roberts, 1996).

Other examples of tyrosine kinase/phosphatase pairs in bacteria include the AmsA/AmsI (BY-kinase/LMW-PTP) pair that takes part in the production of acidic exopolysaccharide, amylovoran, in *Erwinia amylovoran*. Similarly, YwqD(+YwqC)/YwqE (BY-kinase/ polymerase and histindinol (PHP) like phosphatase) is responsible for synthesis of exopolysaccharide in *Bacillus subtilis* (Cozzone et al., 2004).

2.6. Involvement of a BY-kinase/LMW-PTP Pair in *E. coli* K12 Exopolysaccharide Biosynthesis

In the work presented here we focus on the interactions between the BY-kinase Wzc and its corresponding LMW-PTP Wzb from *E. coli* K12. This BY-kinase/LMW-PTP pair and their interactions are representative of similar kinase/phosphatase pairs in both gram-positive and gram-negative species as elaborated above. Thus the Wzc/Wzb pair provides an ideal model system to determine the structural and mechanistic details of the regulation of a bacterial tyrosine kinase by its cognate phosphatase and their influence on exopolysaccharide production (or capsular polysaccharide) and export (or capsular assembly).

Colanic acid production in *E. coli* K12 occurs through a Wzy-dependent (a polysaccharide polymerase) polymerization and export of the assembled polymers to the

plasma membrane (Guo et al., 2008; Obadia et al., 2007). EPS synthesis and export is controlled by a multi-enzyme machine that spans across both inner and outer membranes, and includes a BY-kinase that is regulated by a cytosolic LMW-PTP (Obadia et al., 2007; Wugeditsch et al., 2001). The current model proposes that the biosynthesis of the antigen repeat units is initiated by the glycosyltransferase WecA (WbaP in *E. coli* K30) (Nesper et al., 2003) that belongs to the polyisoprenyl-phosphate N-acetylhexosamine-1-phosphate transferase (PNTP) family that acts at the cytosolic face of the membrane. WecA catalyzes the concerted addition of sugar phosphate units to a polyisoprenoid lipid derivative, undecaprenyl phosphate (*und-P*) to assemble *und-PP*-linked sugar (Guo et al., 2008; Valvano, 2003; Whitfield, 2006). The flippase Wzx assists the transfer of *und-PP*-linked repeat units across the inner membrane (Nesper et al., 2003; Valvano, 2003). The polymerization and elongation of high molecular weight *und-PP*-linked units at the periplasmic face of the inner membrane is facilitated by another integral membrane protein, Wzy (Valvano, 2003). The formation and translocation of the lipid-linked units requires four additional conserved proteins, three of them located in the membrane and one in the cytoplasm (Nesper et al., 2003). High-level polymerization of the *und-PP*-linked repeats requires cyclic autophosphorylation and dephosphorylation (by its cognate phosphatase Wzb) of the C-terminal tyrosine rich tail of the BY-kinase Wzc (Whitfield, 2006). Next, the synthesized polymer is translocated to a periplasm-spanning ring formed by octameric Wza that serves as an export channel (Collins et al., 2007; Nesper et al., 2003). According to the recent electron microscopy (EM) structure of the complex, the periplasmic domain of Wza appears to be in contact with the periplasmic domain of Wzc. This interaction was hypothesized as a trigger for the opening of the central cavity of the periplasmic part of Wza therefore leading to an efficient mechanism of export of the polysaccharides through the inner membrane, periplasm and outer membrane (Collins et al., 2007). In group 1 capsules,

Wzi, a monomeric β-barrel outer membrane protein (Nesper et al., 2003) is involved in modulating the saccharide polymer attachment to the cell surface (Whitfield, 2006). It was found that Wzi is not essential for polymerization and export of the polysaccharide chains however; absence of the Wzi protein fails to produce the coherent structure of the capsule (Nesper et al., 2003) (Figure 6).

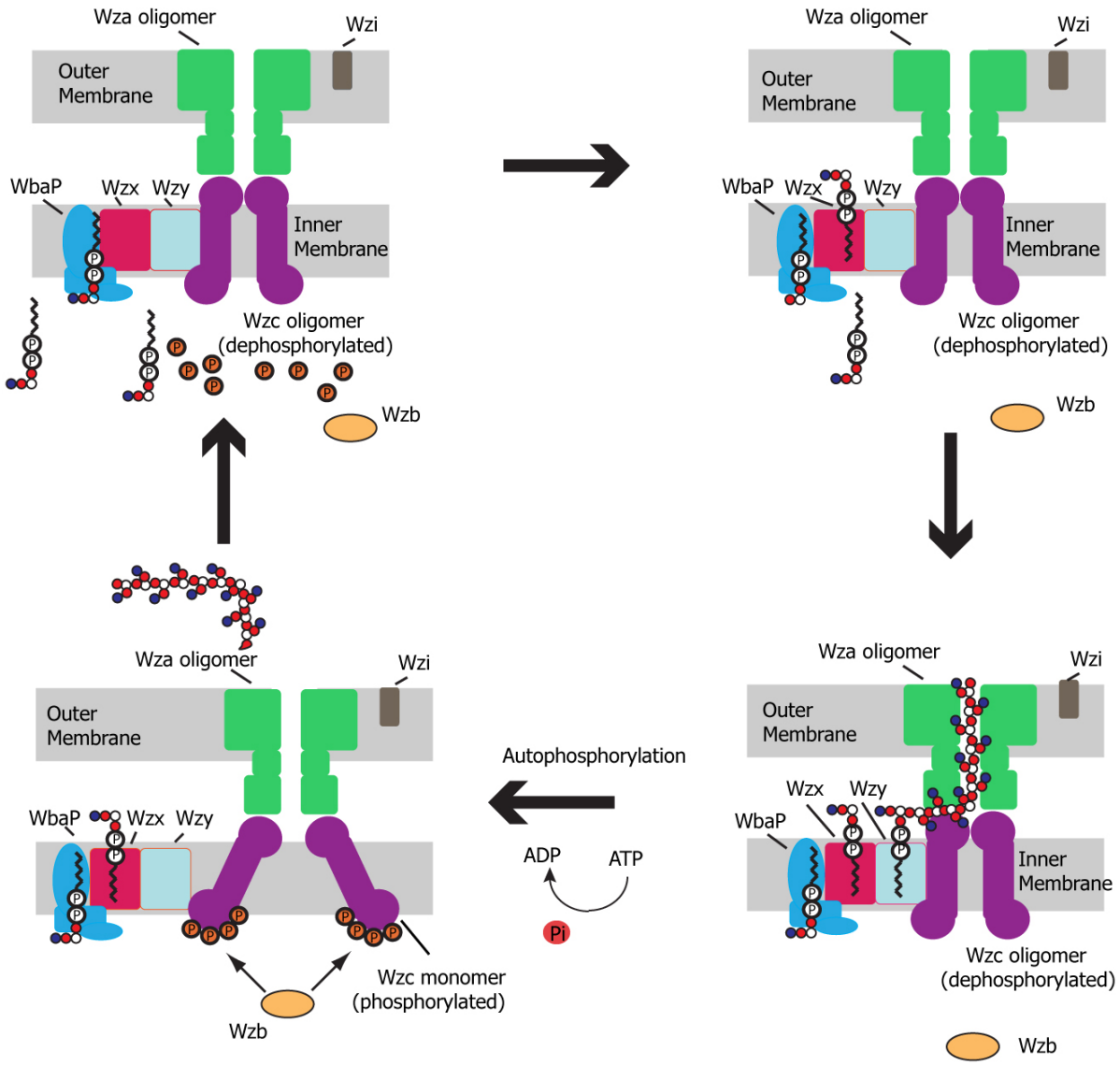

Figure 6: Polysaccharide synthesis and transport in *E. coli* K12. Proposed Wzy dependent colanic acid polymerization and export pathway. This pathway harbors multi enzyme membrane bound machinery and cytoplasmic protein.

It is clear that Wzc BY-kinase and the LMW-PTP Wzb play a crucial role in synthesis and export of the polysaccharide chain. Wzc that does not show any phosphorylation activity on any non-tyrosine can be successfully dephosphorylated by Wzb *in vitro* (Vincent et al., 1999). The catalytic domain (CD) of Wzc (Wzc_{CD}, Ser447-Ala704) does not need the TAD (see section 2.2.1) to undergo phosphorylation of the YC-cluster (Vincent et al., 2000). It has been shown that five of the six tyrosine residues (Tyr708, Tyr710, Tyr711, Tyr 713 and Tyr715) in the YC of Wzc_{CD} are phosphorylated through an intermolecular process (Doublet et al., 2002) although it is unclear whether the phosphorylation of these residues happens simultaneously or sequentially (Grangeasse et al., 2002). It has been shown that dephosphorylation of YC-cluster phosphotyrosine residues by Wzb activates and regulates the colanic acid synthesis (Vincent et al., 2000).

As mention earlier (in section 2.2.1), *in vivo* studies have shown that Wzc can oligomerize and that the catalytic domain is necessary and sufficient for this oligomerization (Doublet et al., 2002). However, as mentioned earlier, the oligomeric state of the BY-kinases had not been clear since it was shown that CapB from *S. aureus* forms an octamer *in crystallo* in the dephosphorylated state (Olivares-Illana et al., 2008) while Wzc (from *E. coli.* K30) appears to be tetrameric in the cryo-EM structure (Collins et al., 2007). In addition, Lee *et. al.* were able to fit the monomeric Etk kinase domain into the EM density and they found that tetrameric form of Etk kinase gave them a best fit. The latest studies suggest that $\mathbf{Wzc_{CD}}$ is octameric in the fully dephosphorylated state and monomeric in the fully phosphorylated state (Bechet et al., 2010).

Based on the inter-monomer interface seen in the crystal structure, the oligomerization interface involves the αA helix (Ser455-Glu461), the βA strand (Val466-Pro471), and the α2 helix (Asp504-Gln525) in addition to the YC. The α2 helix possesses the previously mentioned EX_2RX_2R (Glu508-Arg514) motif where Glu508, Arg511 and

Arg514 make salt bridges with Arg566 and Glu618 of an adjacent protomer (Figure 7) (Bechet et al., 2010). A Glu508Ala/Arg511Ala/Arg514Ala triple-mutant was largely monomeric *in vitro* and severely compromised in its ability to produce colanic acid *in vivo* (Bechet et al., 2010; Olivares-Illana et al., 2008). Thus, it was concluded that the EX_2RX_2R motif was crucial for oligomerization and subsequently colanic acid production (Bechet et al., 2010).

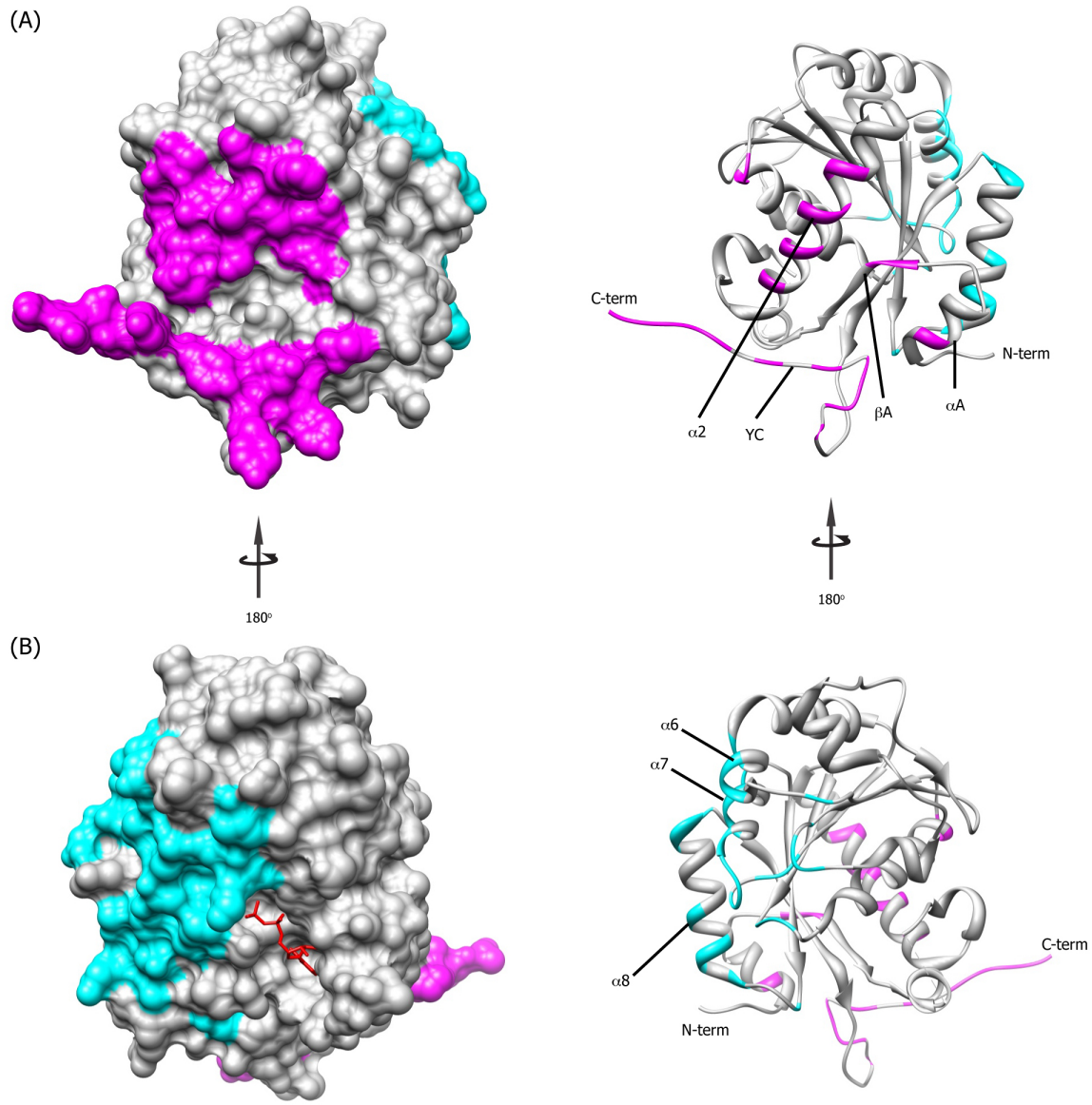

Figure 7: The oligomerization interface of Wzc_{CD}. (A) Oligomerization of Wzc_{CD} mainly involves the αA helix, the βA strand, the α2 helix and the YC (in cyan). (B) Contact occurs with α6, α7 and α8 (in magenta) of a neighboring residue. A bound ADP molecule is shown in red. Contacts between each protomer were found by UCSF CHIMERA using default contact parameters and a Van Der Waals overlap, ($overlap_{ij}$)≥ -0.4 Å and 0.0 Å allowance.

In *E. coli* K12, *wzc* and *wzb* are in an operon within the colanic acid cluster *cps* (Vincent et al., 1999; Whitfield, 2006). There have been several biochemical studies which demostrates that Wzb dephosphorylates YC-phosphorylated Wzc. Thus the cycling between oligomeric forms of dephosphorylated Wzc and monomeric phosphorylated Wzc, a process regulated by Wzb, appears to be central to the biosynthesis and transport of exopolysaccharide colanic acid and capsular polysaccharides, which constitute virulence, factor in bacterial pathogens (Ilan et al., 1999; Obadia et al., 2007; Vincent et al., 1999; Vincent et al., 2000; Wugeditsch et al., 2001). However, the crucial information that is lacking is the nature of interactions between Wzb and Wzc that regulate the phosphorylation-dependent oligomerization state of the latter. Thus this work aims to elucidate the interaction of Wzc and Wzb from *E.coli* K12 strain. This information will be the first step in developing a comprehensive mechanistic model for the regulation of BY-kinase activity by LMW-PTPs in bacteria.

2.7. Nuclear Magnetic Resonance (NMR) Spectroscopy

We use solution state NMR techniques as the principal biophysical tool to study these the interactions between Wzc_{CD} and Wzb. The utility of solution NMR techniques to study the structure and dynamics of proteins has been the subject of numerous books and reviews e.g. Cavanagh et. al. (Cavanagh et al., 2007) and we will not repeat them here. Additionally, the unique sensitive of NMR spectral parameters such as chemical shifts to variations in the chemical environments of nuclei that give rise to them, provides highly sensitive, residue-specific probes to study the formation of complexes, even weak or transient ones (Zuiderweg, 2002). The availability of higher fields, advances in probe technology (Flynn et al., 2000; Styles et al., 1989) and most notably the development of transverse relaxation optimized spectroscopy (TROSY) based techniques and related approaches (Pervushin et al., 1997; Riek et al., 2000; Salzmann et al., 1998; Salzmann et al., 1999) have allowed the study of

large proteins and protein complexes. We take advantage of all these innovations to probe the interactions between Wzc_{CD} and Wzb as described below.

3. Materials and Methods

3.1. Expression and Purification of the Catalytic Domain of Wzc and Full-length Wzb

pQE30 plasmids containing the cytoplasmic fragment of Wzc_{CD} and a construct thereof with the YC-cluster truncated ($Wzc_{CD\Delta C}$), were generous gifts from Dr. Christophe Grangeasse from the Institute of Biology and Chemistry of Proteins, University of Lyon. Initial attempts based on the published protocol (Grangeasse et al., 2002) failed to yield sufficient levels of expression to obtain soluble protein purified to homogeneity necessary for NMR studies. Therefore, Wzc_{CD} and $Wzc_{CD\Delta C}$ were sub-cloned into the pET15b vector system (*Novagen*) between the NdeI and BamHI restriction sites using commercially synthesized primers (*Integrated DNA Technologies*, see Table 1). The pET15b vector was chosen mainly to attain high yields and ease in due to the presence of a cleavable N-terminal His_6-tag.

Similarly, a plasmid encoding Wzb was constructed by amplification of MC4100 *E. coli* K12 cDNA using the primers described in Table 1, and subcloned in to the pET15b vector system between NdeI and BamHI restriction sites.

Plasmid	Primer	5′ to 3′ Sequence	Molecular Weight
Wzc_{CD}	Upstream	AGCTACATATGTCGTTGTTTA ATCGCGGCATTG	32.477 kDa
	Downstream	CCTAGTGGATCCTTATTTCGCA TCCGACTTAT	
$Wzc_{CD\Delta C}$	Upstream	ACTGGCCATATGTCGTTGTTTA ATCGCGCTGGCGCGG	30.413 kDa
	Downstream	ATTATAGGATCCTTACGCGCTG GCGCGG	
Wzb	Upstream	GGG AGG GCA TAT GTT TAA CAA CAT CTT AGT TGT CTG TG	18.872 kDa
	Downstream	AGG AAA TGG ATC CTT ATA CCT GCT CTG CGT TCA AT	

Table 1: Primers used in this study.

After confirmation of the sequences of Wzc_{CD}, $Wzc_{CD\Delta C}$ and Wzb (*Genewiz*) sub-cloned into pET15b vectors, these plasmids were transformed into *E. coli* host strain BL21(DE3) (*Invitrogen*) competent cells. Competent cells were then plated onto ampicillin agar plates and incubated at 37°C for overnight. A single colony was picked and grown in 20 mL of M9 minimal media prepared in 100% H_2O or rich media. Cells were adapted for growth in gradually increasing concentrations of D_2O (10%, 30%, 50%, 75%, 90% and 100%) in 20 mL of M9 media. Finally, cells were inoculated in 20 mL of M9-(100% D_2O) media and grown overnight. This overnight culture was transferred into 1L of M9-(100% D_2O) media containing 1 g of ^{15}N-labeled ammonium chloride (*Cambridge Isotope Laboratories, Inc.*) and 2 g of ^{13}C, ^{2}H- or ^{13}C, ^{1}H- labeled glucose (*Cambridge Isotope Laboratories, Inc.*) as sole nitrogen and carbon sources to obtain either uniformly ^{2}H- or fractionally ^{2}H-labeled samples, respectively (Shekhtman et al., 2002). The cells were grown at 37°C and induced by adding 1mM isopropyl β-D-1-thiogalactopyranoside (IPTG) when the optical density reached the mid-log phase for cell growth. After induction, the cells were grown for 20 hours at 16°C and harvested by centrifugation. In some cases for uniform ^{15}N and fractional ^{2}H labeling, cells were harvested after they reached the mid-log phase by centrifugation at low speed (~4000 rpm) at room temperature. The cell pellet was washed with phosphate buffered-saline (PBS) and re-suspended in an M9-(100%D_2O) media supplemented with ^{15}N ammonium chloride and ^{13}C, ^{1}H-labeled glucose, induced with 1mM IPTG and grown for overnight at 16°C.

The purifications steps mentioned hereafter were performed at 4°C. Cell pellets were suspended in 40 mL lysis buffer (50 mM Phosphate Buffer pH 8.0, 300 mM NaCl, 10% Glycerol, 10 mM β-mercaptoethanol, 10 mM Imidazole and EDTA-free protease inhibitor tablet (*Complete Mini, Roche*). The cells were lysed by sonication and cell debris was removed by centrifugation at 16000 rpm for 45 minutes. The soluble lysate was added to a

pre-equilibrated (with lysis buffer) Ni-NTA affinity column (*Qiagen*), and after an incubation period of 1 hour, the column was washed extensively with lysis buffer and with washing buffer (50 mM Phosphate Buffer pH 8.0, 300 mM NaCl, 10% Glycerol, 10 mM β-mercaptoethanol and 20 mM Imidazole). The protein was eluted with 20mL of elution buffer (50 mM Phosphate Buffer pH 8.0, 300 mM NaCl, 10% Glycerol, 10 mM β-mercaptoethanol and 150 mM Imidazole). The eluted protein was incubated with 1 mM ATP and 1 mM $MgCl_2$ for every 40 μM protein at 4°C for overnight. The eluate was concentrated and purified further by gel filtration chromatography using a Superdex 75 10/300 GL (*GE Health Care*) column, equilibrated with NMR buffer (50 mM Phosphate buffer pH 6.0, 50 mM NaCl, 25 mM DTT, 5 mM EDTA) with 10 mM $MgCl_2$. All fractions containing pure $Wzc_{CD\Delta C}$ (or Wzc_{CD}) were collected and further incubated with ATP overnight at 4°C. NMR samples typically contained 100-300 μM $Wzc_{CD\Delta C}$ (or Wzc_{CD}).

Wzb was grown from freshly transformed *E. coli* BL21(DE3) cells. Uniformly protonated or uniformly ^{2}H-labeled (in addition to uniform ^{15}N or ^{13}C-^{15}N) Wzb samples were prepared as described above for the Wzc constructs using cells grown in M9 media prepared either in 100% H_2O or 100% D_2O. The ATP incubation step described above was omitted. Wzb concentration in NMR samples varied from 100-250 μM.

3.2. NMR Spectroscopy

All NMR experiments were recorded at 25°C using Bruker Avance spectrometers operating at ^{1}H frequencies of 600, 700, 800 or 900 MHz, or on a Varian Innova spectrometer operating at a ^{1}H frequency of 600 MHz. All spectrometers were equipped with cryogenic probes capable of applying pulse-field gradients along the z-axis. Data were processed using NMRPipe, visualized using NMRDraw (Delaglio et al., 1995) and analyzed using the NMRViewJ (Johnson, 2004) software suite.

3.2.1. Backbone Resonance Assignments of $Wzc_{CD\Delta C}$ and Wzb

Sequential assignment of the backbone resonances of $Wzc_{CD\Delta C}$ was performed using 300 μM samples of uniformly ^{15}N, ^{13}C, ^{2}H-labeled utilizing data collected at 800 MHz and 25º C. The following TROSY-based experiments were used - a HNCO/HN(CA)CO pair (512, 32 and 40 complex points with sweep-widths of 13.35, 30 and 13 ppm in ^{1}H, ^{15}N and ^{13}C dimensions respectively), a HNCA/HN(CO)CA pair (512, 32 and 50/40 complex points with sweep-widths of 13.35, 30 and 30 ppm in the ^{1}H, ^{15}N and ^{13}C dimensions respectively), and a HNCACB/HN(CO)CACB pair (512, 32 and 40/42 complex points with sweep widths of 13.35, 30 and 65 ppm in ^{1}H, ^{15}N and ^{13}C dimensions respectively) (Salzmann et al., 1998).

Backbone resonance assignment for Wzb was carried out using 250 μM uniformly ^{15}N-^{13}C labeled samples utilizing data collected at 700 MHz and 25º C. Non-uniformly sampled versions of the following experiments were used - HNCO/HN(CA)CO (512, 32 and 50 complex points with sweep widths of 13, 32 and 13 ppm in ^{1}H, ^{15}N and ^{13}C dimensions respectively), HNCACB/CACB(CO)NH (512, 32 and 50 complex points with sweep widths of 13, 32, 65 ppm in ^{1}H, ^{15}N and ^{13}C dimensions respectively) and HNCA/HN(CO)CA (512, 32, 50 complex points with sweep widths of 10, 32 and 30 ppm in ^{1}H, ^{15}N and ^{13}C dimensions respectively) were collected. A 30% sampling schedule generated by the *sparse.py* script (Lemak et al., 2011) was utilized. Datasets were reconstructed using MDDGui software (Orekhov and Jaravine, 2011) and processed using NMRPipe, visualized by NMRDraw and analyzed using NMRViewJ.

3.2.2. ^{15}N Relaxation Measurements on Wzc_{CD}, $Wzc_{CD\Delta C}$ and Wzb

Spin-lattice and spin-spin relaxation are both exponential decay functions. These relaxations and their relation with relaxation time can be defined by Equation 1 and Equation 2:

$$I = I_0 e^{-Rt} \tag{1}$$

$$T = \frac{1}{R} \tag{2}$$

where I_t is intensity of the particular resonance after a delay t, I_0 is the peak intensity at time 0, R represents either R_1 or R_2 and T (relaxation time) stands for either T_1 or T_2 delay (Morin, 2011; Natarajan et al., 2006).

Steady-state heteronuclear NOE, also known as $\{^1H\}$-^{15}N NOE, gives information about resonance intensity changes due to the cross-relaxation from neighboring spin dipoles i.e. ^1H and ^{15}N. The collection of $\{^1H\}$-^{15}N NOE data requires two different spectra - one with "with proton saturation" and the other "without proton saturation". The NOE measurements (Morin, 2011) and the error in NOE (σ_{NOE}) (Johnson, 2004) are determined by the following equations:

$$NOE = \frac{I_{sat}}{I_{unsat}} \tag{3}$$

$$\sigma_{NOE} = \frac{\sigma_{unsat}}{I_{unsat}} \tag{4}$$

Combining these relaxation experiments, it is possible to measure the motion of resonances in both the fast and slow time scales.

A complete set of R_1 and R_2 measurements were performed using standard pulse sequences (Palmer, 2001) as described previously. $\{^1H\}$-^{15}N NOE data was collected using an improved pulse sequences described recently (Ferrage et al., 2009; Ferrage et al., 2008).

TROSY based backbone relaxation experiments (R_1, R_2 and NOE) were recorded at 900 MHz spectrometer using 300 μM uniformly ^{15}N, ^2H-labeled $Wzc_{CD\Delta C}$ sample at 25°C. An additional set of R_2 values were obtained at 800 MHz (25°C) for the same sample. Relaxation

measurements with 2 s recycle delay were collected with the following relaxation delays R_1: 10, 200, 400, 600, 800, 1000, 1400 and 1800 ms; R_2: 0, 16.32, 32.64, 48.96, 65.28 and 81.60 ms. Steady state $\{^1H\}$-^{15}N NOE values were obtained by recording two spectra with and without proton saturation for 7 s.

A uniformly ^{15}N-labeled, 250 μM sample of Wzb was used for backbone relaxation experiments collected on a 600 MHz spectrometer at 25°C. The $\{^1H\}$-^{15}N NOE values were measured using experiment with and without 8 s of proton saturation. Experiments to measure R_1 and R_2 values were recorded with 1.5 s recycle delays using the following relaxation delays: 10(X2), 50, 100, 200, 400, 600, 800, 1000 ms (R_1) and 0, 16.32, 32.64, 65.28, 130.56, 163.2, 195.6 ms (R_2).

In order to further probe the dynamic and hydrodynamic properties of the protein complexes involving Wzb and either Wzc_{CD} or $Wzc_{CD\Delta C}$, TROSY based transverse relaxation (R_2) experiments were recorded on the complexes at 800 MHz and 25°C. R_2 values were measured for the following samples: (1) A sample containing equimolar (100μM) amounts of uniformly ^{15}N, ^2H-labeled $Wzc_{CD\Delta C}$ and uniformly ^2H-labeled Wzb using the following relaxation delays: 0, 16.32, 32.64, 48.96 and 65.28 ms and a 2 recycle delay; (2) a sample containing equimolar (100 μM) amounts of uniformly ^{15}N, ^2H-labeled Wzc_{CD} and uniformly ^2H-labeled Wzb using the following relaxation delays: 0, 16.32 (X2), 32.64, 48.96 and 65.28 ms with a 2 s recycle delay; (3) a sample containing equimolar amounts (100 μM) of uniformly ^{15}N, ^2H-labeled Wzb and uniformly ^2H-labeled $Wzc_{CD\Delta C}$ with the following relaxation delays 16.32, 32.64, 48.96, 65.28, 97.92, 130.56, 163.2 ms and 16.32, 32.64, 48.9, 65.28, 81.6 ms respectively and a 1.5 s recycle delay; and (4) a sample containing equimolar amounts (100 μM) of uniformly ^{15}N, ^2H-labeled Wzb and uniformly ^2H-labeled Wzc_{CD} with the following relaxation delays 16.32, 32.64, 48.96, 65.28, 97.92, 130.56, 163.2 ms and 16.32, 32.64, 48.9, 65.28, 81.6 ms respectively with a 1.5 s recycle delay.

3.2.3. Methods for the MD/HYDRONMR calculations

The flexible C-terminal tail of the protein has been described by an ensemble of disordered conformations generated by a high temperature molecular dynamic *in vacuo*. Starting from the experimental crystal structure (3LA6), the amino acids whose electron density was missing were introduced using MODELLER (Sali et al., 1995). This starting conformation was energy minimized in the gromos53a5 force field using conjugate gradient algorithm with a tolerance of 1000 kJ mol^{-1} nm^{-1}. Then 200 ns of molecular dynamic simulation were performed in the absence of solvent, periodic boundary conditions and pressure coupling using GROMACS (Hess et al., 2008). Electrostatic interactions were suppressed by imposing an infinite dielectric constant. Velocities were integrated every 0.1 femto seconds, holonomic constraints were applied using the LINCS method (Hess et al., 1997) and the protein was coupled to a 4000 K bath using velocity rescaling with a stochastic term (Bussi et al., 2007) . The correct folding of the Wzc structured domain was maintained imposing a large number (~ 38000) of distance restraints with a force constant of 1000 kJ mol^{-1} nm^{-2}. Snapshots from the MD were extracted every 2.5 ps, and 71 of them were used as input for a HYDRONMR (Garcia de la Torre et al., 2000) calculations performed at 298.15 K and assuming a viscosity of 9.11 millipoises. The radius of the spheres replacing the non-hydrogen atoms for the primary hydrodynamic model was fixed to 3.2 Å, while the range for the mini-beads radii used for extrapolating the shell model was optimized automatically. The position of the amide hydrogens was recalculated automatically assuming a 1.02 Å distance from the nitrogen, and the relaxation values were calculated at 18.8 teslas (800 MHz).

3.2.4. Determination of Wzc_{CD}/$Wzc_{CD\Delta C}$ and Wzb Interactions by NMR Chemical Shift Titration Analysis

In order to define the surfaces on Wzc_{CD} and Wzb that take part in their mutual interactions, we measured chemical shift perturbations for each in the presence of the other. 100 μM uniformly ^{15}N, ^{2}H-labeled Wzc_{CD} or 100 μM uniformly ^{15}N, ^{2}H-labeled $Wzc_{CD\Delta C}$ were separately titrated with uniformly ^{2}H-labeled Wzb at the following concentrations of 25, 50, 75,100 and 200 μM, with TROSY spectra being acquired at each titration point. Similarly, 100 μM uniformly ^{15}N, ^{2}H-labeled Wzb was titrated with either uniformly ^{2}H-labeled $Wzc_{CD\Delta C}$ or uniformly ^{2}H-labeled Wzc_{CD} at the following concentrations - 25 μM, 50 μM, 75 μM and 100 μM and TROSY spectra were recorded at each titration point. All spectra were acquired at 900 MHz and 25°C using sweep widths of 13.35 ppm (512 complex points), 30 ppm (128 complex points) in the ^{1}H and ^{15}N dimensions respectively. Recycle delays of 1.5 s were used and 16 transients were collected per t_1 point.

4. Results and Discussion

4.1. Expression, Purification and Characterization of Wzc_{CD}, $Wzc_{CD\Delta C}$ and Wzb

Two different fragments of the Wzc catalytic domain and full-length Wzb and were purified as described in the previous section and utilized for the biochemical and NMR studies. Relatively high expression levels were achieved for all the proteins. All three proteins were eluted as a single monomeric species from the Superdex 75 10/300 GL (Figure 8) and the purity of proteins were checked by 15% sodium dodecyl sulfate polycrylamide gel electrophoresis (SDS-PAGE) (Figure 9) and mass spectroscopy.

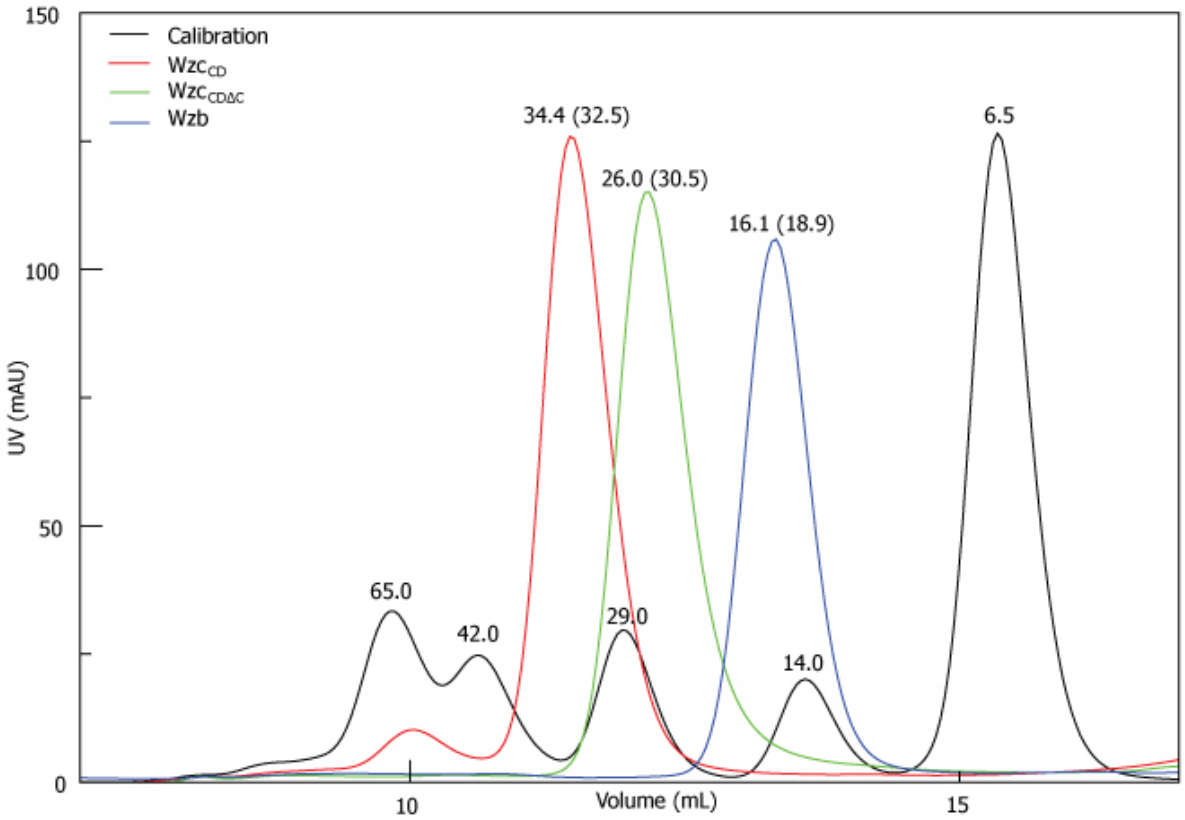

Figure 8: Gel filtration profiles of Wzc$_{CD}$, Wzc$_{CDΔC}$ and Wzb. Gel filtration profiles of Wzc$_{CD}$ (red), Wzc$_{CDΔC}$ (green) and Wzb (blue) using calibrated Superdex 75 column. Molecular weights in kDa are calculated using calibration curve and the corresponding expected molecular weights (in parentheses) are shown.

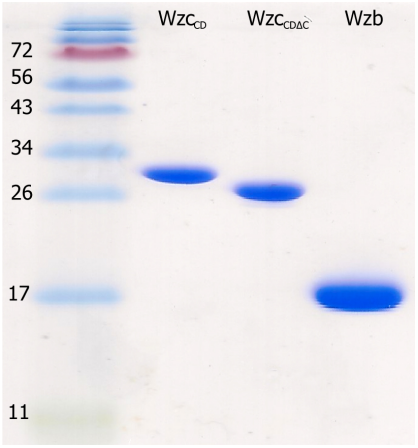

Figure 9: The relevant proteins can be purified to homogeneity. 15% SDS-PAGE gel shows the purity of Wzc$_{CD}$, Wzc$_{CDΔC}$ and Wzb after gel filtration chromatography. All constructs contain N-terminal sequence that includes a His$_6$-tag (Wzc$_{CD}$ and Wzc$_{CDΔC}$ have 21 residues and Wzb has 20 N-terminal His$_6$-tag residues).

4.2. Backbone Resonance Assignments for $Wzc_{CD\Delta C}$

$Wzc_{CD\Delta C}$ is more stable in solution at high concentrations over longer periods of time compared with Wzc_{CD}, and hence we felt that the entire slew of triple resonance experiments could be performed using fewer samples of the former construct making the entire process more economical in terms of labeling supplies. Hence we chose to assign $Wzc_{CD\Delta C}$ first instead of Wzc_{CD}. The ^{15}N, ^{1}H TROSY spectrum of $Wzc_{CD\Delta C}$ displayed excellent dispersion with resonances that had uniform lineshapes (Figure 10). This is in contrast to the complications that arise from the disordered YC in the spectra of Wzc_{CD} as described below.

The backbone assignments of $Wzc_{CD\Delta C}$ were obtained by using TROSY based triple resonance experiments described previously and by using RunAbout semi-automated assignment module in NMRViewJ analysis software (Johnson, 2004). $Wzc_{CD\Delta C}$ (Ser447-Ala704) contains 258 residues including 13 prolines. A total of 231 out of 245 expected amide ^{1}H and ^{15}N resonances were seen/resolved in TROSY spectrum (800 MHz). Of these 72% (177 out of 245) were assigned and peaks that correspond to unassigned residues are plotted on to surface of crystal structure of Wzc (access code 3LA6) (Figure 11). 65.1% (168 out of 258) of C', 75.6% (195 out of 258) of C^{α} and 70.7% (171 out of 242) of C^{β} were assigned. We were able to partially assign the resonances from Walker A (33.3%), Walker A' (50.0%) and RK cluster (50%). However, the resonances corresponding to Walker B motif could not be assigned unambiguously. The missing assignments are likely due to (1) broadening of the peaks due to conformational exchange or (2) the extensive spectral overlap seen for a protein of this size. Although, some of those unassigned peaks in TROSY spectra have resolved peaks in 3D HNCO, they were absent from the other the complementary experiments required to do sequential backbone assignments. Moreover, 8 out of 21 residues in N-terminal tail including His_6-tag, which is likely disordered, were identified in the

spectrum. Thrombin cleavage of the His_6-tag reduced the long-term stability of the protein and hence we did not remove the tag for our NMR studies.

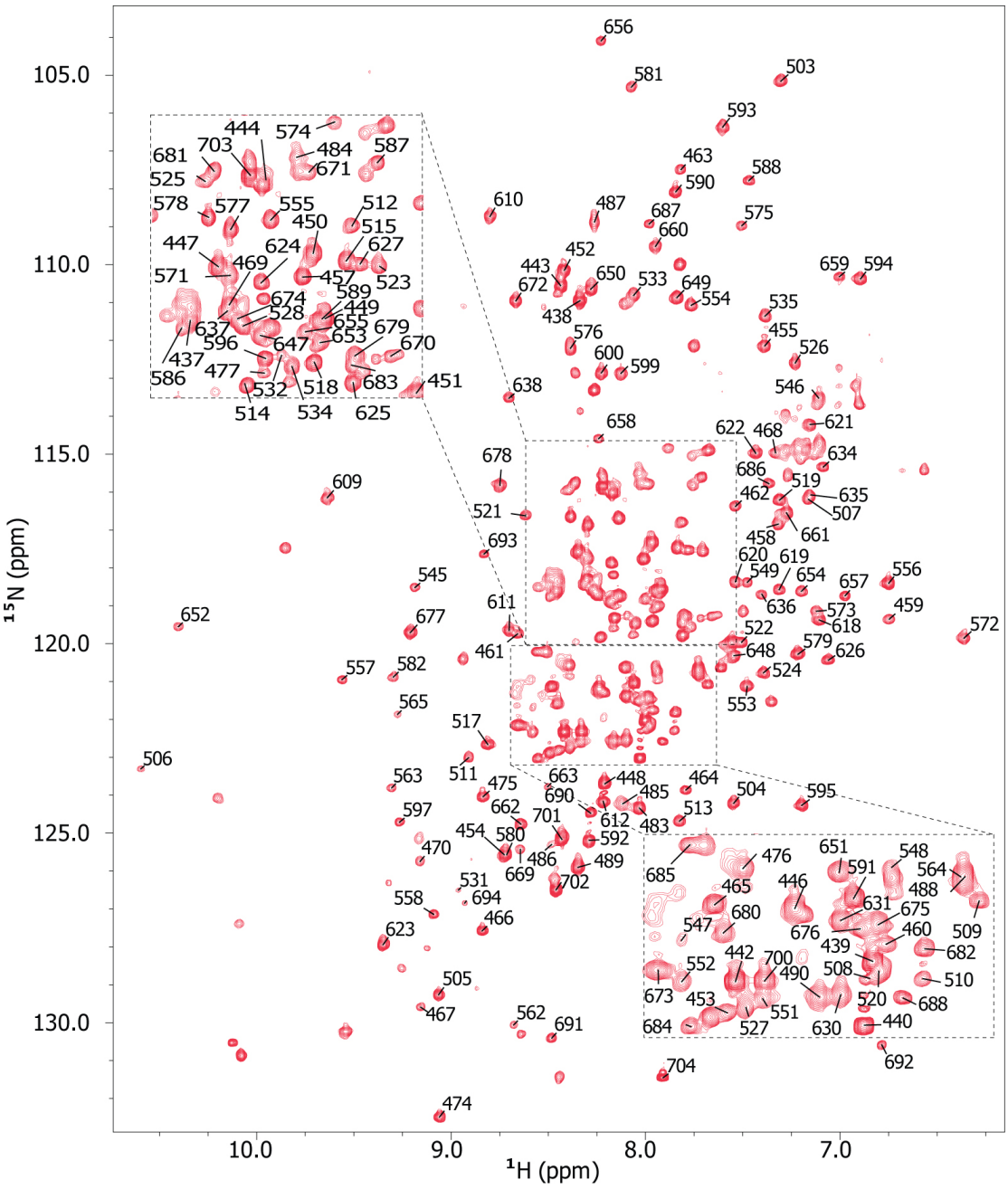

Figure 10: ^{1}H, ^{15}N TROSY spectrum of $Wzc_{CD\Delta C}$. Data collected at a ^{1}H frequency of 900 MHz spectrometer using sweep widths of 13.35 ppm (512 complex points) in the direct dimension and 30 ppm (128 complex points) in indirect dimension with recycle delay of 1.5 s at 25ºC. 100 µM uniformly ^{15}N,^{2}H-labeled $Wzc_{CD\Delta C}$ in a buffer containing 50 mM Phosphate, pH 6.0, 50 mM NaCl, 25 mM DTT, 5 mM EDTA.

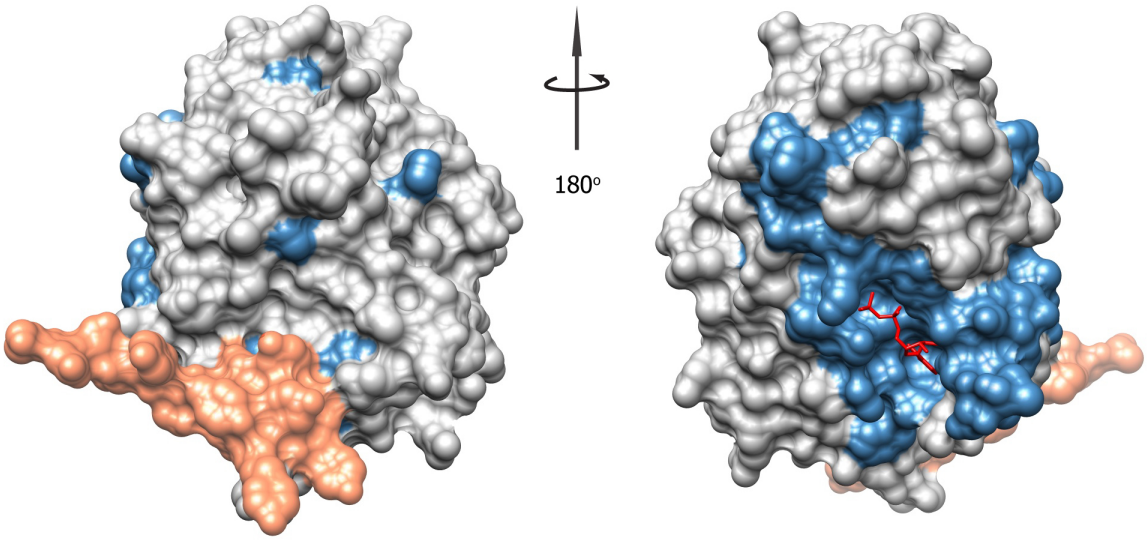

Figure 11: Extent of resonance assignment of $Wzc_{CD\Delta C}$. Unassigned backbone amide resonances obtained from ^{1}H, ^{15}N TROSY spectrum of $Wzc_{CD\Delta C}$ are plotted on Wzc_{CD} surface where unassigned residues are in blue and YC-cluster in coral (not present in the present construct). The ligand ADP (in red) sits in the catalytic site of $Wzc_{CD\Delta C}$.

4.3. NMR Experiments on Wzc_{CD}

An overlay of TROSY spectra of $Wzc_{CD\Delta C}$ and Wzc_{CD} revealed no significant chemical shift changes in the core domain (Ser447-Ala704), indicating that residues in the YC have minimal interactions with the folded core. Resonance assignments of the core domain residues could by and largely be unambiguously transferred to Wzc_{CD} spectrum. The average chemical shift difference between the residues in the core domain of $Wzc_{CD\Delta C}$ and Wzc_{CD} is 0.0125±0.0138 ppm. The only significant differences were found for the extreme C-terminal residues of $Wzc_{CD\Delta C}$ (Ser700-Ala704) for which a simple assignment transfer could not be made (Figure 12). The 16 additional (compared to the $Wzc_{CD\Delta C}$ spectrum) unassigned resonances in the Wzc_{CD} spectrum correspond to the C-terminal tail and we expect to be able to assign them in the future.

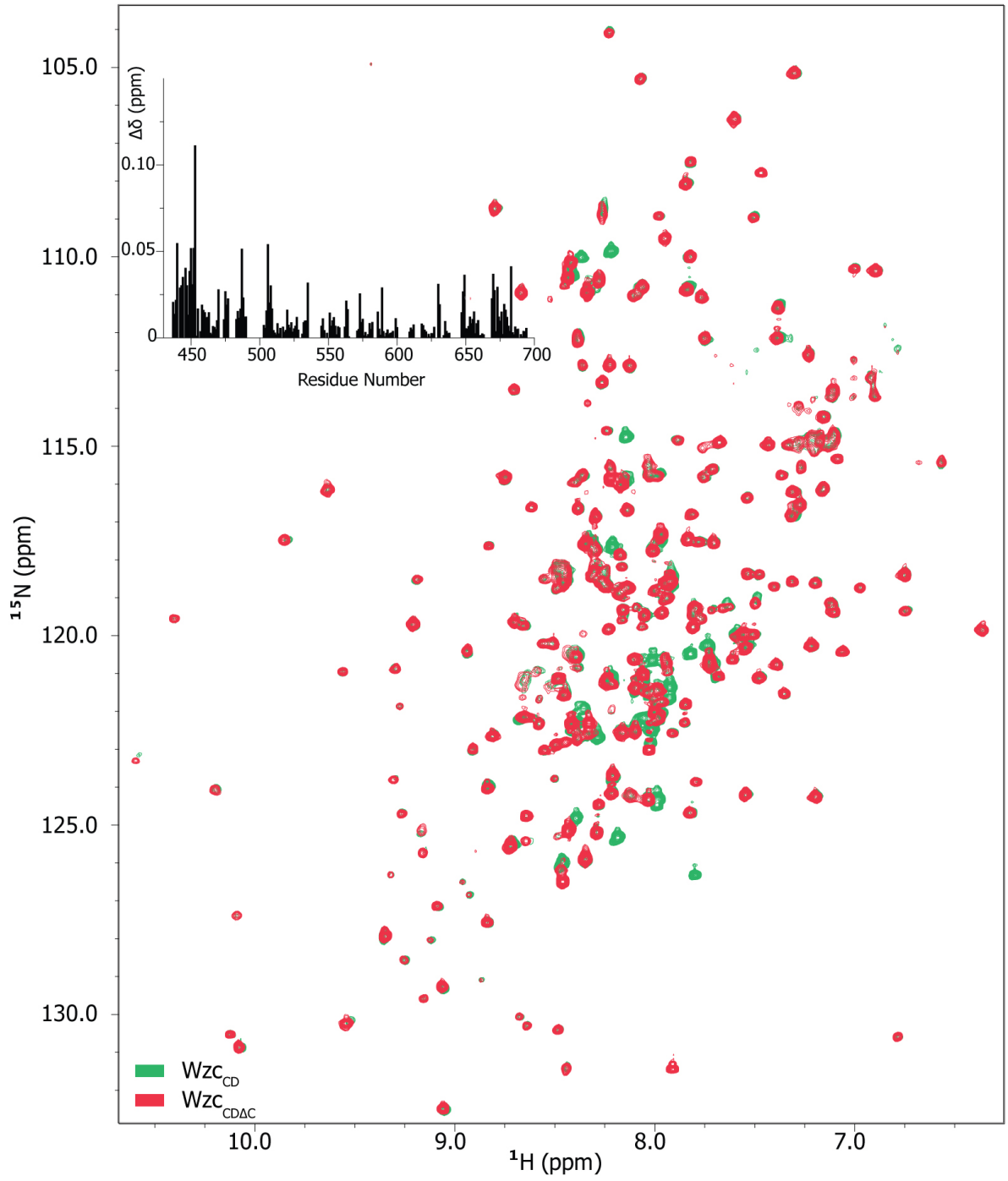

Figure 12: An overlay ^{1}H, ^{15}N-TROSY spectra of $Wzc_{CD\Delta C}$ and Wzc_{CD}. Data collected at a ^{1}H frequency of 900 MHz (25ºC) with sweep widths of 13.35 ppm (512 complex points) in the direct dimension and 30 ppm (128 complex points) in the indirect dimension using a recycle delay of 1.5 s. Samples were 100 µM in a buffer containing 50 mM phosphate, 50 mM NaCl, 25 mM DTT, 5 mM EDTA at pH 6.0. Inset shows the chemical shift difference between the resonances in $Wzc_{CD\Delta C}$ and Wzc_{CD}.

4.4. Backbone Resonance Assignment for Full-length Wzb

The NMR assignments of backbone resonances Wzb are available in the public domain-BMRB databank (BMRB ID: 6934) (Lescop et al., 2006). However, the simple, direct and unambiguous transfer of assignments was not possible, therefore we decided to reassign these resonances using a standard triple-resonance-based assignment strategy.

Our Wzb construct contains 167 residues including a 20-residue N-terminal cloning fragment that contains a cleavable His_6 affinity tag. This N-terminal fragment appeared to provide long-term stability to protein samples at high-concentration and it was not removed for the NMR experiments. Excluding the 6 prolines, a total of 161 backbone amide resonances were expected. We observed 184 distinct resonances in ^{1}H, ^{15}N HSQC spectra (at 600 MHz) including those expected for the sidechains of nitrogen-bearing residues such as Asn and Gln. We were able to unambiguously assign all ^{15}N, ^{1}H resonances corresponding to backbone amides for all Wzb residues (Figure 13). Additionally, 98% (144 out of 147) of C' resonances, 95% (140 out of 147) of C^{α} resonances and 90.6% (126 out of 139) of C^{β} resonances were unambiguously assigned.

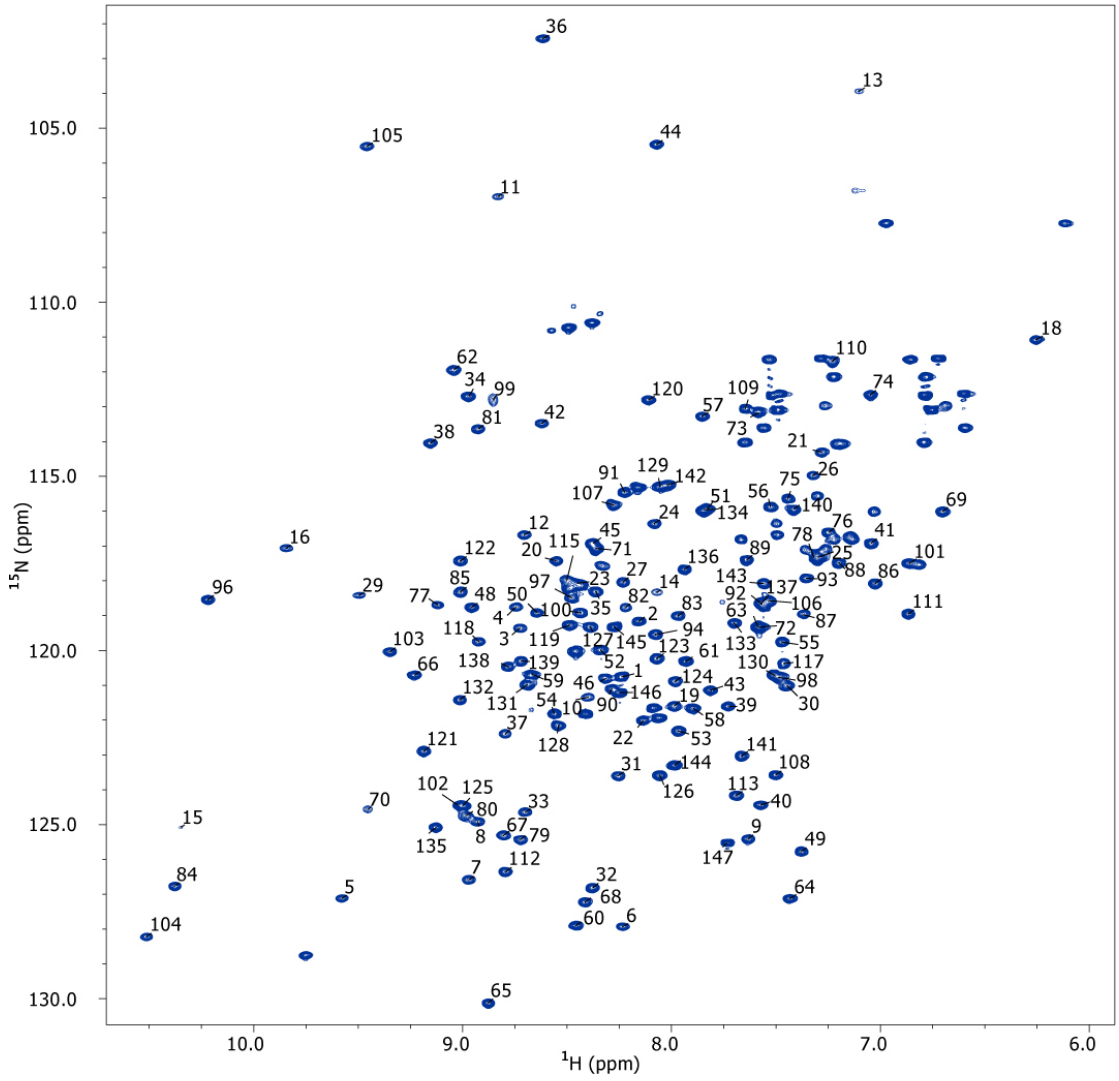

Figure 13: ^{1}H, ^{15}N HSQC spectrum of Wzb. Data collected at a ^{1}H frequency of 800 MHz at 25ºC using sweep widths of 13.0 ppm (512 complex points) in the direct dimension and 32 ppm (128 complex points) in the indirect dimension with a recycle delay of 1.5 s. The NMR sample contained 100 µM Wzb in the following buffer - 50 mM phosphate, 50 mM NaCl, 25 mM DTT, 5 mM EDTA at pH 6.0.

4.5. Identification of the Wzc_{CD}/Wzb Interaction Surface

The ability of Wzb to successfully dephosphorylate the C-terminal tyrosine cluster (YC) of Wzc_{CD} has been previously demonstrated (Vincent et al., 1999). However, the nature of interactions between Wzc_{CD} and Wzb are largely unknown and remains uncharacterized both in location and in geometry. This information is critical in fully elucidating the structural, dynamic and mechanistic determinants of the regulation of a bacterial tyrosine kinase by its cognate phosphatase. NMR chemical shifts are uniquely sensitive to changes in local environment thus provide an excellent means to monitor protein-protein interactions including those that are weak or transient and hence undetectable by other biophysical methods (Zuiderweg, 2002).

We estimated the apparent dissociation constant (K_d) characterizing the interactions between Wzc_{CD} (or $Wzc_{CD\Delta C}$) and Wzb to be around 10 μM. We expect that this relatively strong interaction in solution would likely lead to a significant increase in the effective molecular weight (and the resultant increased rotational correlation time and decrease in spectral quality) for the interacting proteins. Thus, we felt that it would be worthwhile to work using samples with reduced proton density. However, initially we used fully protonated samples. This produced results that while promising were more difficult to allow unambiguous interpretation. Therefore, to better distinguish between global peak attenuation (due to increase in size) and specific attenuations due to interaction, we decided to repeat the titrations using perdeuterated proteins. Uniformly ^{15}N, ^{2}H-labeled $Wzc_{CD\Delta C}$ (or Wzc_{CD}) samples were titrated with uniformly ^{2}H-labeled Wzb using various molar ratios with TROSY spectra being recorded at each titration point. Analyses of these datasets allowed us to identify the surface used by Wzb to dock onto Wzc. Similar titrations employing uniformly ^{15}N, ^{2}H-labeled Wzb and uniformly ^{2}H-labeled $Wzc_{CD\Delta C}$ or Wzc_{CD} allowed the

elucidation of the corresponding docking surface on Wzb in the absence or the presence of the Wzc YC. A detailed analysis is provided below.

4.5.1 Interactions between $Wzc_{CD_{\Delta}C}$ and Wzb using $Wzc_{CD_{\Delta}C}$ as a Probe

In order to determine the $Wzc_{CD_{\Delta}C}$ surface that interacts with Wzb, TROSY spectra of uniformly ^{15}N, ^{2}H-labeled $Wzc_{CD_{\Delta}C}$ in the presence of varying amounts of uniformly ^{2}H-labeled Wzb were recorded. Changes in the intensities and positions of corresponding resonances for the free ($Wzc_{CD_{\Delta}C}$) and bound ($Wzc_{CD_{\Delta}C}$ + Wzb) forms were analyzed to elucidate the interaction surface. These changes could be due to either due to direct binding or allosteric effects resulting in conformational changes upon binding. We found significant chemical shift changes in addition to attenuation in $Wzc_{CD_{\Delta}C}$ resonances in the presence of Wzb. These changes are evident in an overlay of the TROSY spectrum of free $Wzc_{CD_{\Delta}C}$ (red) with that of $Wzc_{CD_{\Delta}C}$ in the presence of an equimolar ratio of Wzb (purple). Chemical shift changes ($\Delta\delta$) and resonance intensity ratios (ΔI) were calculated using Equations 5 and 6, respectively, for each peak.

$$\Delta\delta_i^j = \sqrt{\left(\delta_{0,H}^j - \delta_{i,H}^j\right)^2 + 0.11\left(\delta_0^j - \delta_{i,N}^j\right)^2} \tag{5}$$

$$\Delta I_i^j = 1 - I_i^j / I_0^j \tag{6}$$

The 0 sub-script indexes the ^{1}H or ^{15}N chemical shifts (δ) for $Wzc_{CD_{\Delta}C}$ in the absence of Wzb and the corresponding intensities (I). The *i* and *j* index a particular titration point and the residue number, respectively.

The chemical shift differences (0.016±0.010 ppm) and peak attenuations seen for $Wzc_{CD_{\Delta}C}$ in the presence of an equimolar amount of Wzb are plotted against residue number in Figure 14. Residues for which the resonances were broadened beyond detection are represented by dashed lines in Figure 14B. Most of the chemical shift perturbations and

attenuations were localized around the suggested oligomerization surface in $Wzc_{CD\Delta C}$ (Bechet et al., 2010). On the αA helix, significant chemical shift changes were seen for Ser455 (0.130 ppm), Leu459 (0.053 ppm), Glu461 (0.087 ppm) and peak attenuations for Gln457 and Glu460. For the βA strand: Val466, Tyr467, Ala468 and Ile470 were broadened to the noise level whereas Ser469 showed a large change in chemical shift (0.028 ppm). Furthermore, Asp562, Cys563 that belong to the Walker A' motif also broadened to noise level. Most peaks corresponding to residues on the α2 helix were either significantly attenuated or displayed large chemical shift perturbations (Asp504 (0.128 ppm) and Leu505 (0.174 ppm)) in the presence of Wzb (Figure 14). These include significant chemical shift difference. Most notably, residues Glu508 (shows 45% attenuation), Ala509, Ile510, Arg511, Ser512, Leu513 and Arg514 all of which belong to the EX_2RX_2R motif that has been considered key in the formation of oligomeric Wzc_{CD} (mutation of Glu508, Arg511 and Arg514 to Ala abolishes oligomerization) (Bechet et al., 2010) are attenuated to noise level even in the presence of sub-stoichiometric amounts of Wzb. Additionally, large chemical shift changes were also seen for Lys674 (0.060 ppm) and Glu675 (0.045 ppm) on the C-terminal α-helix (α8) and in Gly692 which is located at the C-terminal β-strand. Interestingly all of these residues are fully conserved in BY-kinases (see Figure 2). In addition, several residues on the α3 helix show significant chemical shift perturbation and attenuation, likely due to conformational changes in the α2 helix upon Wzb binding. Chemical shifts differences (in green), which are 2σ and 3σ (σ = standard deviation) above the mean and attenuations (in orange) are plotted on the crystal structure of Wzc_{CD} (PDB ID: 3LA6) (Figure 15, top and bottom panels). Based on this analysis it appears that Wzb utilizes a surface that is opposite to that bearing the catalytic residues. While the resonance assignments for several residues of the catalytic face are not yet available (see Figure 11), an analysis of the binding surface reveals the presence of negatively charged (Glu460, Glu461, Glu684), positively charged (Arg511, His518 and

Lys691) and hydrophobic residues (Tyr467, Leu505, Met512, Phe519, Leu680) (Figure 15). In the absence of site-specific mutational data it is difficult to interpret the interaction as either hydrophobic or electrostatic. However, our recent NMR results do not reveal any significant modifications in the Wzc_{CD}/Wzb interactions in the presence of increasing quantities of salt. This seems to suggest that electrostatic interactions may not be that crucial in stabilizing the interface.

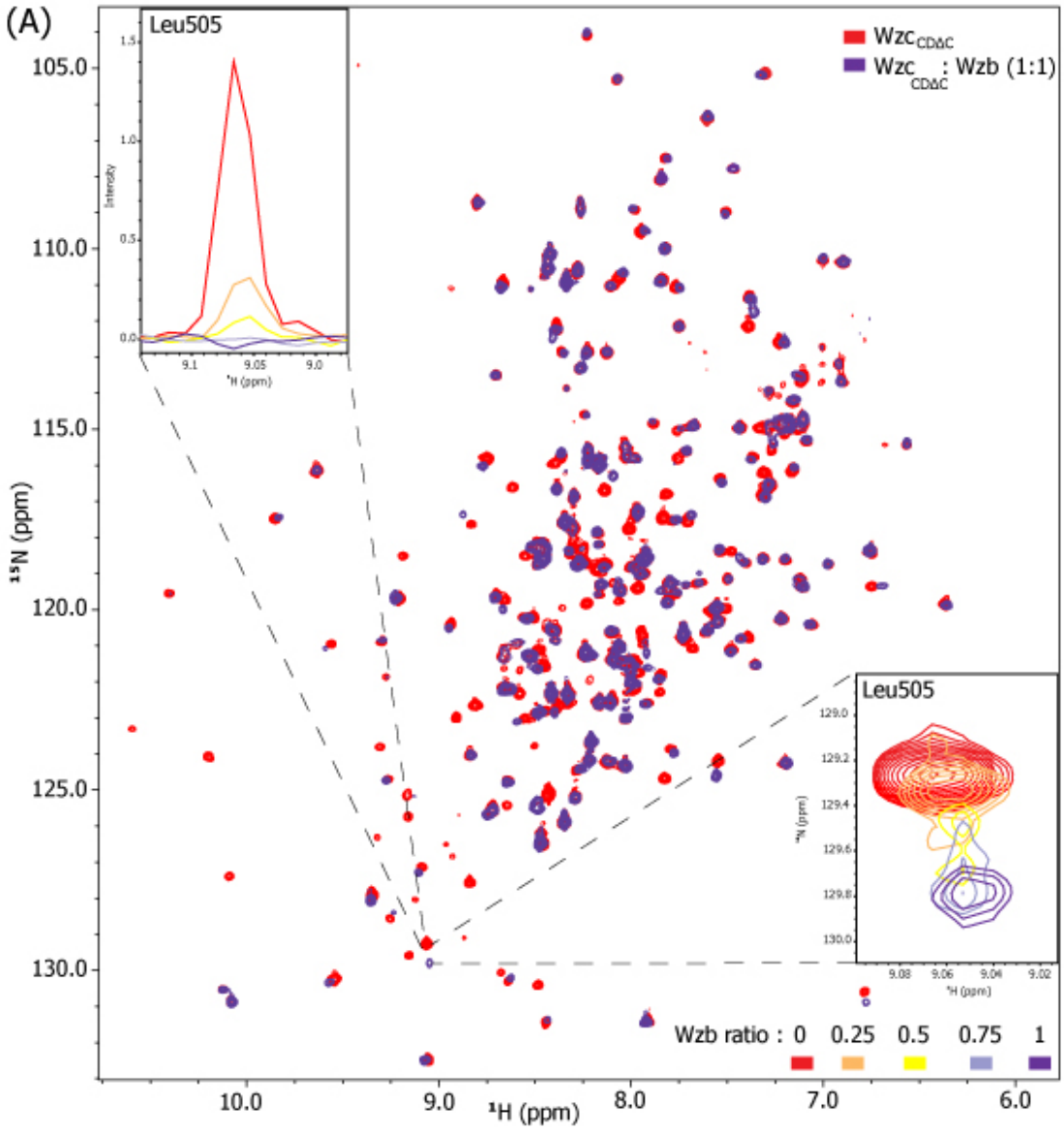
(A)
Leu505
Wzc CDΔC
Wzc CDΔC : Wzb (1:1)
Intensity
¹H (ppm)
¹⁵N (ppm)
Leu505
Wzb ratio : 0 0.25 0.5 0.75 1
¹H (ppm)

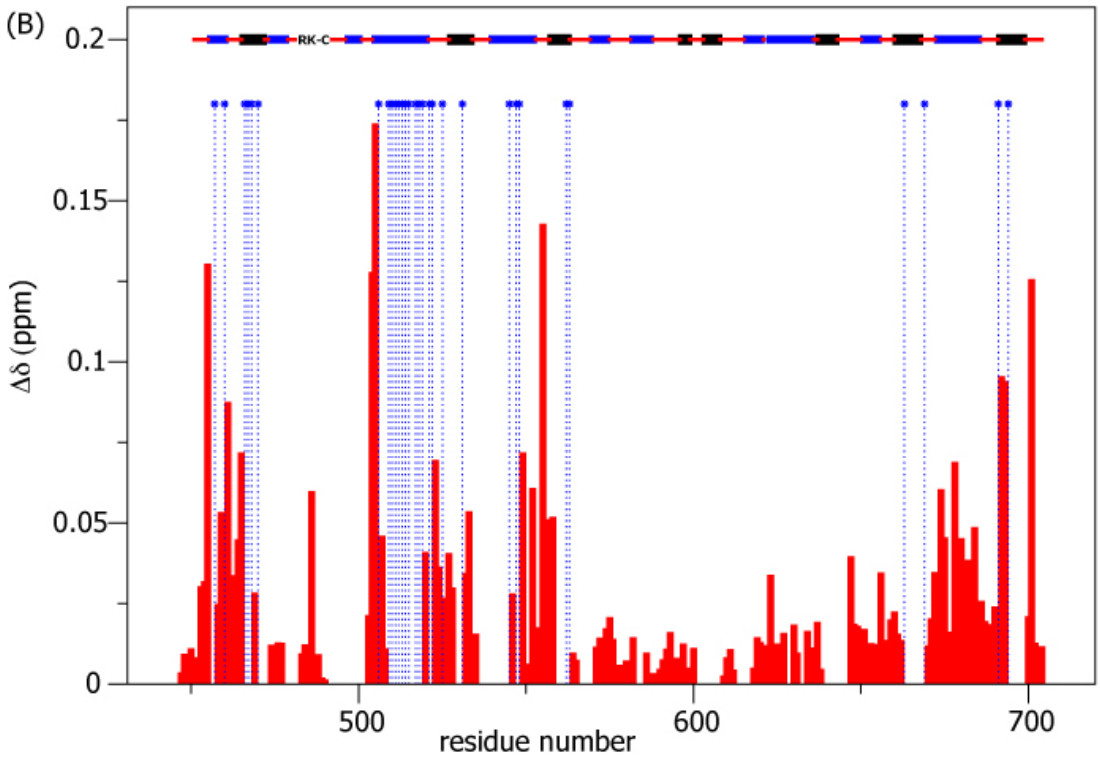

Figure 14: Interactions between $Wzc_{CD_{\Delta}C}$ and Wzb using $Wzc_{CD_{\Delta}C}$ as a Probe. (A) Overlay of the TROSY spectra (900 MHz at 25ºC) of 100 μM uniformly ^{15}N, ^{2}H-labeled $Wzc_{CD_{\Delta}C}$ in the absence (red) or the presence (blue) of an equimolar amount of uniformly ^{2}H-labeled Wzb. Inset: Attenuation and chemical shift changes for Leu505 in the presence of increasing amounts of Wzb. (B) Chemical shift changes for $Wzc_{CD_{\Delta}C}$ in the presence of equimolar amounts of Wzb plotted against residue number. Residues that are broadened beyond the threshold of detection are indicated by blue dashed lines. Regions of secondary structure are depicted as follows: α helices (thick blue lines), β strands (thick black lines), loops (red lines). The disordered RK-C (RK-cluster) is also shown.

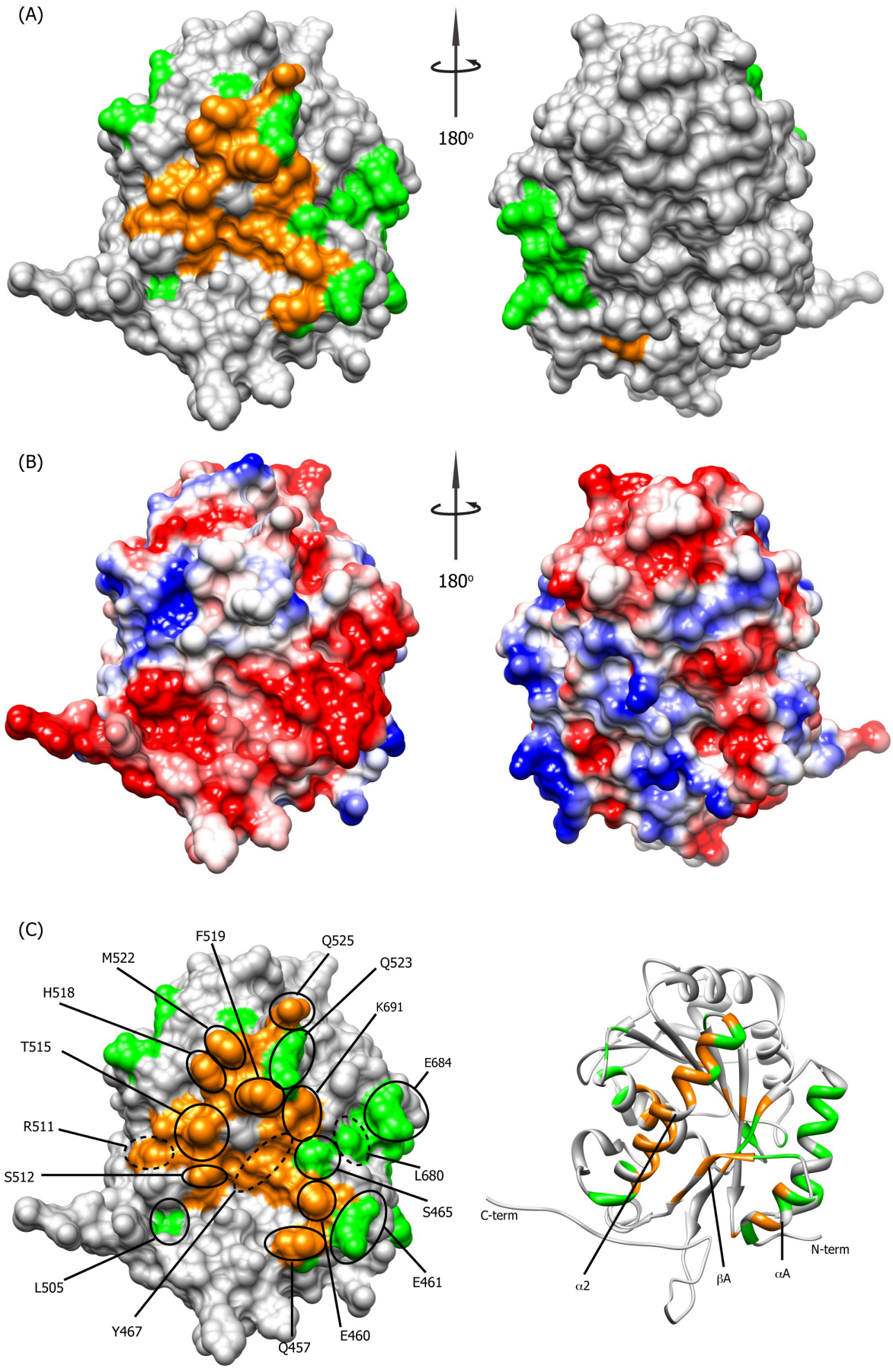
(A)
180°
(B)
180°
(C)
F519
Q525
M522
Q523
H518
K691
T515
E684
R511
L680
S512
S465
L505
E461
Y467
E460
Q457
C-term
N-term
α2
βA
αA

Figure 15: Wzb docking surface on $Wzc_{CD\Delta C}$. (A) The $Wzc_{CD\Delta C}$ surface was generated using UCSF Chimera molecular modeling software (Pettersen et al., 2004). Signal attenuations (orange) and chemical shift changes (green) > 2σ above the mean in the presence of an equimolar amount of Wzb are shown on the $Wzc_{CD\Delta C}$ surface. Unassigned residues in $Wzc_{CD\Delta C}$ are not colored. (B) Charge distribution on the $Wzc_{CD\Delta C}$ surface. The charge distribution (Coulombic) was calculated using UCSF Chimera (Pettersen et al., 2004) and is depicted as a red-blue gradient (-5kT to +5kT). (C) Some of the key residues that lie on the αA, α2 helices and the βA strand (in ribbon representation on the right panel) and which display significant spectral perturbation in the presence of Wzb are circled on the surface (and labeled).

4.5.2. Interactions between Wzc_{CD} and Wzb using Wzc_{CD} as a Probe

The studies described above were repeated using uniformly ^{15}N, ^{2}H-labeled Wzc_{CD} and uniformly ^{2}H-labeled Wzb, with TROSY spectra acquired at each titration point at 25°C. The observed spectral were similar to those seen in the case of $Wzc_{CD\Delta C}$ and Wzb, described above (Figure 16). As in the case of $Wzc_{CD\Delta C}$, the largest changes (chemical shift perturbations and peak attenuations) are observed for the residues, which are part of the putative oligomerization surface, including the αA and α2 helices, and the βA strand (Bechet et al., 2010). As in the case of $Wzc_{CD\Delta C}$ residues in the α3 helix in Wzc_{CD} undergo chemical shift changes and peak attenuation, the conserved residues Lys674, Glu675 and Gly692 also show large chemical shift changes. In addition to Asp562 and Cys563, Met565 that belongs to the Walker A' motif also broadened to noise level (Figure 16). This motif lies in close spatial proximity to the α3 helix in the crystal structure (Bechet et al., 2010). The attenuations in Walker A' could be the result of significant conformational changes in the orientation of the α3 helix upon Wzb binding.

The fully attenuated peaks (in orange) and peaks which show 2σ and 3σ chemical shift differences (in green) are plotted on to the surface of Wzc x-ray crystal structure (access code 3LA6) (Figure 17 top and bottom panel). Figure 17 (bottom right panel) shows the ribbon plot of Wzc_{CD} color coded as explained above. The middle panel of Figure 17 shows

the Coulombic charge distribution of the surface residues of Wzc_{CD}. Interaction surface of Wzc_{CD} upon Wzb binding is matching with the interaction surface of $Wzc_{CD\Delta C}$ upon Wzb binding (Figure 15, Figure 17).

Since the residues present in the tyrosine cluster have not yet been unambiguously assigned, we undertook an overall analysis of the spectral characteristics of these resonances in the presence of Wzb. It was noticed that 8 out of 18 peaks (15 from the tail and three from altered residues most likely Ser700-Ala704) were attenuated. This peak attenuation could be simply due to an overall increase in the rotational correlation time upon Wzb binding. Additionally, 4 peaks also display significant shift perturbations. The spectral changes in the YC are currently being analyzed in greater detail.

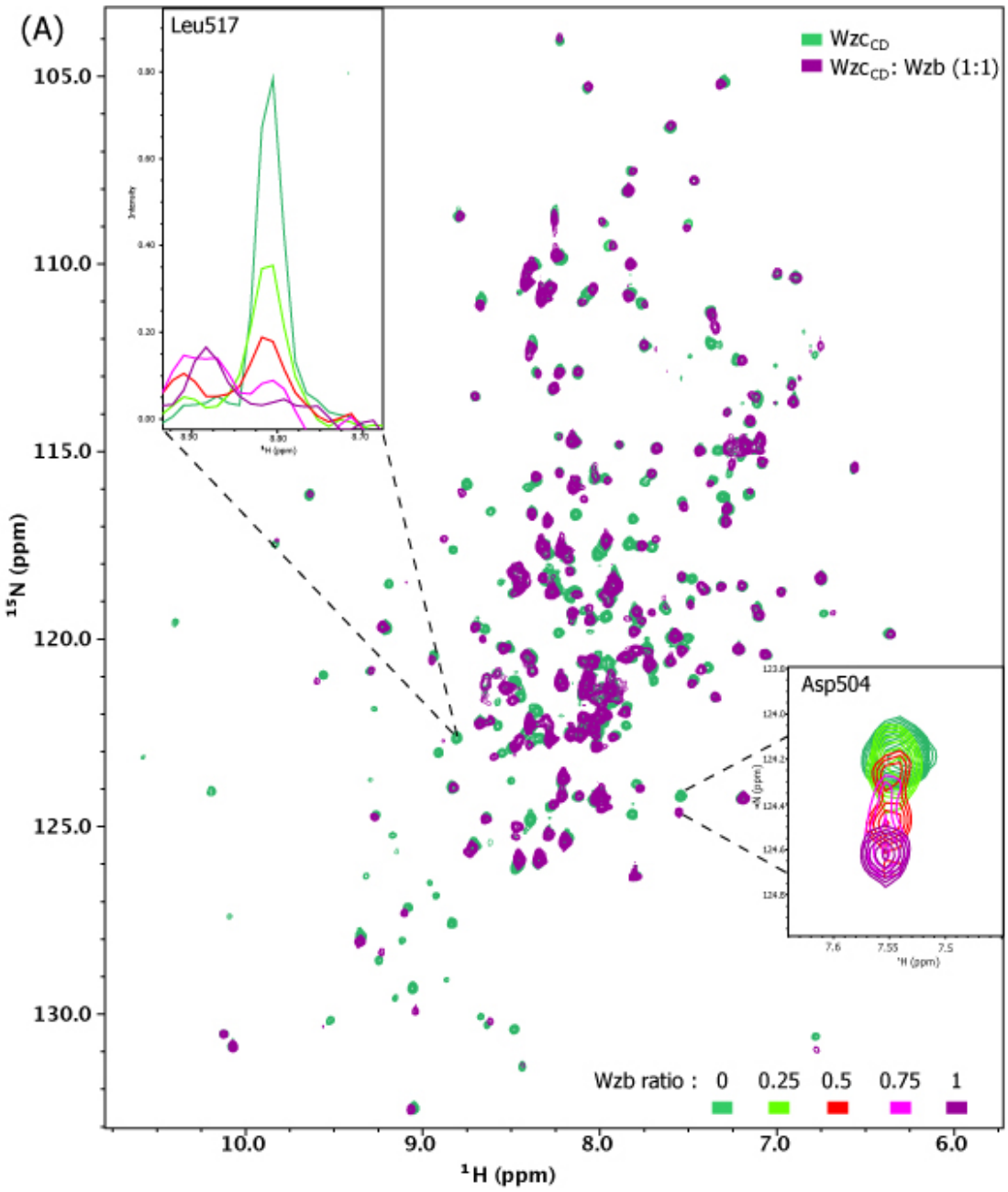
(A)
Leu517
Asp504
Wzc$_{CD}$
Wzc$_{CD}$: Wzb (1:1)
Wzb ratio : 0 0.25 0.5 0.75 1
^{15}N (ppm)
^{1}H (ppm)
105.0
110.0
115.0
120.0
125.0
130.0
10.0
9.0
8.0
7.0
6.0

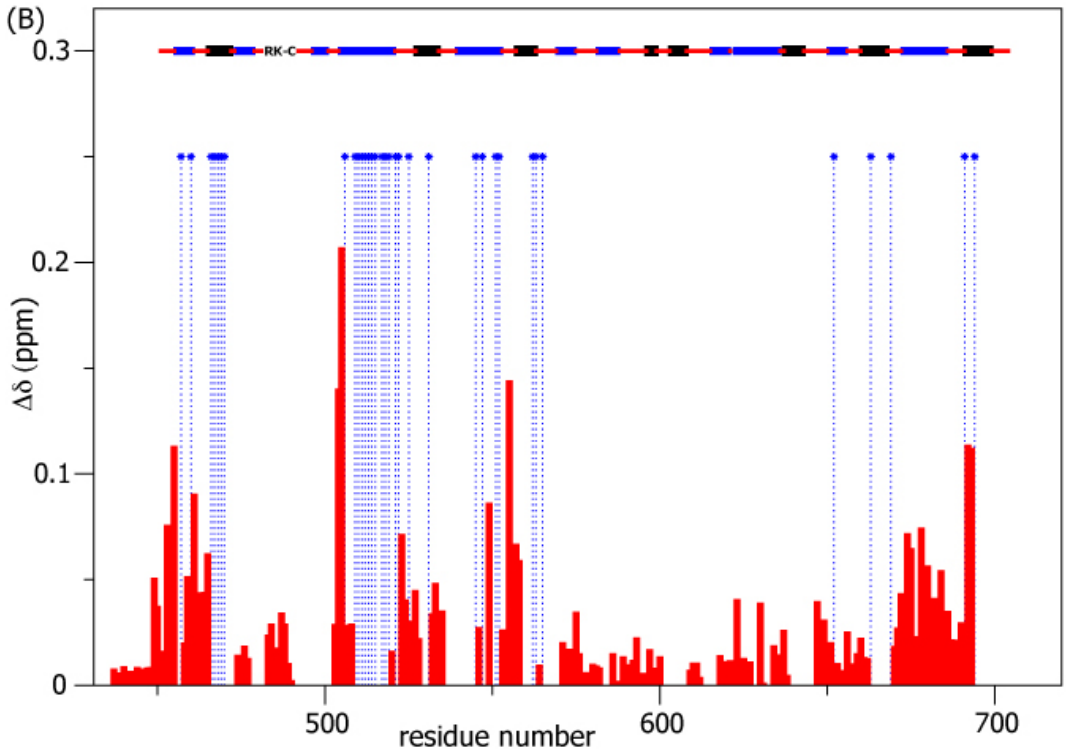

Figure 16: Interactions between Wzc_{CD} and Wzb using Wzc_{CD} as a probe. (A) Overlay of ^{15}N, ^{1}H, TROSY spectra of uniformly ^{2}H, ^{15}N-labeled Wzc_{CD} (900 MHz, 25ºC) in the absence (green) and the presence (purple) of an equimolar amount of uniformly ^{2}H-labeled Wzb. The inset shows examples of peak attenuation (Leu517) and chemical shift changes (Asp504) seen in the presence of increasing amounts of Wzb. (B) Scaled chemical shift changes in Wzc_{CD} in the presence of Wzb at 1:1 molar ratio (in red) are plotted against residue number. Residues that are broadened beyond the observation threshold are indicated as blue dashed vertical lines. Regions of secondary structure in $Wzc_{CD\Delta C}$ are indicated as follows: α helices (thick blue lines), β strands (thick black lines), loops (red lines). The RK-C (RK-cluster) that is found to be disordered in the crystal structure is also indicated.

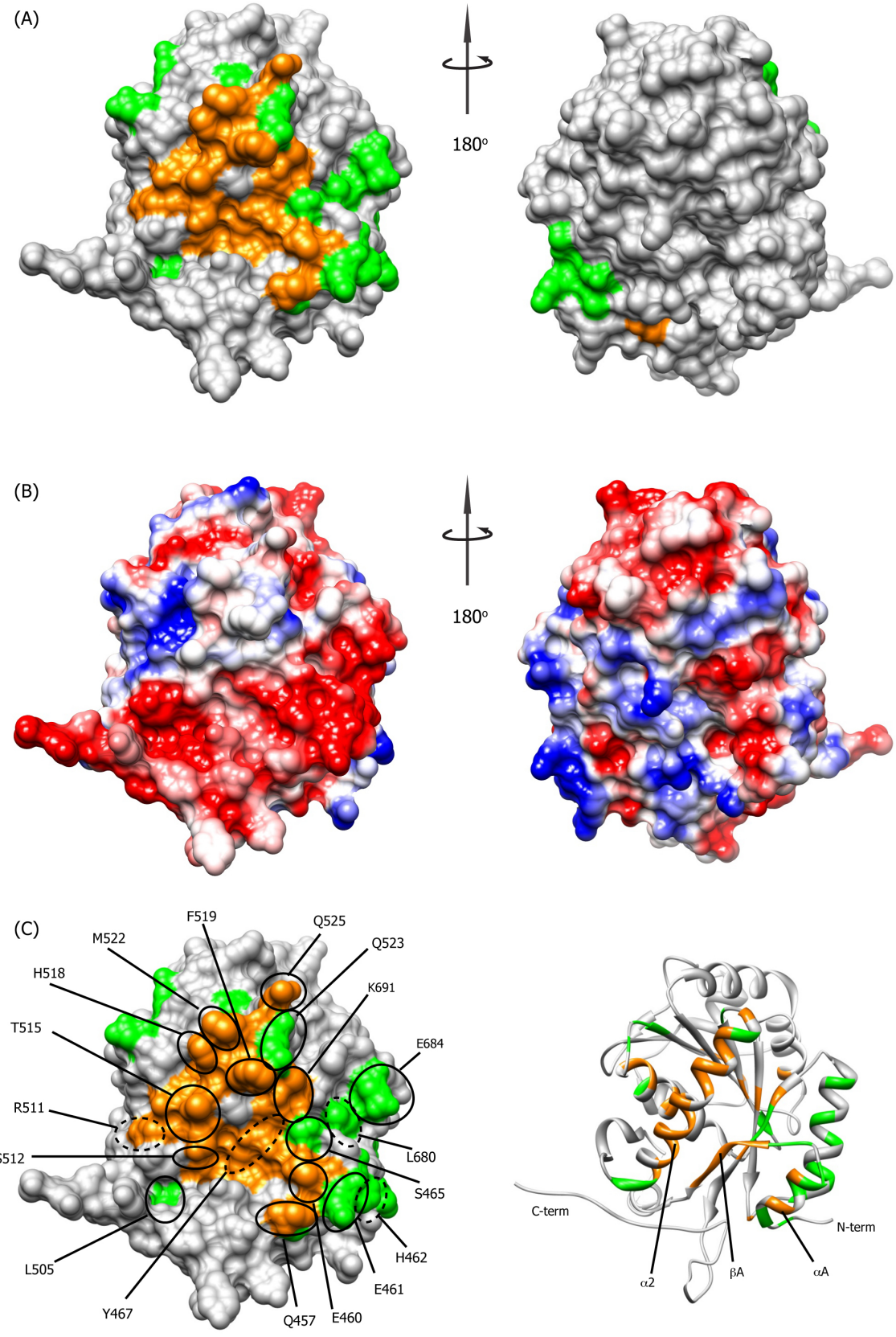
(A)
180°
(B)
180°
(C)
F519
Q525
M522
Q523
H518
K691
T515
E684
R511
S512
L680
S465
H462
L505
E461
Y467
Q457
E460
C-term
N-term
α2
βA
αA

Figure 17: Wzb docking surface on Wzc_{CD}. (A) Wzc_{CD} surface representation in gray was generated by UCSF CHIMERA molecular modeling software (Pettersen et al., 2004). Signal attenuations (orange) and chemical shift changes (green) > 2σ above the mean in the presence of an equimolar amount of Wzb are shown on the Wzc_{CD} surface. Unassigned residues in $Wzc_{CD\Delta C}$ are not colored. (B) Charge distribution on the Wzc_{CD} surface. The charge distribution (Coulombic) was calculated using UCSF Chimera (Pettersen et al., 2004) and is represented using a red-blue gradient from -5 kT (red) to +5 kT (blue) (C) Some of the key residues which undergo changes upon Wzb interaction in the αA, α2 helices and the βA strand in Wzc_{CD} are circled on the surface and the αA, α2 helices and the βA strand are indicated in ribbon diagram.

Based on our results obtained from the titration of $Wzc_{CD\Delta C}$ and Wzc_{CD} with Wzb, it appears that Wzb occludes the oligomerization surface of Wzc, this is where the largest degree of signal attenuation and chemical shift changes are seen. It is therefore likely, that this mode of association constitute a mechanism to prevent Wzc_{CD} monomers from reassociating and shielding the YC during dephosphorylation by Wzb.

4.5.3. Interactions between Wzb and $Wzc_{CD\Delta C}$ using Wzb as a Probe

Having defined the surface on Wzc_{CD} utilized by Wzb in its interactions with the former, we proceeded to identify the corresponding surface on Wzb. Uniformly ^{15}N, ^{2}H-labeled Wzb samples were separately titrated using different molar ratios of either uniformly ^{2}H-labeled $Wzc_{CD\Delta C}$ or uniformly ^{2}H-labeled Wzc_{CD}. Given the large increase in the effective molecular size for Wzb in the complex compared to Wzb in the free state, this labeling scheme allowed a more efficient evaluation of the spectral perturbations resulting from protein-protein interactions.

As described in the Materials and Methods section, TROSY spectra of Wzb were recorded in the presence of increasing amounts of $Wzc_{CD\Delta C}$, and chemical shift changes and attenuations were calculated for each titration point. Figure 18A shows an overlay of the spectra of 100 μM uniformly ^{15}N, ^{2}H-labeled Wzb in the presence of an equimolar amount of

uniformly ^{2}H-labeled $Wzc_{CD\Delta C}$. The residues for which the corresponding resonances show significant chemical shift perturbations (0.014±0.007) and/or signal attenuation are shown in Figure 18B. Peaks belonging to the catalytic residues e.g. Cys9 (attenuated), Arg15 (attenuated) and Ser16 (0.028 ppm) were either attenuated or showed significant chemical shift changes greater than by 1σ above the mean. In addition, peak intensities were reduced to the noise level for the following residues that are highly conserved in LMW-PTPs including Asp77, Ile79, Leu80, Gly99 and Lys100. A large chemical shift change (> 3σ) was seen in the conserved Trp138 (0.038 ppm). We found that 29 of 141 (20.6%) resonances corresponding to Wzb were fully attenuated in the TROSY spectrum in the presence of an equimolar amount of $Wzc_{CD\Delta C}$. All spectral perturbations which include attenuations and chemical shift changes (the overall magnitude of chemical shift changes seen in Wzb were much smaller than those seen for $Wzc_{CD\Delta C}$ or Wzc_{CD}) mapped onto a large surface proximal to the Wzb catalytic site. This large surface harbors residues from the N-terminus Met1, Phe2, Asn3 and Asn4 along with residues from α1, β1, α3, β3 and α4 (residues in β3 and α4 are conserved: Asp77, Ile79, Leu80, Gly99, Lys100) and extreme C-terminus helix. Some of the residues in the catalytic P-loop also perturbed i.e. Val10 (0.032 ppm), Gly11 (0.034 ppm) and Ser16 or attenuated i.e. Cys9 and Arg15, which could represent conformational changes at the catalytic site priming it for catalysis upon $Wzc_{CD\Delta C}$ binding.

Peaks that display chemical shift differences > 2σ (in green) and those that are completely attenuated (in orange) are plotted on a surface representation of Wzb (PDB ID: 2FEK) (Figure 19 top and bottom panel). Figure 19 (bottom right panel) shows a ribbon plot of Wzb using the same coloring scheme. The middle panel of Figure 19 shows the Coulombic charge distribution mapped onto the Wzb surface. The putative Wzc_{CD} recognition surface on Wzb contains positively charged residues: Arg7, Lys31, Arg71, R98 and His106; negatively charged residues: Asp77, Glu29 and Glu96, and hydrophobic

residues: Met1, Phe2, Met97 and Val147. However, as mentioned previously electrostatic interactions do not appear to play a significant role in Wzb/Wzc_{CD} associations. Based on our data with Wzb with $Wzc_{CD\Delta C}$, it was concluded that Wzb binding of $Wzc_{CD\Delta C}$ happens through a site in Wzb proximal to its catalytic site.

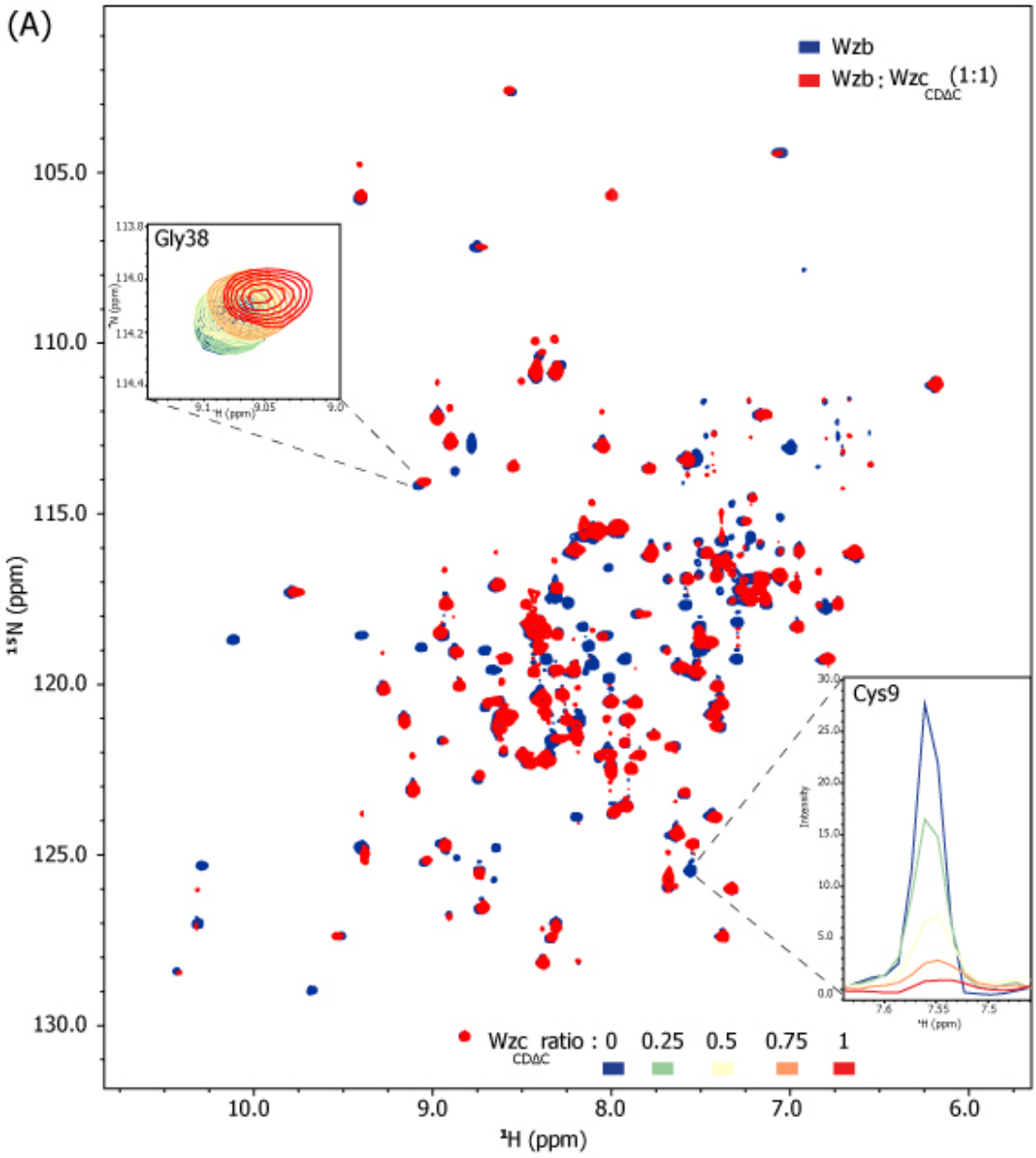
(A)
Wzb
Wzb : Wzc CDΔC (1:1)
Gly38
Cys9
Wzc CDΔC ratio : 0 0.25 0.5 0.75 1
105.0
110.0
115.0
120.0
125.0
130.0
15N (ppm)
10.0
9.0
8.0
7.0
6.0
1H (ppm)

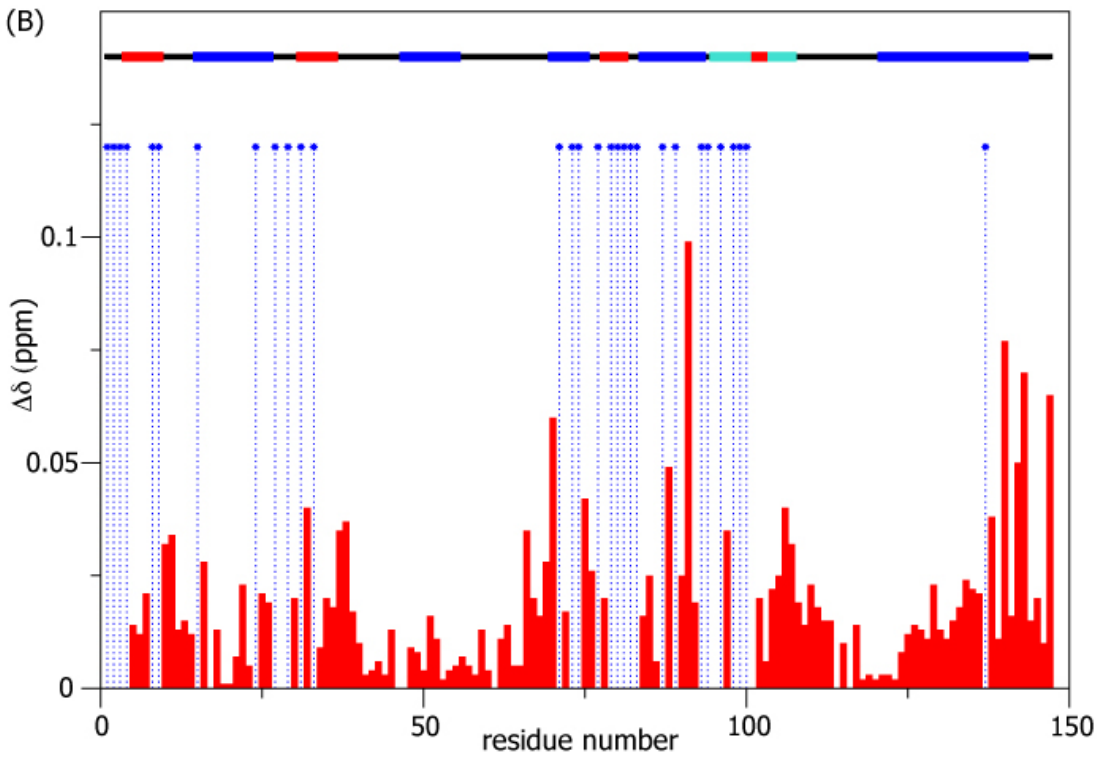

Figure 18: Interactions between Wzb with Wzc_{CD_4C} by monitoring Wzb. (A) Overlay of ^{15}N, ^{1}H, TROSY spectra (900 MHz at 25ºC) of uniformly ^{2}H, ^{15}N-labeled Wzb in the absence (blue) or the presence (red) of an equimolar amount of uniformly ^{2}H-labeled Wzc_{CD_4C}. Representative attenuations (Cys9) and chemical shift changes (Gly38) during the titration course are shown in the inset. (B) Scaled chemical shift changes occurring for the Wzb in the presence of Wzc_{CD_4C} at 1:1 molar ratio (in red). Residues that are broadened beyond the observation threshold are indicated by blue dashed lines. Secondary structural elements are depicted as follows: α helices (thick red lines), β strands (thick blue lines), loops (black lines) and the 3_{10} helix (in cyan).

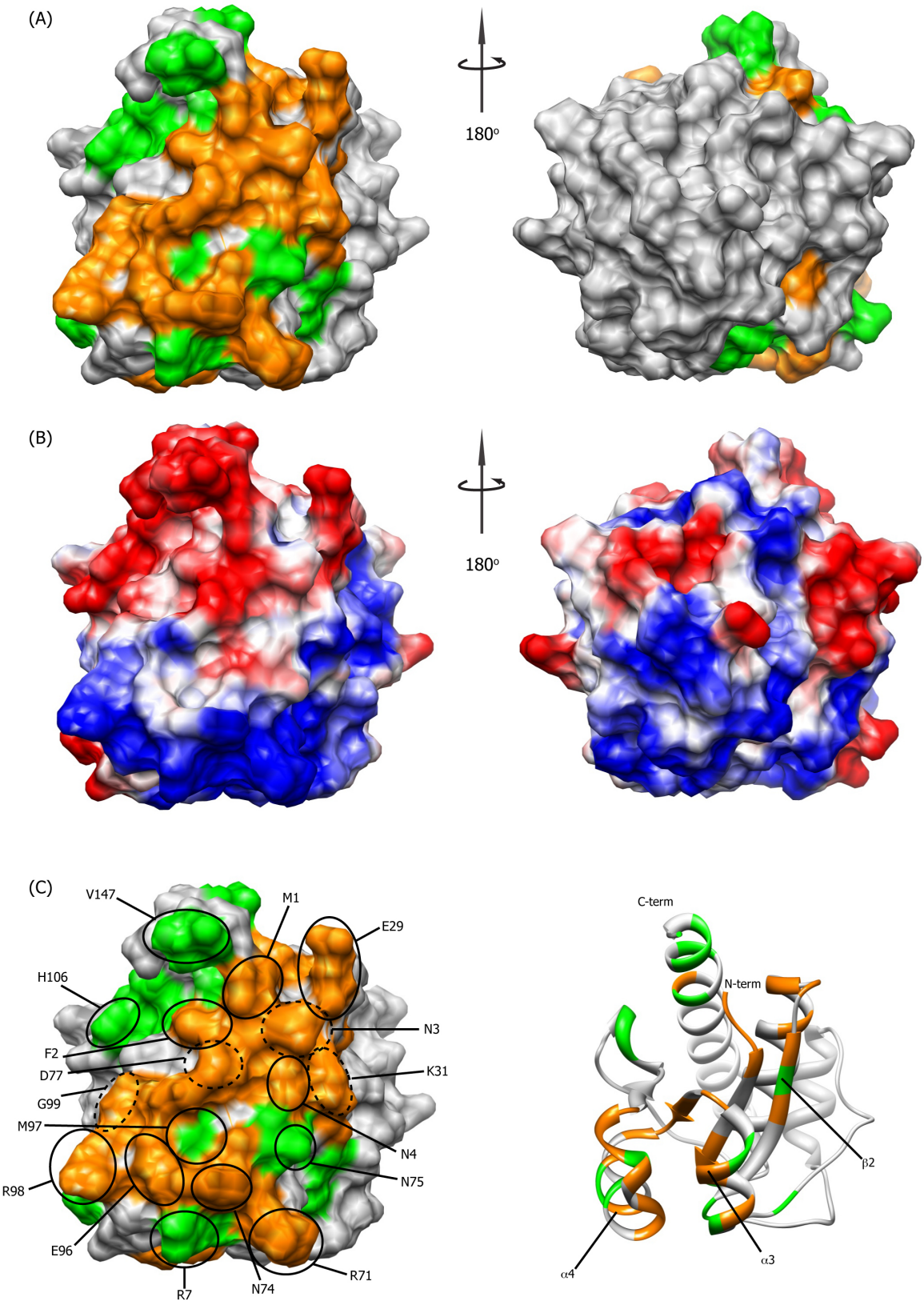
(A)
180°
(B)
180°
(C)
V147
M1
E29
H106
N3
F2
D77
K31
G99
M97
N4
N75
R98
E96
R71
R7
N74
C-term
N-term
β2
α4
α3

Figure 19: Spectral perturbations in Wzb in the presence of $Wzc_{CD\Delta C}$. (A) Signal attenuations (orange) and chemical shift changes > 2σ (in green) in Wzb in the presence of an equimolar amount of $Wzc_{CD\Delta C}$ mapped onto the Wzb surface. (B) The Coulombic surface of Wzb is shown. The charge distribution was calculated using UCSF Chimera (Pettersen et al., 2004) and is depicted using a red (-5kT) to blue (+5kT) gradient. (C) Some of the key residues in Wzb which undergo changes upon interaction with $Wzc_{CD\Delta C}$ are circled on the Wzb surface. The α3, α4 helices and β3 strand are indicated on the corresponding ribbon diagram.

4.5.4. Interactions between Wzb and Wzc_{CD} using Wzb as a Probe

In order to determine whether the YC in Wzc_{CD} played an additional role in Wzb/Wzc_{CD} interactions, we titrated of uniformly ^{15}N, ^{2}H-labeled Wzb with Wzc_{CD} recording TROSY spectra at each step in the titration course (Figure 20). We observed that 43 of 141 (30.5%) of the resonances observable in free Wzb were fully attenuated and some of the resonances show chemical shift perturbations (0.024±0.021) in the presence of an equimolar amount of Wzc_{CD}. The attenuations include some residues for which chemical shift perturbations were observed upon interaction with $Wzc_{CD\Delta C}$ e.g. Gly11 in the P-loop, Gly38 in the α2-β2 loop and Arg70, Asn75 and Tyr76 in the α3 helix. In addition, resonances belonging to the catalytic site, Ile13 and Cys14 that were not significantly perturbed in the $Wzc_{CD\Delta C}$ titrations also show attenuations in the analyzed titration spectrum (Figure 20). Spectral perturbations were seen for resonances corresponding to all P-loop residues and residues proximal to the catalytic site. Overall, these were similar to that observed in the presence of $Wzc_{CD\Delta C}$. The α3 and α4 helices along with the β3 strand that constitute the upper part of the crevice housing the P-loop, show significant perturbations in the presence of Wzc_{CD} (as also seen in $Wzc_{CD\Delta C}$, described previously). As expected, the spectral perturbations seen for Wzb in the presence of Wzc_{CD} or $Wzc_{CD\Delta C}$, are quite similar. This is not unexpected since one would expect that the phosphorylated YC for Wzc_{CD} would be efficiently dephosphorylated by Wzb during sample preparation before the commencement of the NMR experiments.

The results of the titration are shown in Figure 20 and Figure 21. Overall, the nature of interactions of Wzb with Wzc_{CD} is quite similar to that seen for Wzb /$Wzc_{CD\Delta C}$ interactions. However, a marginally wider Wzb surface appears to be perturbed in the presence of Wzc_{CD} (compare Figure 19 and Figure 21). This difference could be due to the YC interactions of Wzb with the YC.

Note, all our experiments on Wzb were performed in phosphate buffer. Thus, one would expect that inorganic phosphate, the product of the dephosphorylation reaction, would be bound at the catalytic site.

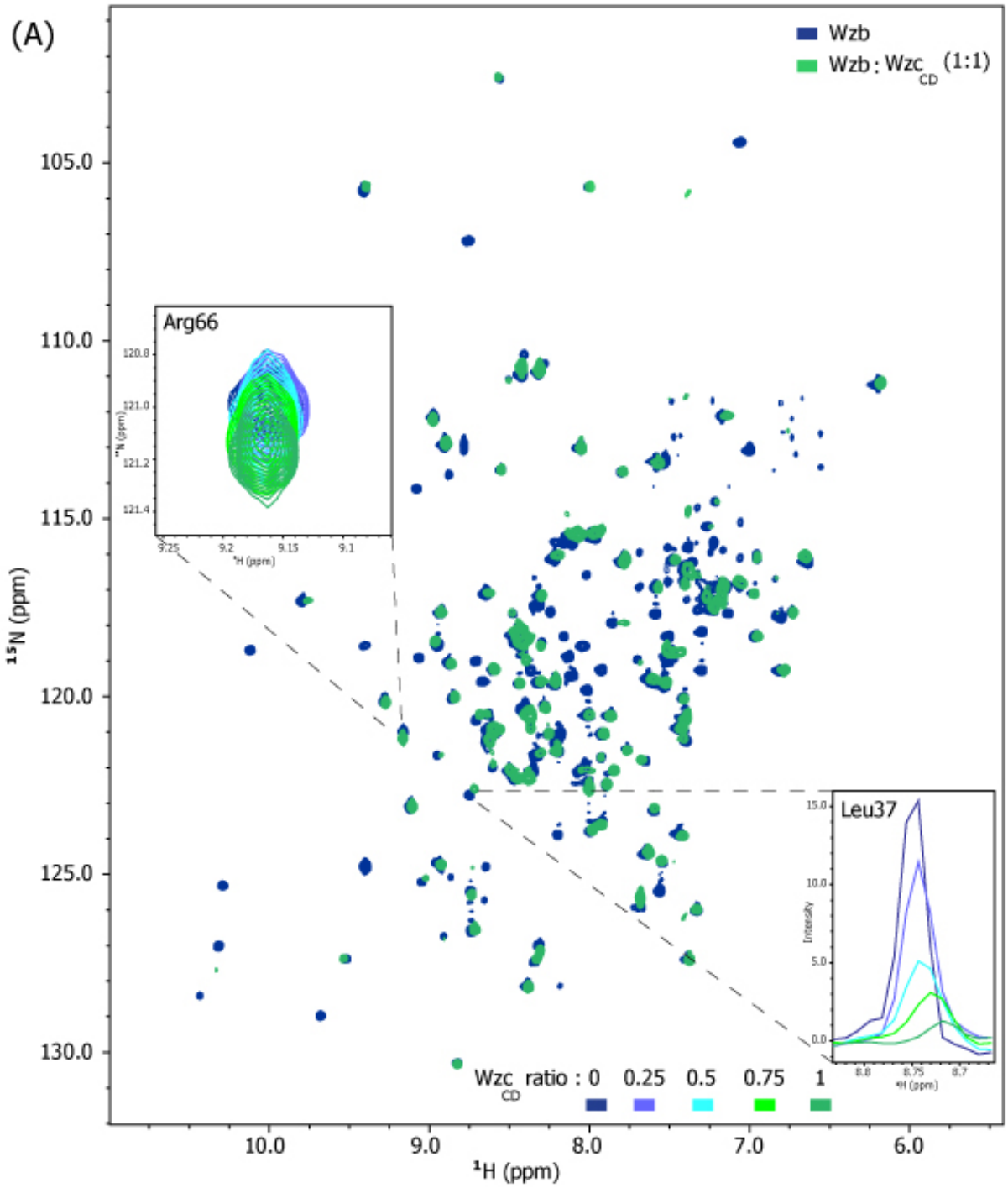
(A)
Wzb
Wzb : Wzc CD (1:1)
Arg66
Leu37
Wzc CD ratio : 0 0.25 0.5 0.75 1
15N (ppm)
1H (ppm)
105.0
110.0
115.0
120.0
125.0
130.0
10.0
9.0
8.0
7.0
6.0

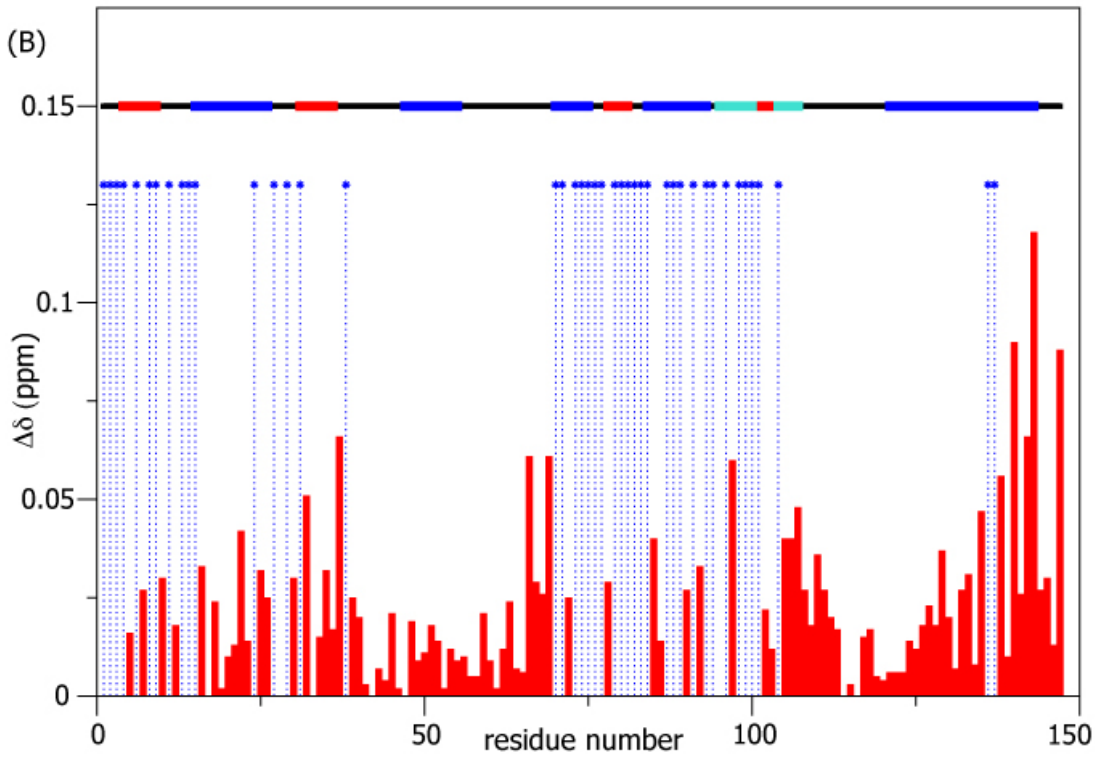

Figure 20: Interactions between Wzb and Wzc_{CD} using Wzb as a probe. (A) Overlay of ^{15}N, ^{1}H, TROSY spectra (900 MHz at 25ºC) of uniformly ^{2}H, ^{15}N-labeled Wzb in the absence (blue) or the presence (green) of an equimolar amount of uniformly ^{2}H-labeled Wzc_{CD}. Insets display representative attenuations (Leu37) chemical shift changes (Arg66) during the titration course. (B) Scaled chemical shift changes in Wzb in the presence of Wzc_{CD} at 1:1 molar ratio (in red). Residues that are broadened beyond the observation threshold are indicated blue dashed vertical lines. Regions of secondary structure in Wzb are indicated as follows: α helices (in thick red lines), β strands (in thick blue lines), loops (black lines) and the 3_{10} helix (in cyan).

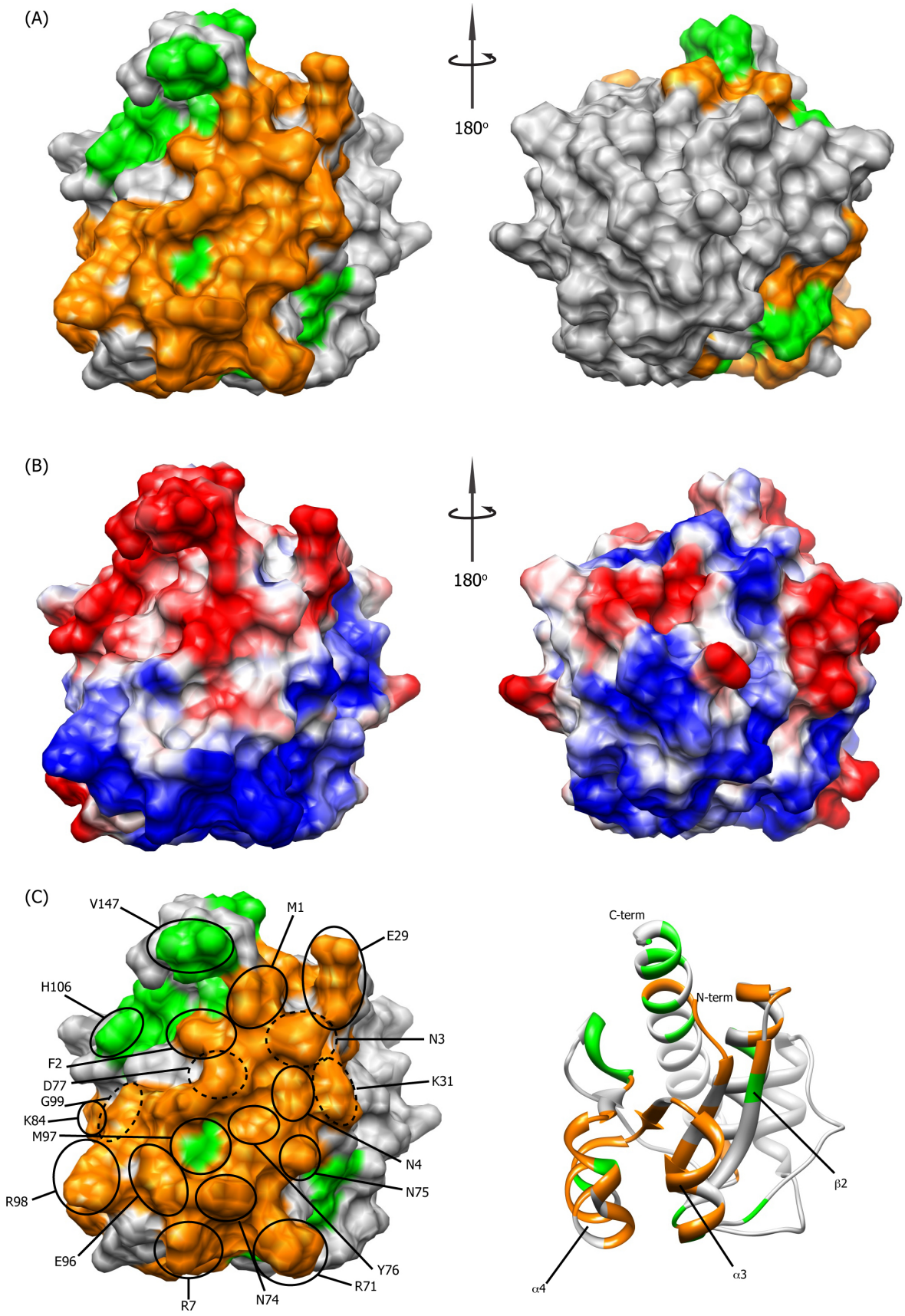
(A)
180°
(B)
180°
(C)
V147
M1
E29
H106
N3
F2
D77
K31
G99
K84
M97
N4
N75
R98
E96
Y76
R71
R7
N74
C-term
N-term
β2
α3
α4

Figure 21: Spectral perturbations in Wzb in the presence of Wzc_{CD} (A) Wzb surface representation in gray was generated by UCSF CHIMERA molecular modeling software (Pettersen et al., 2004). Signal attenuations (orange) and chemical shift changes > 2σ above the mean (in green) for Wzb in the presence of an equimolar amount of Wzc_{CD}, are shown. (B) The Coulombic surface of Wzb is shown. The charge distribution was calculated using UCSF Chimera (Pettersen et al., 2004) using a gradient from -5 kT (red) to +5 kT (blue) (C) Some of the key residues in Wzb which undergo changes in the presence of Wzc_{CD} are circled on the Wzb molecular surface and the α3, α4 helices and the β3 strand are indicated in the corresponding ribbon diagram.

4.5.5. Hallmarks of Wzc_{CD}, $Wzc_{CD\Delta C}$ and Wzb Interactions

In order to define the Wzc_{CD}/Wzb interface, we performed a series of NMR titration experiments by monitoring the interaction of either Wzc_{CD} or $Wzc_{CD\Delta C}$ (using ^{15}N, ^{1}H TROSY experiments) with Wzb. The reverse using TROSY spectra of Wzb in the presence of Wzc_{CD} or $Wzc_{CD\Delta C}$ were also performed. Analyses of these datasets for chemical shift changes and attenuation of resonances, allowed us to define the interface between the catalytic domain of Wzc and Wzb.

Our results indicated that LMW-PTP Wzb docks onto the putative oligomerization surface of Wzc_{CD} (Bechet et al., 2010) that lies opposite to that hosting the catalytic elements of Wzc_{CD}. It has been suggested that Wzc_{CD} oligomers dissociate upon YC phosphorylation (Bechet et al., 2010). It is therefore likely, that monomers are stabilized by interactions with Wzb preventing their reassociation allowing access to the phosphorylated YC that would be occluded in the oligomeric form of Wzc_{CD}.

In addition, it was observed that Wzb docks onto Wzc_{CD}/ $Wzc_{CD\Delta C}$ at a site, which is proximal to the catalytic site. We hypothesize that the spectral perturbations seen for the P-loop residues are likely due to the conformational changes in the upper part of the catalytic site rather than direct binding with Wzc_{CD}/$Wzc_{CD\Delta C}$. Since these perturbations are also observed in the $Wzc_{CD\Delta C}$ that lacks the YC tail, thus may represent reorganization of the Wzb active site to prime it for catalysis upon docking interactions with Wzc_{CD}.

4.6. Dynamic Properties of Wzc_{CD_4C} and Wzb

The spin relaxation experiments, R_1, R_2 and $\{^1H\}$-^{15}N NOE, were recorded on Wzc_{CD_4C}, Wzb and their complexes. These data sets provide deep and detailed information about their dynamics; how these enzymes behave *per se* and along with their partners in solution. These relaxations depend on the probed enzyme's dynamics and are affected by their environment and binding partners.

4.6.1. Dynamic Properties of Wzc_{CD_4C}

We recorded the complete set of experiments at 900 MHz to obtain R_1, R_2 and $\{^1H\}$-^{15}N NOE values on uniformly ^{15}N, ^2H-labeled Wzc_{CD_4C}. Data for 29 peaks out of 176 peaks for which assignments are available, were excluded from the analysis due to spectral overlap. Relaxation rates were extracted from the experimental data using the rate analysis feature of NMRViewJ (Johnson, 2004). The average relaxation rates for structured Wzc_{CD_4C} are as follows: R_1 0.40±0.06 s^{-1}, R_2 32.9± 3.3 s^{-1} and $\{^1H\}$-^{15}N NOE 0.88±0.1 (Figure 22).

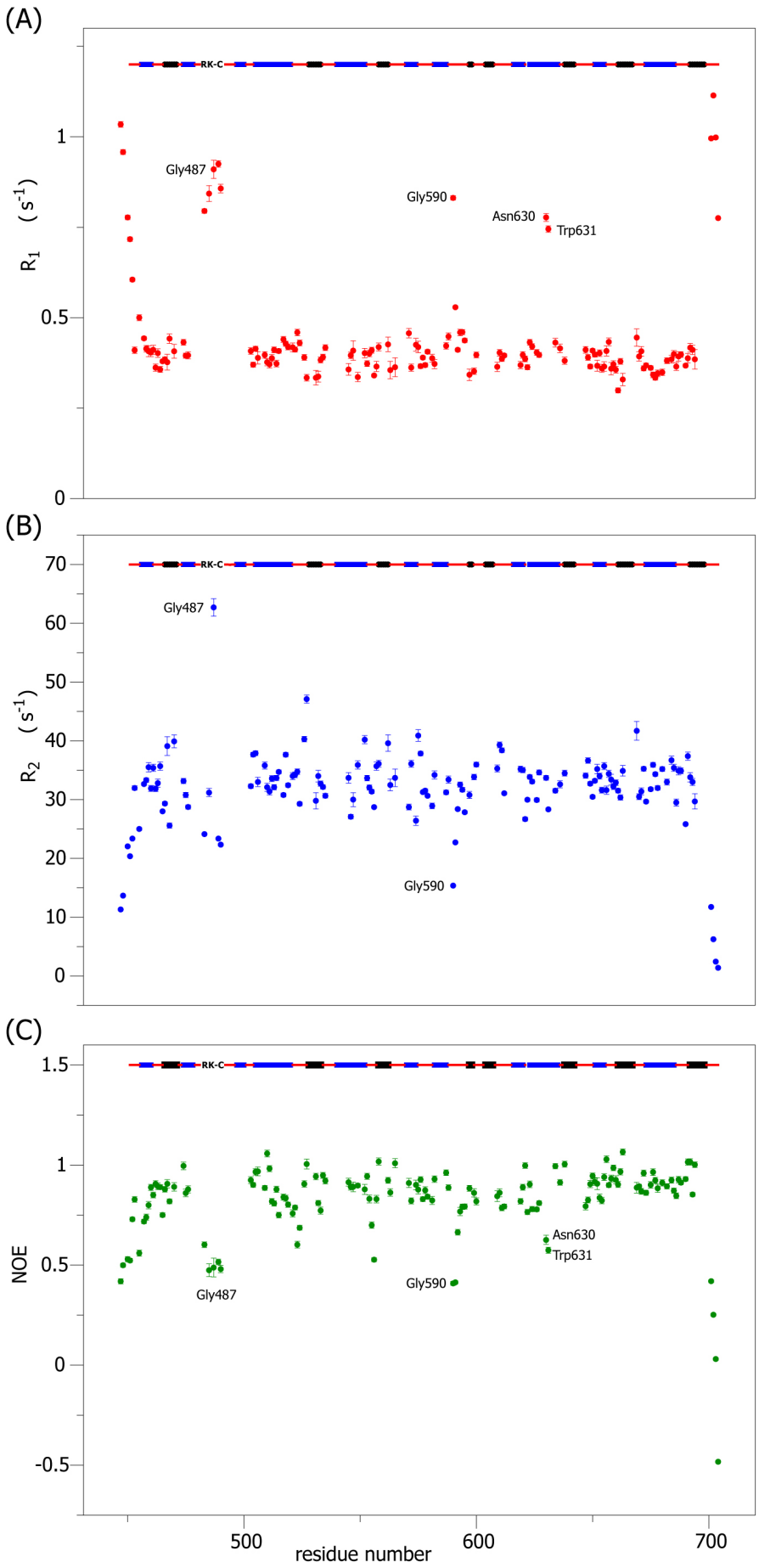
(A)
RK-C
1
0.5
0
R_1 (s^{-1})
Gly487
Gly590
Asn630
Trp631
(B)
RK-C
70
60
50
40
30
20
10
0
R_2 (s^{-1})
Gly487
Gly590
(C)
RK-C
1.5
1
0.5
0
-0.5
NOE
Gly487
Gly590
Asn630
Trp631
500
600
700
residue number

Figure 22: Spin relaxation rates for $Wzc_{CD\Delta C}$. Plots of (A) R_1, (B) R_2 and (C) $\{^1H\}$-^{15}N NOE values for $Wzc_{CD\Delta C}$ are plotted against residue number. Elements of secondary structure are shown on the top of the figure with helices in blue, strands in black and loops in red. Selected outliers in the relaxation rates are labeled.

Some peaks belonging to the RK-cluster (Ser473-Leu496) displayed high R_1 and low R_2 and NOE values. Residues Lys483, Lys489 and Arg490 have R_1 values of 0.8, 0.84 and 0.86 s^{-1} respectively, R_2 values of 24.1, 23.4 and 22.3 s^{-1} respectively, NOE values of 0.6, 0.52 and 0.48 respectively. This is consistent with the fact that the C-terminus of the RK-cluster is not visible in the crystal structure of Wzc (Bechet et al., 2010), suggesting extensive dynamics.

4.6.2. Hydrodynamic and Microdynamic Properties of $Wzc_{CD\Delta C}$

The hydrodynamic properties of uniformly ^{15}N, ^{2}H-labeled $Wzc_{CD\Delta C}$ were determined by program DIFFTENS 2.0 (Ghose et al., 2001a) using R_1, R_2 and $\{^1H\}$-^{15}N NOE at 900 MHz. In addition to previously excluded overlapped peaks, residues with R_2/R_1 values that 1.5σ beyond the mean and those residues with NOE values < 0.75 were excluded from the hydrodynamic analysis. To obtain the amide bond orientations, we utilized the crystal structure of Wzc_{CD} after addition of hydrogen atoms to the amide positions using the program MOLMOL (Koradi et al., 1996) and no further minimization. The analysis yielded axially symmetric model with an axial ratio of 1.12 (Table 2). Given the small rotational anisotropy, an isotropic model was used in all further analyses. The isotropic rotational correlation time (τ_c=1/(6Trace{D})) was found to be 19.4 ns, consistent with that expected for a monomeric species.

Model	D_{xx}	D_{yy}	D_{zz}	α	β	γ	D_{aniso}	D_{asym}
Fully-Asymmetric	0.75 ± 0.06	0.85 ± 0.12	0.94 ± 0.096	165.4 ± 8.0	160.6 ± 3.5	117.6 ± 8.9	1.17	0.10
Axially symmetric	0.82 ± 0.04	0.82 ± 0.04	0.93 ± 0.07	308.7 ± 9.3	146.6 ± 6.4	—	1.12	—
Isotropic	0.86 ± 0.01	0.86 ± 0.01	0.86 ± 0.01	—	—	—	—	—

Table 2: Hydrodynamics of Wzc_{CD_AC} from NMR relaxation rates. D_{ii} (i = x, y, z) are expressed in 10^7 s^{-1}; the angles α, β and γ are in degrees. $D_{aniso}= 2D_{zz}/(D_{xx}+D_{yy})$; $D_{asym}= (D_{yy}-D_{xx})/D_{zz}$

An analysis of the microdynamic parameters of Wzc_{CD_AC} was undertaken using the Lipari-Szabo model-free formalism (Clore et al., 1990; Lipari and Szabo, 1982). However, since the model-free parameters have a highly non-linear dependence on the measured relaxation parameters and may be unreliable in the presence of local motional anisotropy, we also used the reduced spectral density function approach (Ghose et al., 2001a; Natarajan et al., 2006) to obtain a sense of the overall flexibility on a residue-by-residue basis. Of the three sets of reduced spectral density values obtained, namely J(0), J(ω_N) and J(0.87ω_H), J(0.87ω_H) is the most informative, providing information on the sub-ns timescale and should roughly correlate inversely with the Lipari-Szabo generalized order parameter S^2. J(0.87ω_H) was obtained using the following expression (Ghose et al., 2001a; Natarajan et al., 2006)

$$J(0.87\omega_H) = \frac{\gamma_N}{\gamma_H}\frac{1}{5d^2}R_1(1-NOE) \qquad (7)$$

where $d = -\left(\frac{\mu_0\gamma_N\gamma_H\hbar}{8\pi r_{NH}^3}\right)$ and symbols are in their usual meanings.

S^2 and R_{ex} values were obtained using the model-free approach as implemented in the DYNAMICS package (Fushman et al., 1997) (we used the full set of relaxation rates at 900 MHz supplemented with an additional R_2 dataset obtained at 800 MHz to better define the R_{ex} values). R_{ex} values that were 25% less than their corresponding R_2 values were not

interpreted. Microdynamic parameters for those residues that yielded a local correlation time (> 1.9 ns i.e 10% of the overall rotational correlation time) were also not interpreted due to the possible breakdown of the Lipari-Szabo separation of the overall and local motions. Overall $Wzc_{CD\Delta C}$ was found to be quite rigid with an average S^2 value of 0.78±0.26. As expected the N-terminal and the C-terminal residues show low S^2 (0.45±0.28 and 0.08±0.06, respectively) and correspondingly high $J(0.87\omega_H)$ values (33.1±19.2 and 86.4±23.7, respectively, average $J(0.87\omega_H)$ = 11.1±17.2 rad^{-1} ps) values indicating substantial disorder and ps-ns dynamics in the solution (Figure 23). In addition to the extreme termini low S^2 and high $J(0.87\omega_H)$ values were obtained for the loop residues Gly590, Asp591, and Asn630, Trp631 both located on α6. As expected, the RK-cluster also displayed low S^2 (0.26±0.15) and high $J(0.87\omega_H)$ (41.6±6.1) values representing enhanced dynamics on the fast, sub-nanosecond timescale in solution. Interestingly, some residues on the α2 helix - Leu513 (0.47±0.13), His518 (0.33±0.12) and Met522 (0.35±0.12); Gln457 (0.35±0.06) on αA; and Ala468 (0.37±0.13) on βA show relatively low S^2 values. These residues lie on the oligomerization surface of Wzc_{CD}. Further interpretation of the fast dynamics in $Wzc_{CD\Delta C}$ is to likely to be facilitated by a ~10 ns molecular dynamics simulation of $Wzc_{CD\Delta C}$ in explicit solvent, currently underway in the laboratory.

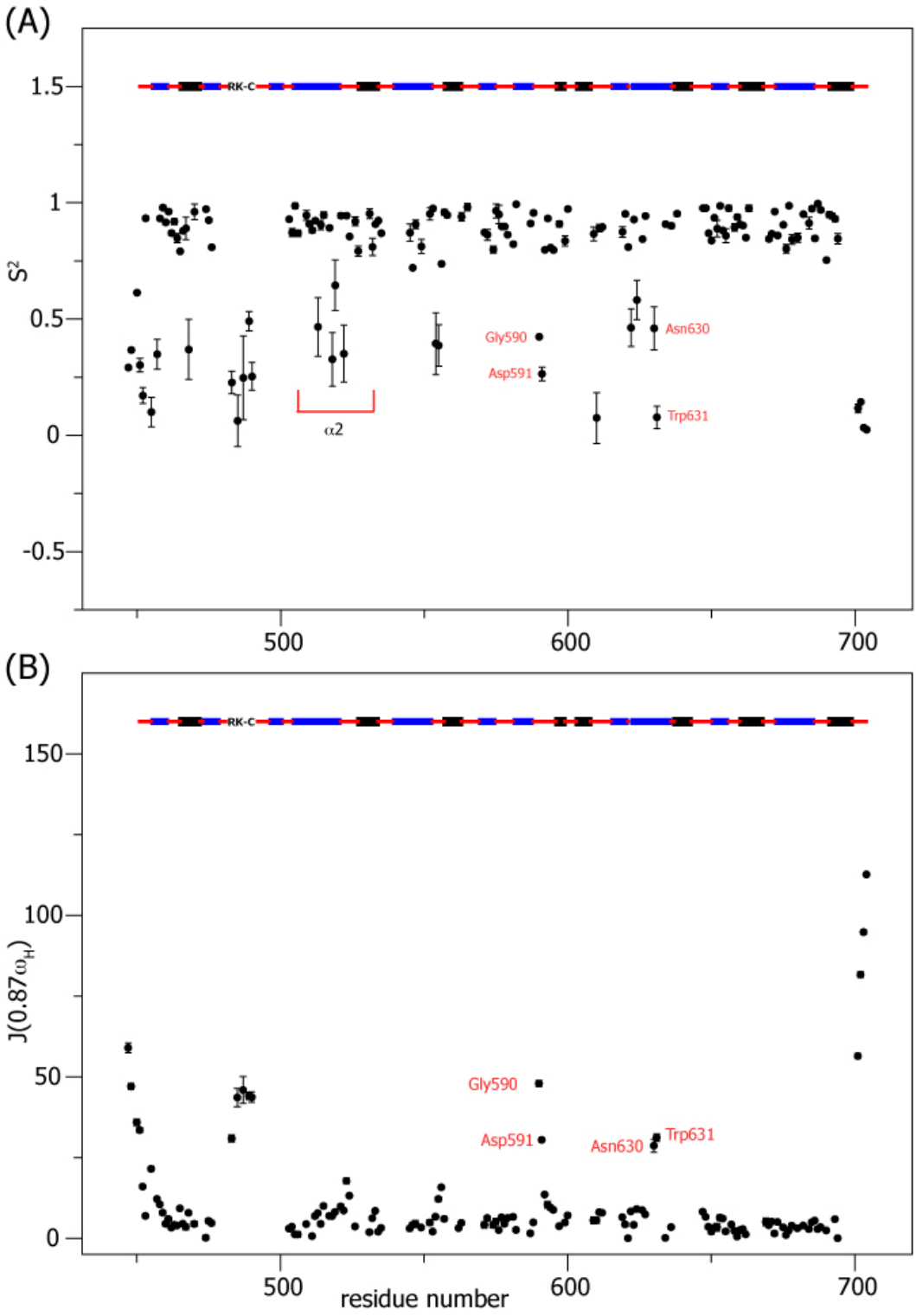

Figure 23: Fast, sub-nanosecond dynamics in Wzc_{CD_4C}. (A) S^2 values were obtained from a Lipari-Szabo model-free analysis utilizing R_1, R_2 and $\{^1H\}$-^{15}N NOE data at 900 MHz supplemented with an additional R_2 dataset at 800 MHz. Selected residues with low S^2 values are indicated. (B) Reduced spectral density values near ^1H Larmor frequency were plotted. Selected residues with elevated $J(0.87\omega_H)$ values are labeled. Secondary structural elements are indicated as before.

Slow conformational dynamics on the μs-ms timescale were obtained as R_{ex} values in the model-free analysis as discussed previously (Figure 24). The largest R_{ex} value was observed for Gly487 53.0±6.9 s^{-1} (R_{ex} values for 900 MHz reported). This residue is located in the RK-cluster. The average R_{ex} values for the RK-cluster was found to be is 27.1±18.5 s^{-1}. As mentioned previously, the RK-cluster was found to possess low S^2 values. Thus, it appears that the RK-cluster is dynamic both on the sub-ns as well as the μs-ms timescale. Significant R_{ex} values were also seen for several residues that constitute the oligomerization surface i.e. Gln457 (19.9±2.1 s^{-1}) on αA, Leu513 (15.3±4.6 s^{-1}) and Met522 (21.4±4.6 s^{-1}) on α2 display significant R_{ex} values suggesting μs-ms timescale dynamics in solution.

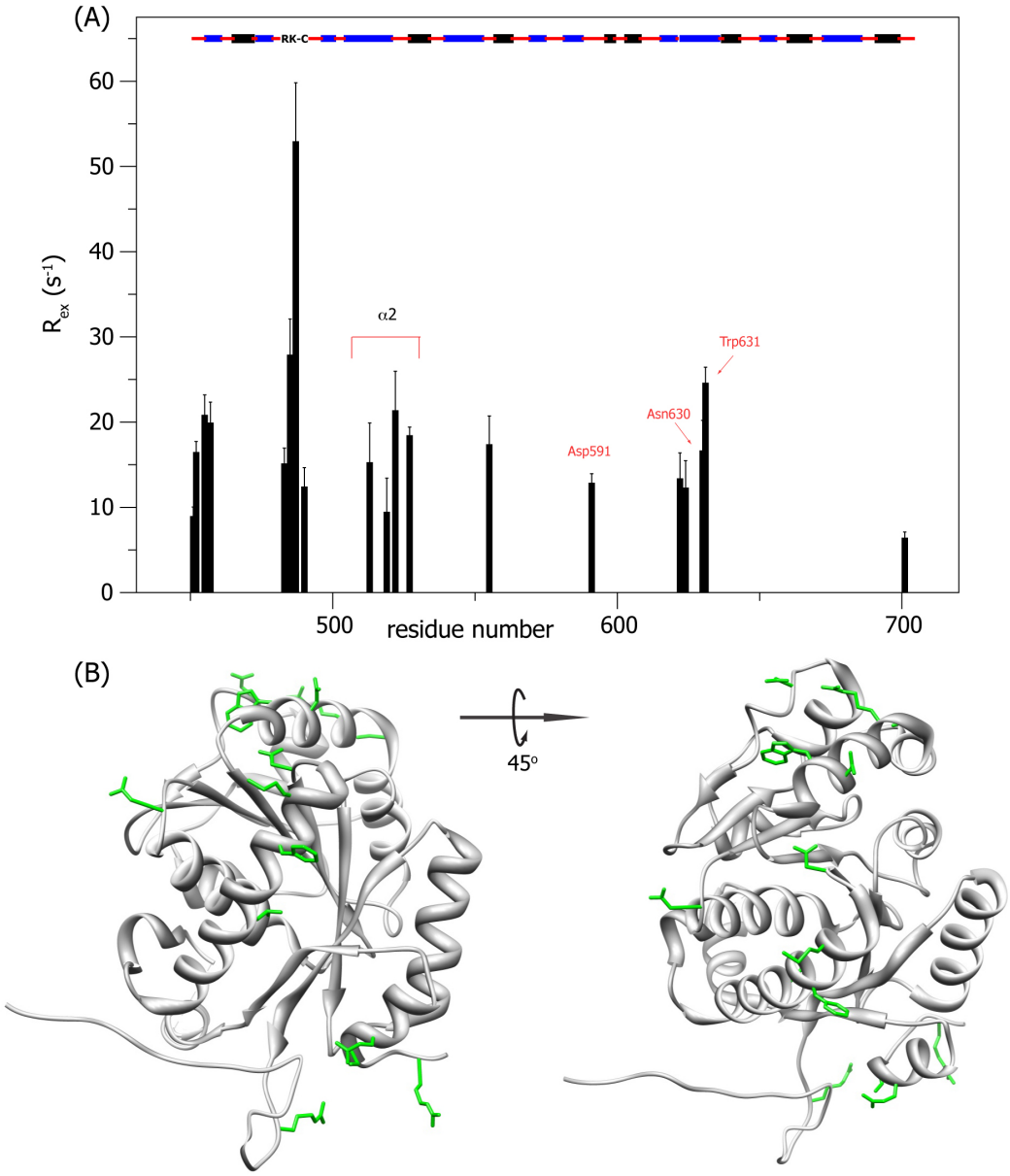

Figure 24: Slow dynamics in $Wzc_{CD\Delta C}$. (A) R_{ex} values calculated from a Lipari-Szabo model-free analysis plotted against residue number. Secondary structural elements are shown as before. (B) Residues with significant R_{ex} values depicted on the structure of Wzc_{CD}.

4.6.3. Further Evidence for the Formation of a Complex between Wzc_{CD} and Wzb

As will be discussed below, measurement of the spin-spin relaxation rates (R_2) values of $Wzc_{CD\Delta C}$ (and Wzc_{CD}) in the presence of equimolar amounts of Wzb, and that of Wzb in the presence equimolar amounts of $Wzc_{CD\Delta C}$ (and Wzc_{CD}) indicate complex formation. Most notably, in the case of the Wzc_{CD}/Wzb complex, it provides additional evidence that Wzb indeed disrupts the oligomerization of Wzc_{CD}.

In order to characterize the hydrodynamic properties of Wzb in the free state, a complete set of R_1, R_2 and $\{^1H\}$-^{15}N NOE relaxation experiments were recorded on ^{15}N-labeled Wzb at 600 MHz and 25°C. While high-quality data could be obtained for all 141 expected resonances, 19 were excluded due to insufficient spectral resolution. Relaxation values were obtained using NMRViewJ (Johnson, 2004). The average relaxation values for Wzb were found to be R_1 1.16±0.05 s^{-1}, R_2 14.5±2.9 s^{-1} and $\{^1H\}$-^{15}N NOE 0.79±0.06 (Figure 25).

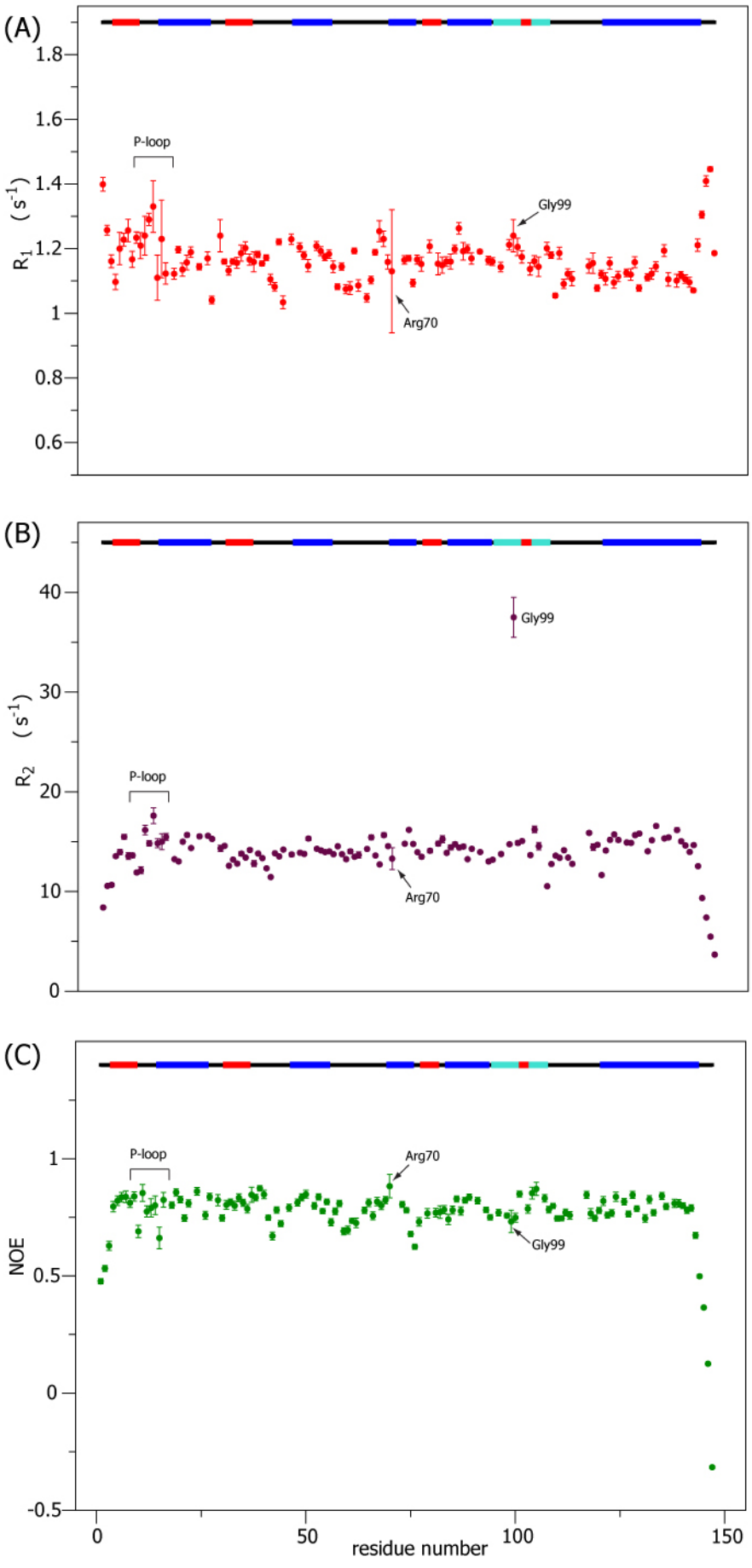
(A)
1.8
1.6
1.4
1.2
1
0.8
0.6
R1 (s-1)
P-loop
Gly99
Arg70
(B)
40
30
20
10
0
R2 (s-1)
Gly99
P-loop
Arg70
(C)
1
0.5
0
-0.5
NOE
P-loop
Arg70
Gly99
0
50
100
150
residue number

Figure 25: Spin relaxation values for ^{15}N-labeled Wzb. Experiments were recorded at 600 MHz at 25°C. Secondary structure elements are represented as follows is drawn at the top of each graph. Think black lines represent loops, red rectangles for β-strands, blue rectangles for α-helices and green rectangles represents the 3_{10} helix.

As in the case of $Wzc_{CD\Delta C}$, the hydrodynamic properties of Wzb were determined using the DIFFTENS 2.0 program (Ghose et al., 2001a). In addition to the overlapped peaks, residues with $\{^1H\}$-^{15}N NOE values < 0.6 and 6 additional peaks that had R_2/R_1 ratios > 1.5σ beyond the standard deviation were excluded from the analysis. Amide vector orientations were obtained from representative models of the NMR structure of Wzb (PDB ID: 2FEK) (Lescop et al., 2006). As shown in Table 3, an axially-symmetric diffusion tensor with an axial ratio of 1.21 was obtained and the effective correlation time was found to be 10.8 ns consistent with that expected for a monomeric species.

Model	D_{xx}	D_{yy}	D_{zz}	α	β	γ	D_{aniso}	D_{asym}
Fully-Asymmetric	1.42 ± 0.06	1.52 ± 0.07	1.78 ± 0.07	95.7 ± 1.5	137.2 ± 1.2	103.1 ± 0.5	1.51	0.05
Axially symmetric	1.46 ± 0.02	1.46 ± 0.02	1.77 ± 0.05	96.7 ± 2.5	136.0 ± 1.2	—	1.21	—
Isotropic	1.54 ± 0.01	1.54 ± 0.01	1.54 ± 0.01	—	—	—	—	—

Table 3: Hydrodynamics of Wzb from NMR relaxation rates. D_{ii} (i = x, y, z) are expressed in 10^7 s^{-1}; the angles α, β and γ are in degrees. $D_{aniso}= 2D_{zz}/(D_{xx}+D_{yy})$; $D_{asym}= (D_{yy}-D_{xx})/D_{zz}$

Having demonstrated that both $Wzc_{CD\Delta C}$ and Wzb were monomeric in solution (rotational correlation times of 19.4 ns and 10.8 ns respectively), we proceeded to measure the spin-spin relaxation rates of uniformly ^{15}N, ^{2}H-labeled $Wzc_{CD\Delta C}$ in the absence or the presence of an equimolar amount of uniformly ^{2}H-labeled Wzb at 800 MHz and 25°C. Data for 25 peaks were excluded due to spectral overlap or low intensity in the protein complex. The average R_2 values for $Wzc_{CD\Delta C}$ (reference) and $Wzc_{CD\Delta C}$/Wzb (complex) were found to be

29.6±3.2 s^{-1} and 40.3±7.4 s^{-1}, respectively (Figure 26). The former rate is consistent with that expected for monomeric $Wzc_{CD\Delta C}$ at 800 MHz. The latter (assuming isotropic overall diffusion) is roughly indicative of a species with a correlation time of around 28 ns roughly consistent with a 1:1 complex. Comparing the relaxation rates in a site-specific manner was not performed.

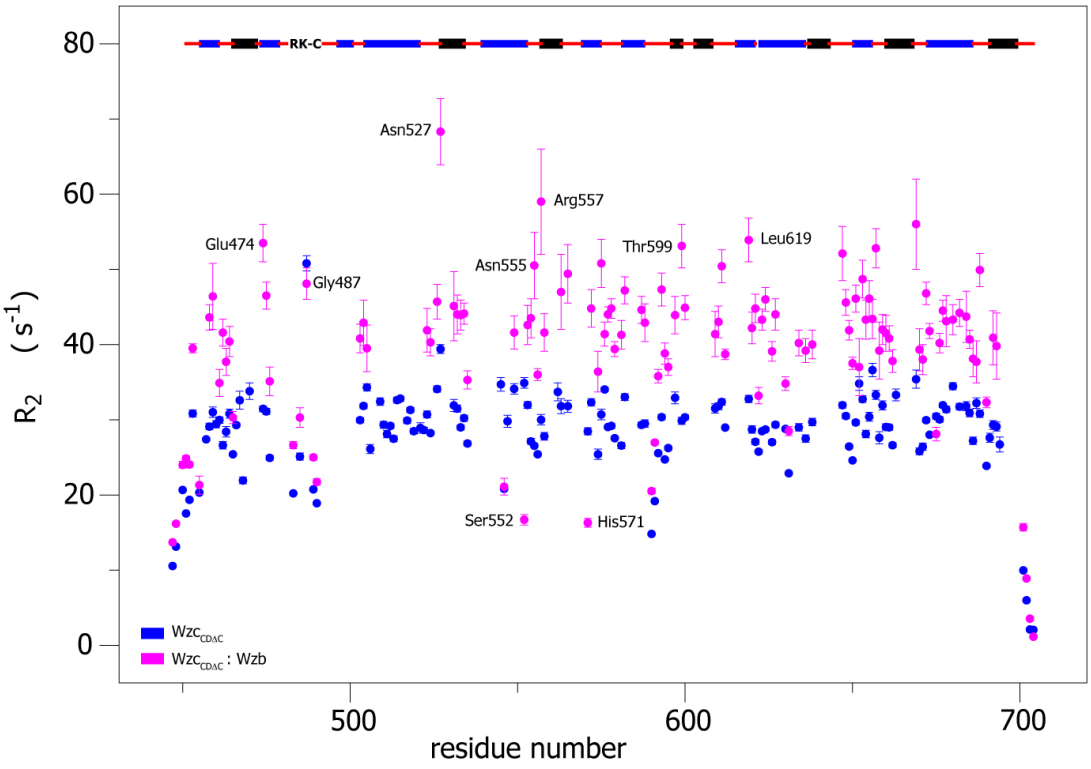

Figure 26: Spin-spin relaxation rates in a $Wzc_{CD\Delta C}$/Wzb complex. R_2 values at 800 MHz spectrometer uniformly ^{15}N, ^{2}H-labeled $Wzc_{CD\Delta C}$ in the absence (blue) or presence (magenta) of uniformly-^{2}H labeled Wzb. R_2 outliers are indicated. Secondary structure elements are shown as before.

Next, we recorded a set of spin-spin relaxation experiments on 100 μM uniformly ^{15}N, ^{2}H-labeled Wzc_{CD} with and without an equimolar amount of uniformly ^{2}H-labeled Wzb at 800 MHz and 25°C. The average transverse relaxation rate for uniformly ^{15}N, ^{2}H-labeled Wzc_{CD} structured regions was found to be 53.6±7.6 s^{-1}. This was significantly larger than that expected for a protein this size. It has been previous shown that the presence of a long disordered tail adds to the hydrodynamic drag (Ghose et al., 2001b). HYDRONMR (Garcia de la Torre et al., 2000) calculations on $Wzc_{CD\Delta C}$ (using a high-temperature MD generated ensemble in vacuum) and Wzc_{CD} predicted (assuming an S^2=1) an overall increase of 50% (clearly an upper limit) in the R_2 value of the latter over that in the former. The observed increase, on the other hand, is found to be ~83%. The magnitude of this increase, even in the most conservative estimates, cannot simply be attributed to the hydrodynamic drag due to the presence of the disordered YC. Therefore, it may be concluded, that partial oligomerization of Wzc_{CD} occurs at the concentration employed for NMR studies. Interestingly, uniformly ^{15}N, ^{2}H-labeled Wzc_{CD} in the presence of equimolar amounts of uniformly ^{2}H-labeled Wzb yielded an average R_2 value of 56.6±8.0 s^{-1} (Figure 27), only a marginal increase. Thus, there could be two possible reasons for this modest increase: (1) the nature of interactions of Wzb with Wzc_{CD} is quite different from its interactions with $Wzc_{CD\Delta C}$ or (2) Wzb binds to and prevents oligomerization of Wzc_{CD} and the associations largely involve Wzc_{CD} and Wzb monomers. However, we have shown that the spectral perturbations on Wzb are essentially the same in the presence of $Wzc_{CD\Delta C}$ or $Wzc_{CD.}$ Additionally, $Wzc_{CD\Delta C}$ and Wzc_{CD} also display similar perturbations in the core residues in the presence of Wzb. Thus scenario (1) appears highly unlikely. This, coupled to the fact we have demonstrated that the Wzb binding surface on $Wzc_{CD\Delta C}$ (or Wzc_{CD}) overlaps with the oligomerization surface of the latter, reinforces scenario (2).

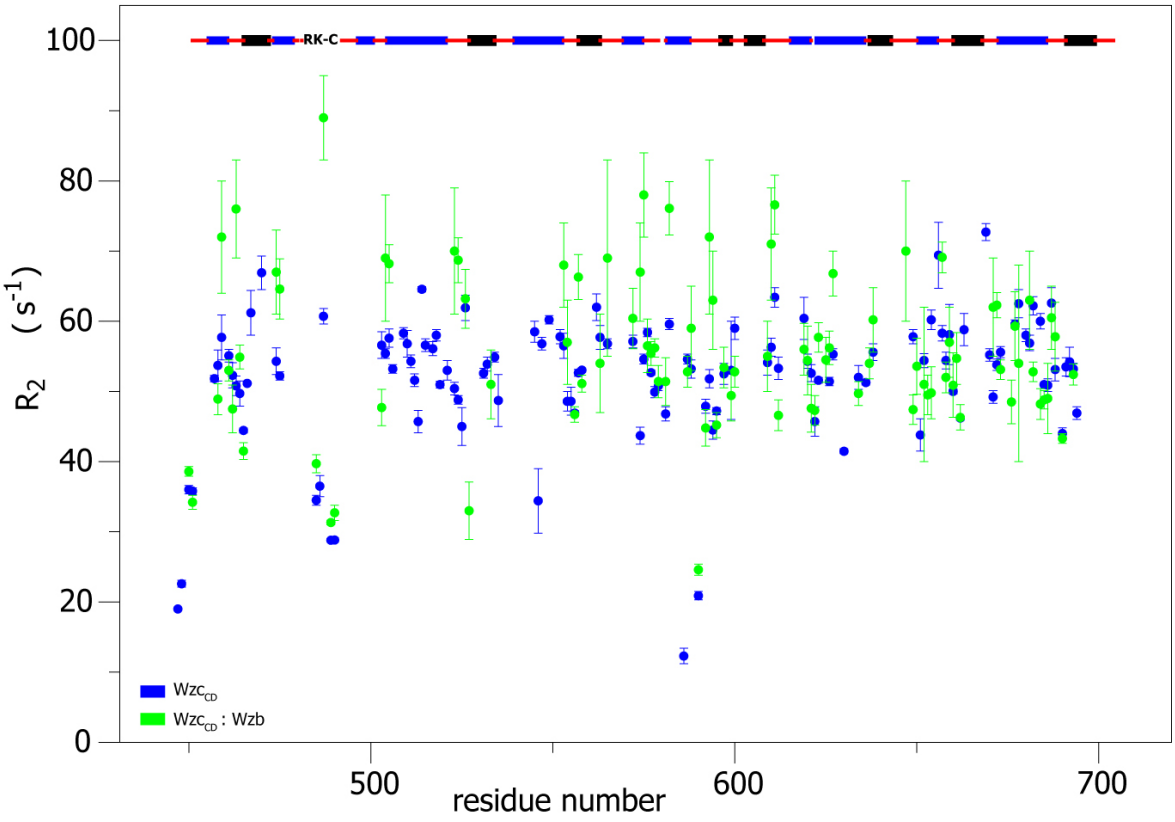

Figure 27: Spin-spin relaxation rates in a Wzc_{CD}/Wzb complex. R_2 values at 800 MHz spectrometer for uniformly ^{15}N, ^{2}H-labeled Wzc_{CD} in the absence (blue) or the presence of an equimolar ratio of uniformly ^{-2}H-labeled Wzb (green).

For a final confirmation of the hydrodynamic properties of the $Wzc_{CD_\Delta C}$/Wzb complex, we measured the spin-spin relaxation rates of uniformly ^{15}N, ^{2}H-labeled Wzb in the presence of ^{2}H-labeled $Wzc_{CD_\Delta C}$ at 800 MHz. The average R_2 for the reference (free Wzb) was 16.3±4.6 s^{-1}. A large increase in the average R_2 value (32.7±3.7 s^{-1}) occurred in the presence of a 1:1 ratio of uniformly-^{2}H labeled $Wzc_{CD_\Delta C}$ (Figure 28). This value is consistent with that (40.3±7.4 s^{-1}, see discussion above) measured for $Wzc_{CD_\Delta C}$ in the presence of an equimolar amount of Wzb. This is only to be expected since the same complex is being probed in both cases and the measured overall hydrodynamic properties are expected to be the same. Minor differences may be attributed to the fact that the internal dynamics of $Wzc_{CD_\Delta C}$ and Wzb in their complex are different, leading to a distinct distribution of R_2 values for each.

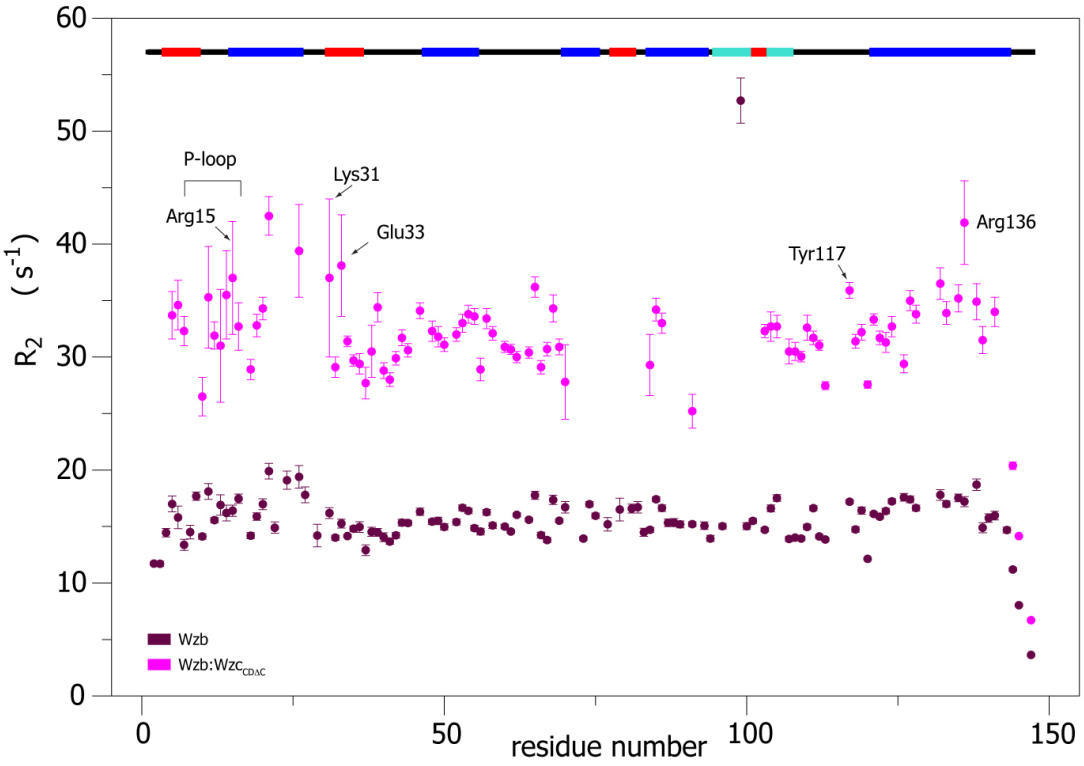

Figure 28: Spin-spin relaxation rates in a Wzb/Wzc$_{CD\Delta C}$ complex. R_2 values at 800 MHz for uniformly ^{15}N, ^{2}H-labeled Wzb in the absence (maroon) and the presence (magenta) of uniformly ^{2}H-labeled Wzc$_{CD\Delta C}$. Secondary structure elements are indicated as before.

5. Conclusions

BY-kinases play a central role in bacterial physiology by regulating the synthesis of polysaccharides responsible for capsule and biofilm formation that facilitate survival under a variety of environmental stress conditions. The polysaccharide assemblies are anti-phagocytic and are often indispensible in avoiding the immune response of host cells for pathogenic species during infection. BY-kinases constitute a unique class of enzymes that do not share any sequence and structural homology with their eukaryal counterparts. *Escherichia coli* K12 cells harbor a BY-kinase Wzc and its LMW-PTP Wzb. Wzc_{CD} (the catalytic domain of Wzc) has 5 phosphorylatable tyrosine residues located at the C-terminal tail that undergo intermolecular autophosphorylation. These tyrosines are subsequently dephosphorylated by Wzb. The phosphorylation/dephosphorylation processes also affects the oligomerization state of Wzc. The cycling between autophosphorylation of Wzc_{CD} resulting in monomer formation and dephosphorylation of this YC-cluster by the cytosolic Wzb and subsequent oligomerization of Wzc_{CD} appears to be indispensible for the synthesis and export of the exopolysaccharide, colanic acid. While large amounts of biological and biochemical data exist on the regulation of Wzc by Wzb, the structural and mechanistic determinants of their interactions were poorly defined.

Towards the goal of identifying the Wzc_{CD}/Wzb interface, we used solution NMR spectroscopy techniques, a powerful and sensitive biophysical method to decipher molecular interactions *in vitro*. After assigning the spectral resonances for Wzc_{CD} and Wzb, we performed a series of titrations by probing both enzymes. Our data indicated that $Wzc_{CD\Delta C}$ utilizes a surface that largely overlaps with its putative oligomerization surface, to bind Wzc. Wzb, on the other hand utilizes a site that proximal to its catalytic site, likely to allow easy access to its substrate, the phosphorylated YC of Wzc_{CD}.

While the research described here provides significant insight into the nature of the Wzc/Wzb interface, it requires confirmation through site-directed mutational analysis and testing their effects both *in vitro* and *in vivo* through specific physiological readouts – production of colanic acid and cellular viability under stress conditions. Given the conservation of BY-kinase/LMW-PTP pairs in both gram-negative and gram-positive species and the proven clinical importance of bacterial capsules in the pathogenesis of species such as *S. aureus* (O'Riordan and Lee, 2004) and *S. pneumoniae* (Morona et al., 2006), it would be worthwhile to undertake analyses similar to the work described here in a larger group of bacterial species.

REFERENCES

Alonso, A., Sasin, J., Bottini, N., Friedberg, I., Osterman, A., Godzik, A., Hunter, T., Dixon, J., and Mustelin, T. (2004). Protein tyrosine phosphatases in the human genome. Cell *117*, 699-711.

Bakal, C.J., and Davies, J.E. (2000). No longer an exclusive club: eukaryotic signalling domains in bacteria. Trends Cell Biol *10*, 32-38.

Bechet, E., Gruszczyk, J., Terreux, R., Gueguen-Chaignon, V., Vigouroux, A., Obadia, B., Cozzone, A.J., Nessler, S., and Grangeasse, C. (2010). Identification of structural and molecular determinants of the tyrosine-kinase Wzc and implications in capsular polysaccharide export. Mol Microbiol *77*, 1315-1325.

Bechet, E., Guiral, S., Torres, S., Mijakovic, I., Cozzone, A.J., and Grangeasse, C. (2009). Tyrosine-kinases in bacteria: from a matter of controversy to the status of key regulatory enzymes. Amino Acids *37*, 499-507.

Bottini, N., Bottini, E., Gloria-Bottini, F., and Mustelin, T. (2002). Low-molecular-weight protein tyrosine phosphatase and human disease: in search of biochemical mechanisms. Arch Immunol Ther Exp (Warsz) *50*, 95-104.

Burnett, G., and Kennedy, E.P. (1954). The enzymatic phosphorylation of proteins. J Biol Chem *211*, 969-980.

Bussi, G., Donadio, D., and Parrinello, M. (2007). Canonical sampling through velocity rescaling. J Chem Phys *126*, 014101.

Cavanagh, J., Fairbrother, W.J., Palmer, A.G., 3rd, Rance, M., and Skelton, N.J. (2007). Protein NMR spectroscopy: Principles and practice (Elsevier academic press).

Clore, G.M., Szabo, A., and al., e. (1990). Deviations from the simple two-parameter model-free approach to the interpretation of nitrogen-15 nuclear magnetic relaxation of proteins. J Am Chem Soc *112*, 4989-4936.

Cohen, P. (2002). The origins of protein phosphorylation. Nat Cell Biol *4*, E127-130.

Collet, J.F., Stroobant, V., Pirard, M., Delpierre, G., and Van Schaftingen, E. (1998). A new class of phosphotransferases phosphorylated on an aspartate residue in an amino-terminal DXDX(T/V) motif. J Biol Chem *273*, 14107-14112.

Collins, R.F., Beis, K., Clarke, B.R., Ford, R.C., Hulley, M., Naismith, J.H., and Whitfield, C. (2006). Periplasmic protein-protein contacts in the inner membrane protein Wzc form a tetrameric complex required for the assembly of Escherichia coli group 1 capsules. J Biol Chem *281*, 2144-2150.

Collins, R.F., Beis, K., Dong, C., Botting, C.H., McDonnell, C., Ford, R.C., Clarke, B.R., Whitfield, C., and Naismith, J.H. (2007). The 3D structure of a periplasm-spanning platform required for assembly of group 1 capsular polysaccharides in Escherichia coli. Proc Natl Acad Sci U S A *104*, 2390-2395.

Cozzone, A.J. (2005). Role of protein phosphorylation on serine/threonine and tyrosine in the virulence of bacterial pathogens. J Mol Microbiol Biotechnol *9*, 198-213.

Cozzone, A.J., Grangeasse, C., Doublet, P., and Duclos, B. (2004). Protein phosphorylation on tyrosine in bacteria. Arch Microbiol *181*, 171-181.

Delaglio, F., Grzesiek, S., Vuister, G.W., Zhu, G., Pfeifer, J., and Bax, A. (1995). NMRPipe: a multidimensional spectral processing system based on UNIX pipes. J Biomol NMR *6*, 277-293.

Doublet, P., Grangeasse, C., Obadia, B., Vaganay, E., and Cozzone, A.J. (2002). Structural organization of the protein-tyrosine autokinase Wzc within Escherichia coli cells. J Biol Chem *277*, 37339-37348.

Duclos, B., Grangeasse, C., Vaganay, E., Riberty, M., and Cozzone, A.J. (1996). Autophosphorylation of a bacterial protein at tyrosine. J Mol Biol *259*, 891-895.

Dutta, K., Cox, C.J., Basavappa, R., and Pascal, S.M. (2008). 15N relaxation studies of Apo-Mts1: a dynamic S100 protein. Biochemistry *47*, 7637-7647.

Ferrage, F., Cowburn, D., and Ghose, R. (2009). Accurate sampling of high-frequency motions in proteins by steady-state 15N-{1H} nuclear Overhauser effect measurements in the presence of cross-correlated relaxation. J Am Chem Soc *131*, 6048-6049.

Ferrage, F., Piserchio, A., Cowburn, D., and Ghose, R. (2008). On the measurement of 15N-{1H} nuclear Overhauser effects. J Magn Reson *192*, 302-313.

Fiaschi, T., Chiarugi, P., Buricchi, F., Giannoni, E., Taddei, M.L., Talini, D., Cozzi, G., Zecchi-Orlandini, S., Raugei, G., and Ramponi, G. (2001). Low molecular weight protein-tyrosine phosphatase is involved in growth inhibition during cell differentiation. J Biol Chem *276*, 49156-49163.

Flynn, P.F., Mattiello, D.L., Hill, H.D.W., and Wand, A.J. (2000). Optimal Use of Cryogenic Probe Technology in NMR Studies of Proteins. J Am Chem Soc *122*, 4823-4824.

Fushman, D., Cahill, S., and Cowburn, D. (1997). The main-chain dynamics of the dynamin pleckstrin homology (PH) domain in solution: analysis of 15N relaxation with monomer/dimer equilibration. J Mol Biol *266*, 173-194.

Gao, R., and Stock, A.M. (2009). Biological insights from structures of two-component proteins. Annu Rev Microbiol *63*, 133-154.

Garcia de la Torre, J., Huertas, M.L., and Carrasco, B. (2000). HYDRONMR: prediction of NMR relaxation of globular proteins from atomic-level structures and hydrodynamic calculations. J Magn Reson *147*, 138-146.

Ghose, R., Fushman, D., and Cowburn, D. (2001a). Determination of the rotational diffusion tensor of macromolecules in solution from nmr relaxation data with a combination of exact and approximate methods--application to the determination of interdomain orientation in multidomain proteins. J Magn Reson *149*, 204-217.

Ghose, R., Shekhtman, A., Goger, M.J., Ji, H., and Cowburn, D. (2001b). A novel, specific interaction involving the Csk SH3 domain and its natural ligand. Nat Struct Biol *8*, 998-1004.

Goujon, M., McWilliam, H., Li, W., Valentin, F., Squizzato, S., Paern, J., and Lopez, R. (2010). A new bioinformatics analysis tools framework at EMBL-EBI. Nucleic Acids Res *38*, W695-699.

Grangeasse, C., Cozzone, A.J., Deutscher, J., and Mijakovic, I. (2007). Tyrosine phosphorylation: an emerging regulatory device of bacterial physiology. Trends Biochem Sci *32*, 86-94.

Grangeasse, C., Doublet, P., and Cozzone, A.J. (2002). Tyrosine phosphorylation of protein kinase Wzc from Escherichia coli K12 occurs through a two-step process. J Biol Chem *277*, 7127-7135.

Grangeasse, C., Doublet, P., Vaganay, E., Vincent, C., Deleage, G., Duclos, B., and Cozzone, A.J. (1997). Characterization of a bacterial gene encoding an autophosphorylating protein tyrosine kinase. Gene *204*, 259-265.

Guo, H., Yi, W., Song, J.K., and Wang, P.G. (2008). Current understanding on biosynthesis of microbial polysaccharides. Curr Top Med Chem *8*, 141-151.

Hagelueken, G., Huang, H., Mainprize, I.L., Whitfield, C., and Naismith, J.H. (2009). Crystal structures of Wzb of Escherichia coli and CpsB of Streptococcus pneumoniae, representatives of two families of tyrosine phosphatases that regulate capsule assembly. J Mol Biol *392*, 678-688.

Hanks, S.K., Quinn, A.M., and Hunter, T. (1988). The protein kinase family: conserved features and deduced phylogeny of the catalytic domains. Science *241*, 42-52.

Hess, B., Bekker, H., Berendsen, H.J.C., and Fraaije, J. (1997). G. E. M. LINCS: A linear constraint solver for molecular simulations.

. J Comp Chem *18*, 1463-1472.

Hess, B., Kutzner, C., Van Der Spoel, D., and Lindahl, E. (2008). GROMACS 4: Algorithms for Highly Efficient, Load-Balanced, and Scalable Molecular Simulation. J Chem Theory Comput *4*.

Holm, L., and Rosenstrom, P. (2010). Dali server: conservation mapping in 3D. Nucleic Acids Res *38*, W545-549.

Hunter, T. (1995). Protein kinases and phosphatases: the yin and yang of protein phosphorylation and signaling. Cell *80*, 225-236.

Ilan, O., Bloch, Y., Frankel, G., Ullrich, H., Geider, K., and Rosenshine, I. (1999). Protein tyrosine kinases in bacterial pathogens are associated with virulence and production of exopolysaccharide. EMBO J *18*, 3241-3248.

Jadeau, F., Bechet, E., Cozzone, A.J., Deleage, G., Grangeasse, C., and Combet, C. (2008). Identification of the idiosyncratic bacterial protein tyrosine kinase (BY-kinase) family signature. Bioinformatics *24*, 2427-2430.

Johnson, B.A. (2004). Using NMRView to visualize and analyze the NMR spectra of macromolecules. Methods Mol Biol *278*, 313-352.

Johnson, L.N. (2009). The regulation of protein phosphorylation. Biochem Soc Trans *37*, 627-641.

Kennelly, P.J., and Potts, M. (1996). Fancy meeting you here! A fresh look at "prokaryotic" protein phosphorylation. J Bacteriol *178*, 4759-4764.

Kim, H.S., Lee, S.J., Yoon, H.J., An, D.R., Kim do, J., Kim, S.J., and Suh, S.W. (2011). Crystal structures of YwqE from Bacillus subtilis and CpsB from Streptococcus pneumoniae, unique metal-dependent tyrosine phosphatases. J Struct Biol *175*, 442-450.

Klein, G., Dartigalongue, C., and Raina, S. (2003). Phosphorylation-mediated regulation of heat shock response in Escherichia coli. Mol Microbiol *48*, 269-285.

Kobir, A., Shi, L., Boskovic, A., Grangeasse, C., Franjevic, D., and Mijakovic, I. (2011). Protein phosphorylation in bacterial signal transduction. Biochim Biophys Acta *1810*, 989-994.

Kolot, M., Gorovits, R., Silberstein, N., Fichtman, B., and Yagil, E. (2008). Phosphorylation of the integrase protein of coliphage HK022. Virology *375*, 383-390.

Koradi, R., Billeter, M., and Wuthrich, K. (1996). MOLMOL: a program for display and analysis of macromolecular structures. J Mol Graph *14*, 51-55, 29-32.

Krebs, E.G., and Fischer, E.H. (1956). The phosphorylase b to a converting enzyme of rabbit skeletal muscle. Biochim Biophys Acta *20*, 150-157.

Lacour, S., Bechet, E., Cozzone, A.J., Mijakovic, I., and Grangeasse, C. (2008). Tyrosine phosphorylation of the UDP-glucose dehydrogenase of Escherichia coli is at the crossroads of colanic acid synthesis and polymyxin resistance. PLoS One *3*, e3053.

Larkin, M.A., Blackshields, G., Brown, N.P., Chenna, R., McGettigan, P.A., McWilliam, H., Valentin, F., Wallace, I.M., Wilm, A., Lopez, R.*, et al.* (2007). Clustal W and Clustal X version 2.0. Bioinformatics *23*, 2947-2948.

Lee, D.C., Zheng, J., She, Y.M., and Jia, Z. (2008). Structure of Escherichia coli tyrosine kinase Etk reveals a novel activation mechanism. EMBO J *27*, 1758-1766.

Leipe, D.D., Wolf, Y.I., Koonin, E.V., and Aravind, L. (2002). Classification and evolution of P-loop GTPases and related ATPases. J Mol Biol *317*, 41-72.

Lemak, A., Gutmanas, A., Chitayat, S., Karra, M., Fares, C., Sunnerhagen, M., and Arrowsmith, C.H. (2011). A novel strategy for NMR resonance assignment and protein structure determination. J Biomol NMR *49*, 27-38.

Lescop, E., Hu, Y., Xu, H., Hu, W., Chen, J., Xia, B., and Jin, C. (2006). The solution structure of Escherichia coli Wzb reveals a novel substrate recognition mechanism of

prokaryotic low molecular weight protein-tyrosine phosphatases. J Biol Chem *281*, 19570-19577.

Lipari, G., and Szabo, A. (1982). Model-free approach to the interpretation of nuclear magnetic resonance relaxation in macromolecules. 2. . J Am Chem Soc *104*, 4559-4570.

Manai, M., and Cozzone, A.J. (1982). Endogenous protein phosphorylation in Escherichia coli extracts. Biochem Biophys Res Commun *107*, 981-988.

Mijakovic, I., Musumeci, L., Tautz, L., Petranovic, D., Edwards, R.A., Jensen, P.R., Mustelin, T., Deutscher, J., and Bottini, N. (2005). In vitro characterization of the Bacillus subtilis protein tyrosine phosphatase YwqE. J Bacteriol *187*, 3384-3390.

Morin, S. (2011). A practical guide to protein dynamics from 15N spin relaxation in solution. Prog Nucl Magn Reson Spectrosc *59*, 245-262.

Morona, J.K., Morona, R., and Paton, J.C. (2006). Attachment of capsular polysaccharide to the cell wall of Streptococcus pneumoniae type 2 is required for invasive disease. Proc Natl Acad Sci U S A *103*, 8505-8510.

Munoz-Dorado, J., Inouye, S., and Inouye, M. (1991). A gene encoding a protein serine/threonine kinase is required for normal development of M. xanthus, a gram-negative bacterium. Cell *67*, 995-1006.

Natarajan, A., Ghose, R., and Hill, J.M. (2006). Structure and dynamics of ASC2, a pyrin domain-only protein that regulates inflammatory signaling. J Biol Chem *281*, 31863-31875.

Nesper, J., Hill, C.M., Paiment, A., Harauz, G., Beis, K., Naismith, J.H., and Whitfield, C. (2003). Translocation of group 1 capsular polysaccharide in Escherichia coli serotype K30. Structural and functional analysis of the outer membrane lipoprotein Wza. J Biol Chem *278*, 49763-49772.

O'Riordan, K., and Lee, J.C. (2004). Staphylococcus aureus capsular polysaccharides. Clin Microbiol Rev *17*, 218-234.

Obadia, B., Lacour, S., Doublet, P., Baubichon-Cortay, H., Cozzone, A.J., and Grangeasse, C. (2007). Influence of tyrosine-kinase Wzc activity on colanic acid production in Escherichia coli K12 cells. J Mol Biol *367*, 42-53.

Olivares-Illana, V., Meyer, P., Bechet, E., Gueguen-Chaignon, V., Soulat, D., Lazereg-Riquier, S., Mijakovic, I., Deutscher, J., Cozzone, A.J., Laprevote, O.*, et al.* (2008). Structural basis for the regulation mechanism of the tyrosine kinase CapB from Staphylococcus aureus. PLoS Biol *6*, e143.

Orekhov, V.Y., and Jaravine, V.A. (2011). Analysis of non-uniformly sampled spectra with multi-dimensional decomposition. Prog Nucl Magn Reson Spectrosc *59*, 271-292.

Orskov, I., Orskov, F., Jann, B., and Jann, K. (1977). Serology, chemistry, and genetics of O and K antigens of Escherichia coli. Bacteriol Rev *41*, 667-710.

Ostrovsky, P.C., and Maloy, S. (1995). Protein phosphorylation on serine, threonine, and tyrosine residues modulates membrane-protein interactions and transcriptional regulation in Salmonella typhimurium. Genes Dev *9*, 2034-2041.

Palmer, A.G., 3rd (2001). Nmr probes of molecular dynamics: overview and comparison with other techniques. Annu Rev Biophys Biomol Struct *30*, 129-155.

Palmer, A.G., 3rd (2004). NMR characterization of the dynamics of biomacromolecules. Chem Rev *104*, 3623-3640.

Pereira, S.F., Goss, L., and Dworkin, J. (2011). Eukaryote-like serine/threonine kinases and phosphatases in bacteria. Microbiol Mol Biol Rev *75*, 192-212.

Pervushin, K., Riek, R., Wider, G., and Wuthrich, K. (1997). Attenuated T2 relaxation by mutual cancellation of dipole-dipole coupling and chemical shift anisotropy indicates an avenue to NMR structures of very large biological macromolecules in solution. Proc Natl Acad Sci U S A *94*, 12366-12371.

Pettersen, E.F., Goddard, T.D., Huang, C.C., Couch, G.S., Greenblatt, D.M., Meng, E.C., and Ferrin, T.E. (2004). UCSF Chimera--a visualization system for exploratory research and analysis. J Comput Chem *25*, 1605-1612.

Rafter, G.W. (1964). Identification of a New Form of Bound Phosphoserine in Escherichia Coli. J Biol Chem *239*, 1044-1047.

Ramponi, G., and Stefani, M. (1997). Structure and function of the low Mr phosphotyrosine protein phosphatases. Biochim Biophys Acta *1341*, 137-156.

Rayapureddi, J.P., Kattamuri, C., Steinmetz, B.D., Frankfort, B.J., Ostrin, E.J., Mardon, G., and Hegde, R.S. (2003). Eyes absent represents a class of protein tyrosine phosphatases. Nature *426*, 295-298.

Reid, A.N., and Whitfield, C. (2005). functional analysis of conserved gene products involved in assembly of Escherichia coli capsules and exopolysaccharides: evidence for molecular recognition between Wza and Wzc for colanic acid biosynthesis. J Bacteriol *187*, 5470-5481.

Riek, R., Pervushin, K., and Wuthrich, K. (2000). TROSY and CRINEPT: NMR with large molecular and supramolecular structures in solution. Trends Biochem Sci *25*, 462-468.

Roberts, I.S. (1996). The biochemistry and genetics of capsular polysaccharide production in bacteria. Annu Rev Microbiol *50*, 285-315.

Rudolph, J. (2007). Cdc25 phosphatases: structure, specificity, and mechanism. Biochemistry *46*, 3595-3604.

Sali, A., Potterton, L., Yuan, F., van Vlijmen, H., and Karplus, M. (1995). Evaluation of comparative protein modeling by MODELLER. Proteins *23*, 318-326.

Salzmann, M., Pervushin, K., Wider, G., Senn, H., and Wuthrich, K. (1998). TROSY in triple-resonance experiments: new perspectives for sequential NMR assignment of large proteins. Proc Natl Acad Sci U S A *95*, 13585-13590.

Salzmann, M., Wider, G., Pervushin, K., and Wuthrich, K. (1999). Improved sensitivity and coherence selection for [15N,1H]-TROSY elements in triple resonance experiments. J Biomol NMR *15*, 181-184.

Schaapveld, R., Wieringa, B., and Hendriks, W. (1997). Receptor-like protein tyrosine phosphatases: alike and yet so different. Mol Biol Rep *24*, 247-262.

Shekhtman, A., Ghose, R., Goger, M., and Cowburn, D. (2002). NMR structure determination and investigation using a reduced proton (REDPRO) labeling strategy for proteins. FEBS Lett *524*, 177-182.

Siniossoglou, S., Hurt, E.C., and Pelham, H.R. (2000). Psr1p/Psr2p, two plasma membrane phosphatases with an essential DXDX(T/V) motif required for sodium stress response in yeast. J Biol Chem *275*, 19352-19360.

Stevenson, G., Andrianopoulos, K., Hobbs, M., and Reeves, P.R. (1996). Organization of the Escherichia coli K-12 gene cluster responsible for production of the extracellular polysaccharide colanic acid. J Bacteriol *178*, 4885-4893.

Styles, P., Soffe, N.F., and Scott, C.A. (1989). An improved cryogenically cooled probe for high-resolution NMR. J Magn Reson *84*, 376-378.

Tabernero, L., Aricescu, A.R., Jones, E.Y., and Szedlacsek, S.E. (2008). Protein tyrosine phosphatases: structure-function relationships. FEBS J *275*, 867-882.

Tarrant, M.K., and Cole, P.A. (2009). The chemical biology of protein phosphorylation. Annu Rev Biochem *78*, 797-825.

Tonks, N.K., Diltz, C.D., and Fischer, E.H. (1988). Purification of the major protein-tyrosine-phosphatases of human placenta. J Biol Chem *263*, 6722-6730.

Tootle, T.L., Silver, S.J., Davies, E.L., Newman, V., Latek, R.R., Mills, I.A., Selengut, J.D., Parlikar, B.E., and Rebay, I. (2003). The transcription factor Eyes absent is a protein tyrosine phosphatase. Nature *426*, 299-302.

Valvano, M.A. (2003). Export of O-specific lipopolysaccharide. Front Biosci *8*, s452-471.

Vega, C., Chou, S., Engel, K., Harrell, M.E., Rajagopal, L., and Grundner, C. (2011). Structure and Substrate Recognition of the Staphylococcus aureus Protein Tyrosine Phosphatase PtpA. J Mol Biol *413*, 24-31.

Vincent, C., Doublet, P., Grangeasse, C., Vaganay, E., Cozzone, A.J., and Duclos, B. (1999). Cells of Escherichia coli contain a protein-tyrosine kinase, Wzc, and a phosphotyrosine-protein phosphatase, Wzb. J Bacteriol *181*, 3472-3477.

Vincent, C., Duclos, B., Grangeasse, C., Vaganay, E., Riberty, M., Cozzone, A.J., and Doublet, P. (2000). Relationship between exopolysaccharide production and protein-tyrosine phosphorylation in gram-negative bacteria. J Mol Biol *304*, 311-321.

Wang, W.Q., Sun, J.P., and Zhang, Z.Y. (2003). An overview of the protein tyrosine phosphatase superfamily. Curr Top Med Chem *3*, 739-748.

West, A.H., and Stock, A.M. (2001). Histidine kinases and response regulator proteins in two-component signaling systems. Trends Biochem Sci *26*, 369-376.

Whitfield, C. (2006). Biosynthesis and assembly of capsular polysaccharides in Escherichia coli. Annu Rev Biochem *75*, 39-68.

Wu, J., Ohta, N., Zhao, J.L., and Newton, A. (1999). A novel bacterial tyrosine kinase essential for cell division and differentiation. Proc Natl Acad Sci U S A *96*, 13068-13073.

Wugeditsch, T., Paiment, A., Hocking, J., Drummelsmith, J., Forrester, C., and Whitfield, C. (2001). Phosphorylation of Wzc, a tyrosine autokinase, is essential for assembly of group 1 capsular polysaccharides in Escherichia coli. J Biol Chem *276*, 2361-2371.

Xu, H., Xia, B., and Jin, C. (2006). Solution structure of a low-molecular-weight protein tyrosine phosphatase from Bacillus subtilis. J Bacteriol *188*, 1509-1517.

Zhang, M., Stauffacher, C.V., Lin, D., and Van Etten, R.L. (1998). Crystal structure of a human low molecular weight phosphotyrosyl phosphatase. Implications for substrate specificity. J Biol Chem *273*, 21714-21720.

Zhang, W., Munoz-Dorado, J., Inouye, M., and Inouye, S. (1992). Identification of a putative eukaryotic-like protein kinase family in the developmental bacterium Myxococcus xanthus. J Bacteriol *174*, 5450-5453.

Zhang, Z.Y., and Van Etten, R.L. (1990). Purification and characterization of a low-molecular-weight acid phosphatase--a phosphotyrosyl-protein phosphatase from bovine heart. Arch Biochem Biophys *282*, 39-49.

Zuiderweg, E.R. (2002). Mapping protein-protein interactions in solution by NMR spectroscopy. Biochemistry *41*, 1-7.